Filtered Mass Density Function for Design Simulation of High Speed Airbreathing Propulsion Systems

by

T.G. Drozda, R.M. Sheikhi and P. Givi
Department of Mechanical and Aerospace Engineering
State University of New York at Buffalo
Buffalo, NY 14260-4400

Annual Report Submitted to
The NASA Langley Research Center

Progress Report on Activities Supported Under Grant NAG 1-2238

for the Period

September 1, 2000 - August 31, 2001

Contents

Filtered Mass Density Function for Design Simulation of High Speed Airbreathing Propulsion Systems

T.G. Drozda, R.M. Sheikhi and P. Givi
Department of Mechanical and Aerospace Engineering
State University of New York at Buffalo
Buffalo, NY 14260-4400

Abstract

The objective of this research is to develop and implement new methodology for large eddy simulation of (LES) of high-speed reacting turbulent flows. We have just completed two (2) years of Phase I of this research. This annual report provides a brief and up-to-date summary of our activities during the period: September 1, 2000 through August 31, 2001.

In the work within the past year, a methodology termed "velocity-scalar filtered density function" (VSFDF) is developed and implemented for large eddy simulation (LES) of turbulent flows. In this methodology the effects of the unresolved subgrid scales (SGS) are taken into account by considering the joint probability density function (PDF) of all of the components of the velocity and scalar vectors. An exact transport equation is derived for the VSFDF in which the effects of the unresolved SGS convection, SGS velocity-scalar source, and SGS scalar-scalar source terms appear in closed form. The remaining unclosed terms in this equation are modeled.

A system of stochastic differential equations (SDEs) which yields statistically equivalent results to the modeled VSFDF transport equation is constructed. These SDEs are solved numerically by a Lagrangian Monte Carlo procedure. The consistency of the proposed SDEs and the convergence of the Monte Carlo solution are assessed by comparison with results obtained by an Eulerian LES procedure in which the corresponding transport equations for the first two SGS moments are solved. The unclosed SGS convection, SGS velocity-scalar source, and SGS scalar-scalar source in the Eulerian LES are replaced by corresponding terms from VSFDF equation. The consistency of the results is then analyzed for a case of two dimensional mixing layer.

Technical Monitor

Dr. J. Philip Drummond (Hypersonic Propulsion Branch, NASA LaRC, Mail Stop 197, Tel: 757-864-2298) is the Technical Monitor of this Grant.

Personnel

Dr. Peyman Givi is the PI of this project. One Graduate Research Assistant (RA), Mr. Tomasz G. Drozda, is being supported by this Grant. We also acknowledge collaborations with Professor Stephen B. Pope (Cornell University) on various aspects of this project.

1 Introduction

The probability density function (PDF) approach has proven useful for large eddy simulation (LES) of turbulent reacting flows.[7,12,14,15,17,24,26-30] The formal means of conducting such LES is by consideration of the "filtered density function" (FDF) which is essentially the filtered fine-grained PDF of the transport quantities. In all previous contributions, the FDF of the "scalar" quantities is considered: Gao and O'Brien,[14] Colucci *et al.*[24] and Réveillon and Vervisch[26] developed a transport equation for the FDF in constant density turbulent reacting flows. Jaberi *et al.*[28] extended the methodology for LES of variable density flows by consideration of the "filtered mass density function" (FMDF), which is essentially the mass weighted FDF. The fundamental property of the PDF methods is exhibited by the closed form nature of the chemical source term appearing in the transport equation governing the FDF (FMDF). This property is very important as evidenced in several applications of FDF for LES of a variety of turbulent reacting flows.[24,26-29] However, since the FDF of only the scalar quantities are considered, all of the "hydrodynamic" effects are modeled. In all previous LES/FDF simulations, these effects have been modeled via "non-FDF" methods.

The objective of the work conducted this year is to extend the PDF methodology to also include the SGS velocity-scalars. This is facilitated by consideration of the joint "velocity-scalar filtered density function" (VSFDF). With the definition of the VSFDF, the mathematical framework for its implementation in LES is established. A transport equation is developed for the VSFDF in which the effects of SGS convection are shown to appear in closed form. The unclosed terms in this equation are modeled in a fashion similar to those in the Reynolds-averaged simulation (RAS) procedures. A Lagrangian Monte Carlo procedure is developed and implemented for numerical simulation of the modeled VFDF transport equation. The consistency of this procedure is assessed by comparing the first two moments of the VFDF with those obtained by the Eulerian finite difference solutions of the same moments transport equations.

2 Formulation

We consider an incompressible (unit density), isothermal, turbulent reacting flow involving N_s species. For the mathematical description of this flow, the primary transport variables are the velocity vector $u_i(\mathbf{x},t)$ $(i=1,2,3)$, the pressure $p(\mathbf{x},t)$, and the species' mass fractions $\phi_\alpha(\mathbf{x},t)$ $(\alpha=1,2,\ldots,N_s)$. The equations which govern the transport of these variables in space (x_i) and time (t) are

$$\frac{\partial u_k}{\partial x_k} = 0 \tag{1a}$$

$$\frac{\partial u_i}{\partial t} + \frac{\partial u_k u_i}{\partial x_k} = -\frac{\partial p}{\partial x_i} + \frac{\partial \sigma_{ik}}{\partial x_k} \tag{1b}$$

$$\frac{\partial \phi_\alpha}{\partial t} + \frac{\partial u_k \phi_\alpha}{\partial x_k} = -\frac{\partial J_k^\alpha}{\partial x_k} + S_\alpha(\boldsymbol{\phi}) \tag{1c}$$

where $S_\alpha(\mathbf{x},t)$ denotes the chemical reaction term for species α, and $\boldsymbol{\phi} \equiv [\phi_1,\ \phi_2,\ldots\phi_{N_s}]$ denotes the scalar array. Assuming a Newtonian flow with Fick's law of diffusion, we have:

$$\sigma_{ik} = \nu\left(\frac{\partial u_i}{\partial x_k} + \frac{\partial u_k}{\partial x_i}\right) \tag{2}$$

$$J_k^\alpha = -\Gamma^\alpha \frac{\partial \phi_\alpha}{\partial x_k} \tag{3}$$

where ν is the kinematic viscosity and is assumed constant, and Γ^α is the density weighted diffusion coefficient of species α. The Schmidt number, Sc, is defined as: $\Gamma^\alpha = \frac{\nu}{Sc^\alpha}$.

LES involves the use of the spatial filtering[6,32]

$$\langle f(x,t)\rangle = \int_{-\infty}^{+\infty} f(x',t)G(x',x)dx' \tag{4}$$

where function $G(x',x)$ is a filter function, $\langle f(x,t)\rangle$ is the filtered value of the transport variable $f(x,t)$. Applying such a filter to the governing Eq.(1a-1c) yields filtered equations

$$\frac{\partial \langle u_k\rangle}{\partial x_k} = 0 \tag{5a}$$

$$\frac{\partial \langle u_i\rangle}{\partial t} + \frac{\partial \langle u_k\rangle\langle u_i\rangle}{\partial x_k} = -\frac{\partial \langle p\rangle}{\partial x_i} + \nu \frac{\partial^2 \langle u_i\rangle}{\partial x_k \partial x_k} - \frac{\partial \tau(u_k,u_i)}{\partial x_k} \tag{5b}$$

$$\frac{\partial \langle \phi_\alpha\rangle}{\partial t} + \frac{\partial \langle u_k\rangle\langle \phi_\alpha\rangle}{\partial x_k} = \Gamma^\alpha \frac{\partial^2 \langle \phi_\alpha\rangle}{\partial x_k \partial x_k} - \frac{\partial \tau(u_k,\phi_\alpha)}{\partial x_k} + \langle S_\alpha(\phi)\rangle \tag{5c}$$

where the subgrid scale terms(SGS), τ, are in general defined as

$$\tau(a_i,b_j) = \langle a_i b_j\rangle - \langle a_i\rangle\langle b_j\rangle \tag{6}$$

and satisfy following transport equations

$$\begin{aligned}\frac{\partial \tau(u_i,u_j)}{\partial t} + \frac{\partial \langle u_k\rangle \tau(u_i,u_j)}{\partial x_k} &= \nu \frac{\partial^2 \tau(u_i,u_j)}{\partial x_k \partial x_k} - \tau(u_k,u_i)\frac{\partial \langle u_j\rangle}{\partial x_k} - \tau(u_k,u_j)\frac{\partial \langle u_i\rangle}{\partial x_k} - \\ &- \left[2\nu\tau\left(\frac{\partial u_i}{\partial x_k},\frac{\partial u_j}{\partial x_k}\right) + \tau\left(u_i,\frac{\partial p}{\partial x_j}\right) + \tau\left(u_j,\frac{\partial p}{\partial x_i}\right)\right] - \frac{\partial \tau(u_k,u_i,u_j)}{\partial x_k}\end{aligned} \tag{7}$$

The first unclosed term in the square bracket is dissipation and is often labeled as, ϵ_{ik}. The next two terms correspond to velocity-pressure scrambling and are labeled in literature as, Π_{ik}.

$$\begin{aligned}\frac{\partial \tau(\phi_\alpha,\phi_\beta)}{\partial t} + \frac{\partial \langle u_k\rangle \tau(\phi_\alpha,\phi_\beta)}{\partial x_k} &= \Gamma^\alpha \frac{\partial^2 \tau(\phi_\alpha,\phi_\beta)}{\partial x_k \partial x_k} - \tau(u_k,\phi_\alpha)\frac{\partial \langle \phi_\beta\rangle}{\partial x_k} - \\ &- \tau(u_k,\phi_\beta)\frac{\partial \langle \phi_\alpha\rangle}{\partial x_k} - \left[2\Gamma^\alpha\tau\left(\frac{\partial \phi_\alpha}{\partial x_k},\frac{\partial \phi_\beta}{\partial x_k}\right)\right] + \tau(\phi_\alpha,S_\beta) + \tau(\phi_\beta,S_\alpha) - \\ &- \frac{\partial \tau(u_k,\phi_\alpha,\phi_\beta)}{\partial x_k}\end{aligned} \tag{8}$$

where the term in square bracket is the scalar dissipation.

$$\begin{aligned}\frac{\partial\tau(u_i,\phi_\alpha)}{\partial t} &+ \frac{\partial\langle u_k\rangle\tau(u_i,\phi_\alpha)}{\partial x_k} = \left(\frac{\nu+\Gamma^\alpha}{2}\right)\frac{\partial^2\tau(u_i,\phi_\alpha)}{\partial x_k\partial x_k} - \tau(u_k,u_i)\frac{\partial\langle\phi_\alpha\rangle}{\partial x_k} - \\ &- \tau(u_k,\phi_\alpha)\frac{\partial\langle u_i\rangle}{\partial x_k} - \Bigg[(\nu+\Gamma^\alpha)\,\tau\left(\frac{\partial u_i}{\partial x_k},\frac{\partial\phi_\alpha}{\partial x_k}\right) + \tau\left(\phi_\alpha,\frac{\partial p}{\partial x_i}\right) + \\ &+ \left(\frac{\nu-\Gamma^\alpha}{2}\right)\left(\tau\left(u_i,\frac{\partial^2\phi_\alpha}{\partial x_k\partial x_k}\right) - \tau\left(\phi_\alpha,\frac{\partial^2 u_i}{\partial x_k\partial x_k}\right)\right)\Bigg] \\ &+ \tau(u_i,S_\alpha) - \frac{\partial\tau(u_k,u_i,\phi_\alpha)}{\partial x_k}\end{aligned} \tag{9}$$

where the first term in square bracket is the velocity-scalar dissipation, next term is scalar-pressure scrambling, and the last two terms are velocity-scalar diffusion and scalar-velocity diffusion terms. All of the terms in square brackets are the unclosed terms that need to be modeled. Triple subgrid scale terms, τ, are generally defined as

$$\begin{aligned}\tau(a_i,b_j,c_k) &= \langle a_ib_jc_k\rangle - \langle a_i\rangle\tau(b_j,c_k) - \\ &\quad -\langle b_j\rangle\tau(a_i,c_k) - \langle c_k\rangle\tau(a_i,b_j) - \langle a_i\rangle\langle b_j\rangle\langle c_k\rangle\end{aligned} \tag{10}$$

A Velocity-Scalar Filtered Density Function

The "velocity-scalar filtered density function" (VSFDF), denoted from here on as P, is formally defined as

$$P\left(\boldsymbol{V},\boldsymbol{\psi};x,t\right) = \int_{-\infty}^{+\infty}\varrho\left(\boldsymbol{V},\boldsymbol{\psi};\boldsymbol{U}(x',y),\boldsymbol{\phi}(x',t)\right)G(x'-x)dx' \tag{11}$$

$$\varrho\left(\boldsymbol{V},\boldsymbol{\psi};\boldsymbol{U}(x',y),\boldsymbol{\phi}(x',t)\right) = \prod_{i=1}^{3}\delta\left(V_i-u_i(x,t)\right)\times\prod_{\alpha=1}^{N_s}\delta\left(\psi_\alpha-\phi_\alpha(x,t)\right) \tag{12}$$

where δ denotes the delta function, $\boldsymbol{V},\boldsymbol{\psi}$ are the velocity and scalar state vectors respectively. Term ϱ represents so called "fine-grained" density[30] and hence Eq.(11) defines VSFDF as the spatially filtered value of the fine-grained density. In other words, VSFDF represents a density in the velocity-scalar space of the fluid around x weighted by filter G, at a time t. With the filter properties specified in Eq.(13-17), P has all of the properties of the probability density function(PDF).[1]

$$G(x',x) \equiv G(x'-x) \tag{13}$$

$$G(x) = G(-x) \tag{14}$$

$$G(x) \geq 0, \text{for all x} \tag{15}$$

$$\int_{-\infty}^{+\infty}x^mG(x)dx \equiv \text{moments exist for } m>0 \tag{16}$$

$$\int_{-\infty}^{+\infty}G(x)dx = 1 \tag{17}$$

Following the procedure of Pope,[1] a VSFDF transport equation can be derived by considering a time derivative of Eq.(11).

$$\begin{aligned}\frac{\partial P}{\partial t}+\frac{\partial}{\partial x_k}\left(V_k P\right) &= \Gamma\frac{\partial^2 P}{\partial x_k \partial x_k}+\frac{\partial\langle p\rangle}{\partial x_k}\frac{\partial P}{\partial V_k}-\frac{\partial}{\partial \psi_\alpha}\left[S_\alpha(\psi)P\right]+\\ &+\frac{\partial}{\partial V_k}\left[\left(\left\langle\frac{\partial p}{\partial x_k}|\boldsymbol{V},\boldsymbol{\psi}\right\rangle-\frac{\partial\langle p\rangle}{\partial x_k}\right)P\right]-\\ &-\frac{\partial^2}{\partial V_i \partial V_j}\left[\left\langle\Gamma\frac{\partial u_i}{\partial x_k}\frac{\partial u_j}{\partial x_k}|\boldsymbol{V},\boldsymbol{\psi}\right\rangle P\right]-\\ &-\frac{\partial^2}{\partial \psi_\alpha \partial \psi_\beta}\left[\left\langle\Gamma\frac{\partial \psi_\alpha}{\partial x_k}\frac{\partial \psi_\beta}{\partial x_k}|\boldsymbol{V},\boldsymbol{\psi}\right\rangle P\right]-\\ &-\frac{\partial^2}{\partial V_i \partial \psi_\alpha}\left[\left\langle 2\Gamma\frac{\partial u_i}{\partial x_k}\frac{\partial \psi_\alpha}{\partial x_k}|\boldsymbol{V},\boldsymbol{\psi}\right\rangle P\right]\end{aligned} \tag{18}$$

where $\Gamma=\Gamma^\alpha=\nu$, and consequently $Sc^\alpha=1$. A quick check of the above equation can be made by integrating it according to Eq.(22) to obtain appropriate moment equations. These equations should match with Eq.(5a-5c), and Eq.(7-9)

B Modeled VSFDF Transport Equation

A closure needs to be provided for the conditional terms on the RHS of VSFDF Eq.(18) to allow for a solution. Haworth and Pope[2] proposed that the Generalized Langevin Model (GLM) be employed in this task. An extension of their strategy allows us to present a combination of GLM and linear mean square estimation(LMSE)[3,8,25] model

$$\begin{aligned}&\frac{\partial}{\partial V_k}\left[\left(\left\langle\frac{\partial p}{\partial x_k}|\boldsymbol{V},\boldsymbol{\psi}\right\rangle-\frac{\partial\langle p\rangle}{\partial x_k}\right)P\right]-\frac{\partial^2}{\partial V_i \partial V_j}\left[\left\langle\Gamma\frac{\partial u_i}{\partial x_k}\frac{\partial u_j}{\partial x_k}|\boldsymbol{V},\boldsymbol{\psi}\right\rangle P\right]-\\ &\frac{\partial^2}{\partial \psi_\alpha \partial \psi_\beta}\left[\left\langle\Gamma\frac{\partial \psi_\alpha}{\partial x_k}\frac{\partial \psi_\beta}{\partial x_k}|\boldsymbol{V},\boldsymbol{\psi}\right\rangle P\right]-\frac{\partial^2}{\partial V_i \partial \psi_\alpha}\left[\left\langle 2\Gamma\frac{\partial u_i}{\partial x_k}\frac{\partial \psi_\alpha}{\partial x_k}|\boldsymbol{V},\boldsymbol{\psi}\right\rangle P\right]\approx\\ &\approx\Gamma\frac{\partial\langle u_i\rangle}{\partial x_k}\frac{\partial\langle u_j\rangle}{\partial x_k}\frac{\partial^2 f}{\partial V_i \partial V_j}+2\Gamma\frac{\partial\langle u_i\rangle}{\partial x_k}\frac{\partial^2 f}{\partial x_k \partial V_i}-\\ &-\frac{\partial}{\partial V_i}\left[G_{ij}\left(V_j-\langle u_j\rangle\right)f\right]+\frac{1}{2}C_0\epsilon\frac{\partial^2 f}{\partial V_k \partial V_k}+\\ &+\frac{\partial}{\partial \psi_\alpha}\left[C_{\phi_\alpha}\omega\left(\psi_\alpha-\langle\phi_\alpha\rangle\right)f\right]+\\ &+\Gamma\frac{\partial\langle\phi_\alpha\rangle}{\partial x_k}\frac{\partial\langle\phi_\beta\rangle}{\partial x_k}\frac{\partial^2 f}{\partial \psi_\alpha \partial \psi_\beta}+2\Gamma\frac{\partial\langle u_i\rangle}{\partial x_k}\frac{\partial\langle\phi_\alpha\rangle}{\partial x_k}\frac{\partial^2 f}{\partial V_i \partial \psi_\alpha}+2\Gamma\frac{\partial\langle\phi_\alpha\rangle}{\partial x_k}\frac{\partial^2 f}{\partial x_k \partial \psi_\alpha}\end{aligned} \tag{19}$$

Above model offers full consistency with the exact equations, however, as will become more clear in the following section, the last line can not be included because it violates scalar field realizability conditions.

C Stochastic System

The most convenient way of solving VSFDF equation is by the Lagrangian Monte Carlo procedure. Eulerian Monte Carlo schemes exist, but they are shown to produce excessive artificial diffusion, which greatly degrades LES results.[24] Lagrangian Monte Carlo scheme is based on the principle of equivalent systems.[1] This principle states that two stochastic systems with different instantaneous behaviors may produce identical statistics and satisfy the same Fokker-Plank (PDF, FDF) equation. The following is then true: a set of SDEs produces one, and only one, Fokker-Plank equation, while a Fokker-Plank equation can result from many different sets of SDEs. In this light one may consider a set of stochastic differential equations as the most precise way of describing a random process, and its Fokker-Plank analogous to a "filter" of this random process. Lagrangian Monte Carlo scheme is provided by the following general form of a stochastic diffusion process

$$
\begin{aligned}
dX_i &= D_i^X(t)dt + B^X(t)dW_i^X(t) && \text{(20a)}\\
dU_i &= D_i^U(t)dt + B^U(t)dW_i^U(t) + \\
&+ F_{ij}^{UX}(t)dW_j^X(t) + F_{i\alpha}^{U\phi}(t)dW_\alpha^\phi(t) && \text{(20b)}\\
d\psi_\alpha &= D_\alpha^\phi(t)dt + B^\phi(t)dW_\alpha^\phi(t) + \\
&+ F_{\alpha j}^{\phi X}(t)dW_j^X(t) + F_{\alpha j}^{\phi U}(t)dW_j^U(t) && \text{(20c)}
\end{aligned}
$$

Above set consists of a standard stochastic drift (D) and diffusion (B) terms. In addition, diffusional coupling is introduced between variables by adding extra diffusion terms (F). All of the terms (D, B, F) are implicitly functions of the state variables, that is, $D(t) = D(\mathbf{X}(t), \boldsymbol{V}(t), \boldsymbol{\psi}_\alpha(t); t)$, $B(t) = B(\mathbf{X}(t), \boldsymbol{V}(t), \boldsymbol{\psi}_\alpha(t); t)$, $F(t) = F(\mathbf{X}(t), \boldsymbol{V}(t), \boldsymbol{\psi}_\alpha(t); t)$. The W terms denote independent Wiener-Lévy processes.[16] The corresponding Fokker-Planck equation is

$$
\begin{aligned}
\frac{\partial f^\star}{\partial t} &= -\frac{\partial}{\partial x_i}\left(D_i^X f^\star\right) - \frac{\partial}{\partial V_i}\left(D_i^U f^\star\right) - \frac{\partial}{\partial \psi_\alpha}\left(D_\alpha^\phi f^\star\right) + \\
&+ \frac{\partial}{\partial x_i \partial x_j}\left(b_{ij}^{XX} f^\star\right) + \frac{\partial}{\partial x_i \partial V_j}\left(b_{ij}^{XU} f^\star\right) + \frac{\partial}{\partial x_i \partial \psi_j}\left(b_{ij}^{X\phi} f^\star\right) + \\
&+ \frac{\partial}{\partial V_i \partial x_j}\left(b_{ij}^{UX} f^\star\right) + \frac{\partial}{\partial V_i \partial V_j}\left(b_{ij}^{UU} f^\star\right) + \frac{\partial}{\partial V_i \partial \psi_j}\left(b_{ij}^{U\phi} f^\star\right) + \\
&+ \frac{\partial}{\partial \psi_i \partial x_j}\left(b_{ij}^{\phi X} f^\star\right) + \frac{\partial}{\partial \psi_i \partial V_j}\left(b_{ij}^{\phi U} f^\star\right) + \frac{\partial}{\partial \psi_i \partial \psi_j}\left(b_{ij}^{\phi\phi} f^\star\right) \qquad \text{(21)}
\end{aligned}
$$

where $b_{ij} = \left[\Sigma(t)\Gamma(t)\Sigma^T(t)\right]$,[16] Σ is the diffusion matrix and Γ is the covariance matrix of the Wiener-Lévy processes, W^X,W^U,and W^ϕ.

The above equations implicitly describe a set of moment transport equations. These transport equations can be found either by applying Itô formula[16] to the SDEs and applying a filtering operation, or by integrating the Fokker-Plank equation. In the later case the integration takes on a form

$$
\langle Q(x,t)\rangle = \int_{-\infty}^{+\infty}\int_{-\infty}^{+\infty} Q(\boldsymbol{V},\boldsymbol{\psi};x,t) f(\boldsymbol{V},\boldsymbol{\psi};x,t) d\boldsymbol{V} d\boldsymbol{\psi} \qquad \text{(22)}
$$

where Q is a random variable, $\langle Q\rangle$ is its filtered value, and f is its PDF.

C.1 Fully Consistent System

Pope[1] and Gicquel[31] have proposed a system of stochastic differential equations (SDEs), based on the VSFDF model in Eq.(19). A set of random variables, X, U, ϕ, that correspond to the position, velocity and scalar value respectively is introduced into a stochastic diffusion process. The unknown coefficients are found by comparing the moments of the below set with the exact set of moment equations, i.e. Eq.(5a-9)

$$dX_i = U_i dt + \sqrt{\nu_1} dW_i^X \tag{23a}$$

$$dU_i = \left[-\frac{\partial \langle p \rangle}{\partial x_i} + \nu_2 \frac{\partial^2 \langle u_i \rangle}{\partial x_k \partial x_k} + G_{ij} \left(V_j - \langle u_j \rangle \right) \right] dt + \\ + \sqrt{\nu_3} \frac{\partial \langle u_i \rangle}{\partial x_k} dW_k^X + \sqrt{C_0 \epsilon} dW_i^U \tag{23b}$$

$$d\psi_\alpha = \left[\nu_\alpha \frac{\partial^2 \langle \phi_\alpha \rangle}{\partial x_k \partial x_k} - C_{\phi_\alpha} \omega \left(\psi_\alpha - \langle \phi_\alpha \rangle \right) + S_\alpha(\psi) \right] dt + \\ + \sqrt{\nu_{S_\alpha}} \frac{\partial \langle \phi_\alpha \rangle}{\partial x_k} dW_k^X \tag{23c}$$

The above set of equations contains a model for the unclosed terms in Eq.(18). It should be noted here that the first and the last terms in Eq.(23c) violate realizability of the scalar field and are the source of the terms appearing on the last line in Eq.(19). In particular, these terms would allow a mixture fraction, for example, to extend beyond physical range of 0 to 1.
Computation of the Fokker-Plank[16] equation, or the PDF(in this case it is also a FDF), for the diffusion process in equations above, yields

$$\frac{\partial f}{\partial t} + \frac{\partial}{\partial x_k} \left(V_k f \right) = \left[\frac{\partial \langle p \rangle}{\partial x_k} - \left(\nu_2 - \sqrt{\nu_1 \nu_3} \right) \frac{\partial^2 \langle u_i \rangle}{\partial x_k \partial x_k} \right] \frac{\partial f}{\partial V_i} - \frac{\partial}{\partial V_i} \left[G_{ij} \left(V_j - \langle u_j \rangle \right) f \right] - \\ - \left[\nu_\alpha - \sqrt{\nu_1 \nu_{S_\alpha}} \right] \frac{\partial^2 \langle \phi_\alpha \rangle}{\partial x_k \partial x_k} \frac{\partial f}{\partial \psi_\alpha} + \frac{\partial}{\partial \psi_\alpha} \left[C_{\phi_\alpha} \omega \left(\psi_\alpha - \langle \phi_\alpha \rangle \right) f \right] - \frac{\partial}{\partial \psi_\alpha} \left[S_\alpha(\psi) f \right] + \\ + \frac{\nu_1}{2} \frac{\partial^2 f}{\partial x_k \partial x_k} + \sqrt{\nu_1 \nu_3} \frac{\partial \langle u_j \rangle}{\partial x_i} \frac{\partial^2 f}{\partial x_i \partial V_j} + \sqrt{\nu_1 \nu_{S_\alpha}} \frac{\partial \langle \phi_\alpha \rangle}{\partial x_i} \frac{\partial^2 f}{\partial x_i \partial \psi_\alpha} \\ + \frac{\nu_3}{2} \frac{\partial \langle u_i \rangle}{\partial x_k} \frac{\partial \langle u_j \rangle}{\partial x_k} \frac{\partial^2 f}{\partial V_i \partial V_j} + \frac{1}{2} C_0 \epsilon \frac{\partial^2 f}{\partial V_k \partial V_k} + \frac{1}{2} \sqrt{\nu_{S_\alpha} \nu_{S_\beta}} \frac{\partial \langle \phi_\alpha \rangle}{\partial x_k} \frac{\partial \langle \phi_\beta \rangle}{\partial x_k} \frac{\partial^2 f}{\partial \psi_\alpha \partial \psi_\beta} + \\ + \sqrt{\nu_3 \nu_{S_\alpha}} \frac{\partial \langle u_i \rangle}{\partial x_k} \frac{\partial \langle \phi_\alpha \rangle}{\partial x_k} \frac{\partial^2 f}{\partial V_i \partial \psi_\alpha} \tag{24}$$

The moment transport equations resulting from integration Eq.(22) are

$$\frac{\partial \langle u_k \rangle}{\partial x_k} = 0 \tag{25a}$$

$$\frac{\partial \langle u_i \rangle}{\partial t} + \frac{\partial \langle u_k \rangle \langle u_i \rangle}{\partial x_k} = -\frac{\partial \langle p \rangle}{\partial x_i} + \left(\frac{\nu_1}{2} + \nu_2 - \sqrt{\nu_1 \nu_3} \right) \frac{\partial^2 \langle u_i \rangle}{\partial x_k \partial x_k} - \frac{\partial \tau(u_k, u_i)}{\partial x_k} \tag{25b}$$

$$\frac{\partial \langle \phi_\alpha \rangle}{\partial t} + \frac{\partial \langle u_k \rangle \langle \phi_\alpha \rangle}{\partial x_k} = \left(\nu_\alpha - \sqrt{\nu_1 \nu_{S_\alpha}} + \frac{\nu_1}{2} \right) \frac{\partial^2 \langle \phi_\alpha \rangle}{\partial x_k \partial x_k} + \langle S_\alpha(\phi) \rangle - \frac{\partial \tau(u_k, \phi_\alpha)}{\partial x_k} \tag{25c}$$

The SGS moment equations are

$$\begin{aligned}\frac{\partial\tau(u_i,u_j)}{\partial t} &+ \frac{\partial\langle u_k\rangle\tau(u_i,u_j)}{\partial x_k} = \frac{\nu_1}{2}\frac{\partial^2\tau(u_i,u_j)}{\partial x_k\partial x_k} - \tau(u_k,u_i)\frac{\partial\langle u_j\rangle}{\partial x_k} - \tau(u_k,u_j)\frac{\partial\langle u_i\rangle}{\partial x_k} + \\ &+ (\nu_1 - 2\sqrt{\nu_1\nu_3} + \nu_3)\frac{\partial\langle u_i\rangle}{\partial x_k}\frac{\partial\langle u_j\rangle}{\partial x_k} - \\ &+ [G_{ik}\tau(u_k,u_j) + G_{jk}\tau(u_k,u_i) + C_0\epsilon\delta_{ij}] - \frac{\partial\tau(u_k,u_i,u_j)}{\partial x_k}\end{aligned} \tag{26}$$

$$\begin{aligned}\frac{\partial\tau(\phi_\alpha,\phi_\beta)}{\partial t} &+ \frac{\partial\langle u_k\rangle\tau(\phi_\alpha,\phi_\beta)}{\partial x_k} = \frac{\nu_1}{2}\frac{\partial^2\tau(\phi_\alpha,\phi_\beta)}{\partial x_k\partial x_k} - \tau(u_k,\phi_\alpha)\frac{\partial\langle\phi_\beta\rangle}{\partial x_k} - \tau(u_k,\phi_\beta)\frac{\partial\langle\phi_\alpha\rangle}{\partial x_k} + \\ &+ \left(\nu_1 - \sqrt{\nu_1\nu_{S_\alpha}} - \sqrt{\nu_1\nu_{S_\beta}} + \sqrt{\nu_{S_\alpha}\nu_{S_\beta}}\right)\frac{\partial\langle\phi_\alpha\rangle}{\partial x_k}\frac{\partial\langle\phi_\beta\rangle}{\partial x_k} - \\ &- [(C_{\phi_\alpha} + C_{\phi_\beta})\omega\tau(\phi_\alpha,\phi_\beta)] + \tau(\phi_\alpha,S_\beta) + \tau(\phi_\beta,S_\alpha) - \frac{\partial\tau(u_k,\phi_\alpha,\phi_\beta)}{\partial x_k}\end{aligned} \tag{27}$$

$$\begin{aligned}\frac{\partial\tau(u_i,\phi_\alpha)}{\partial t} &+ \frac{\partial\langle u_k\rangle\tau(u_i,\phi_\alpha)}{\partial x_k} = \frac{\nu_1}{2}\frac{\partial^2\tau(u_i,\phi_\alpha)}{\partial x_k\partial x_k} - \tau(u_k,u_i)\frac{\partial\langle\phi_\alpha\rangle}{\partial x_k} - \tau(u_k,\phi_\alpha)\frac{\partial\langle u_i\rangle}{\partial x_k} + \\ &+ \left(\nu_1 - \sqrt{\nu_1\nu_3} - \sqrt{\nu_1\nu_{S_\alpha}} + \sqrt{\nu_3\nu_{S_\alpha}}\right)\frac{\partial\langle u_i\rangle}{\partial x_k}\frac{\partial\langle\phi_\alpha\rangle}{\partial x_k} + \\ &+ [G_{ik}\tau(u_k,\phi_\alpha) - C_{\phi_\alpha}\omega\tau(u_i,\phi_\alpha)] + \tau(u_i,S_\alpha) - \frac{\partial\tau(u_k,u_i,\phi_\alpha)}{\partial x_k}\end{aligned} \tag{28}$$

A comparison of above set to the corresponding exact moment equations reveals that the fully consistent stochastic system can be achieved if the coefficients in the SDE's Eq.(30a-30c) are set as follows:

$$\nu_1 = \nu_2 = \nu_3 = \nu_\alpha = \nu_{S_{\alpha,\beta,\ldots}} = 2\Gamma \tag{29}$$

A fully consistent stochastic systems becomes:

$$dX_i = U_i dt + \sqrt{2\Gamma}dW_i^X \tag{30a}$$

$$\begin{aligned}dU_i &= \left[-\frac{\partial\langle p\rangle}{\partial x_i} + 2\Gamma\frac{\partial^2\langle u_i\rangle}{\partial x_k\partial x_k} + G_{ij}\left(V_j - \langle u_j\rangle\right)\right]dt + \\ &+\sqrt{2\Gamma}\frac{\partial\langle u_i\rangle}{\partial x_k}dW_k^X + \sqrt{C_0\epsilon}dW_i^U\end{aligned} \tag{30b}$$

$$\begin{aligned}d\psi_\alpha &= \left[2\Gamma\frac{\partial^2\langle\phi_\alpha\rangle}{\partial x_k\partial x_k} - C_{\phi_\alpha}\omega\left(\psi_\alpha - \langle\phi_\alpha\rangle\right) + S_\alpha(\boldsymbol{\psi})\right]dt + \\ &+\sqrt{2\Gamma}\frac{\partial\langle\phi_\alpha\rangle}{\partial x_k}dW_k^X\end{aligned} \tag{30c}$$

The Fokker-Planck equation is:

$$\begin{aligned}\frac{\partial f}{\partial t} &+ \frac{\partial}{\partial x_k}\left(V_k f\right) = \Gamma\frac{\partial^2 f}{\partial x_k \partial x_k} + \frac{\partial \langle p\rangle}{\partial x_k}\frac{\partial f}{\partial V_k} + \\ &+ \Gamma\frac{\partial\langle u_i\rangle}{\partial x_k}\frac{\partial\langle u_j\rangle}{\partial x_k}\frac{\partial^2 f}{\partial V_i \partial V_j} + 2\Gamma\frac{\partial\langle u_i\rangle}{\partial x_k}\frac{\partial^2 f}{\partial x_k \partial V_i} - \\ &- \frac{\partial}{\partial V_i}\left[G_{ij}\left(V_j - \langle u_j\rangle\right) f\right] + \frac{1}{2}C_0\epsilon\delta_{ij}\frac{\partial^2 f}{\partial V_i \partial V_j} + \\ &+ \frac{\partial}{\partial \psi_\alpha}\left[C_{\phi_\alpha}\omega\left(\psi_\alpha - \langle\phi_\alpha\rangle\right) f\right] \end{aligned} \tag{31}$$

and the corresponding moment equations obtained by integration Eq.(22) are

$$\frac{\partial\langle u_k\rangle}{\partial x_k} = 0 \tag{32a}$$

$$\frac{\partial\langle u_i\rangle}{\partial t} + \frac{\partial\langle u_k\rangle\langle u_i\rangle}{\partial x_k} = -\frac{\partial\langle p\rangle}{\partial x_i} + \Gamma\frac{\partial^2\langle u_i\rangle}{\partial x_k \partial x_k} - \frac{\partial\tau(u_k,u_i)}{\partial x_k} \tag{32b}$$

$$\frac{\partial\langle\phi_\alpha\rangle}{\partial t} + \frac{\partial\langle u_k\rangle\langle\phi_\alpha\rangle}{\partial x_k} = \Gamma\frac{\partial^2\langle\phi_\alpha\rangle}{\partial x_k \partial x_k} + \langle S_\alpha\left(\boldsymbol{\phi}\right)\rangle - \frac{\partial\tau(u_k,\phi_\alpha)}{\partial x_k} \tag{32c}$$

$$\begin{aligned}\frac{\partial\tau(u_i,u_j)}{\partial t} &+ \frac{\partial\langle u_k\rangle\tau(u_i,u_j)}{\partial x_k} = \Gamma\frac{\partial^2\tau(u_i,u_j)}{\partial x_k \partial x_k} - \tau(u_k,u_i)\frac{\partial\langle u_j\rangle}{\partial x_k} - \tau(u_k,u_j)\frac{\partial\langle u_i\rangle}{\partial x_k} + \\ &+ \left[G_{ik}\tau(u_k,u_j) + G_{jk}\tau(u_k,u_i) + C_0\epsilon\delta_{ij}\right] - \frac{\partial\tau(u_k,u_i,u_j)}{\partial x_k}\end{aligned} \tag{33}$$

$$\begin{aligned}\frac{\partial\tau(\phi_\alpha,\phi_\beta)}{\partial t} &+ \frac{\partial\langle u_k\rangle\tau(\phi_\alpha,\phi_\beta)}{\partial x_k} = \Gamma\frac{\partial^2\tau(\phi_\alpha,\phi_\beta)}{\partial x_k \partial x_k} - \tau(u_k,\phi_\alpha)\frac{\partial\langle\phi_\beta\rangle}{\partial x_k} - \tau(u_k,\phi_\beta)\frac{\partial\langle\phi_\alpha\rangle}{\partial x_k} - \\ &- \left[(C_{\phi_\alpha} + C_{\phi_\beta})\omega\tau(\phi_\alpha,\phi_\beta)\right] + \tau(\phi_\alpha,S_\beta) + \tau(\phi_\beta,S_\alpha) - \frac{\partial\tau(u_k,\phi_\alpha,\phi_\beta)}{\partial x_k}\end{aligned} \tag{34}$$

$$\begin{aligned}\frac{\partial\tau(u_i,\phi_\alpha)}{\partial t} &+ \frac{\partial\langle u_k\rangle\tau(u_i,\phi_\alpha)}{\partial x_k} = \Gamma\frac{\partial^2\tau(u_i,\phi_\alpha)}{\partial x_k \partial x_k} - \tau(u_k,u_i)\frac{\partial\langle\phi_\alpha\rangle}{\partial x_k} - \tau(u_k,\phi_\alpha)\frac{\partial\langle u_i\rangle}{\partial x_k} + \\ &+ \left[G_{ik}\tau(u_k,\phi_\alpha) - C_{\phi_\alpha}\omega\tau(u_i,\phi_\alpha)\right] + \tau(u_i,S_\alpha) - \frac{\partial\tau(u_k,u_i,\phi_\alpha)}{\partial x_k}\end{aligned} \tag{35}$$

where the terms in square brackets provide closure to the corresponding unclosed terms in the exact Eq.(5a-5c), and Eq.(7-9).

C.2 VSFDF System for Consistency Assessment

The stochastic system of SDEs presented in previous section is fully consistent with exact filtered equations and capable of simulating convection and reaction terms in a fully closed form. We have showed this

mathematically in prior sections, however, it is necessary to also show that numerically, such a system indeed produces results comparable with, most commonly used, Eulerian finite difference schemes. This task is accomplished by solving a somewhat simpler and realizable system of SDEs

$$dX_i = U_i dt + \sqrt{2\Gamma} dW_i^X \tag{36a}$$

$$dU_i = \left[-\frac{\partial \langle p \rangle}{\partial x_i} + 2\Gamma \frac{\partial^2 \langle u_i \rangle}{\partial x_k \partial x_k} + G_{ij} \left(V_j - \langle u_j \rangle \right) \right] dt + \tag{36b}$$

$$+ \sqrt{2\Gamma} \frac{\partial \langle u_i \rangle}{\partial x_k} dW_k^X + \sqrt{C_0 \epsilon} dW_i^U$$

$$d\psi_\alpha = -C_{\phi_\alpha} \omega \left(\psi_\alpha - \langle \phi_\alpha \rangle \right) dt \tag{36c}$$

Above system employs a fully consistent hydrodynamic system and LMSE[3] model for scalar mixing. The Fokker-Plank[16](PDF) equation for this system is

$$\begin{aligned} \frac{\partial f}{\partial t} &+ \frac{\partial}{\partial x_k} \left(V_k f \right) = \Gamma \frac{\partial^2 f}{\partial x_k \partial x_k} + \frac{\partial \langle p \rangle}{\partial x_k} \frac{\partial f}{\partial V_k} + \\ &+ \Gamma \frac{\partial \langle u_i \rangle}{\partial x_k} \frac{\partial \langle u_j \rangle}{\partial x_k} \frac{\partial^2 f}{\partial V_i \partial V_j} + 2\Gamma \frac{\partial \langle u_i \rangle}{\partial x_k} \frac{\partial^2 f}{\partial x_k \partial V_i} - \\ &- \frac{\partial}{\partial V_i} \left[G_{ij} \left(V_j - \langle u_j \rangle \right) f \right] + \frac{1}{2} C_0 \epsilon \delta_{ij} \frac{\partial^2 f}{\partial V_i \partial V_j} + \\ &+ \frac{\partial}{\partial \psi_\alpha} \left[C_{\phi_\alpha} \omega \left(\psi_\alpha - \langle \phi_\alpha \rangle \right) f \right] \end{aligned} \tag{37}$$

and the corresponding moment equations obtained by integration Eq.(22) are

$$\frac{\partial \langle u_k \rangle}{\partial x_k} = 0 \tag{38a}$$

$$\frac{\partial \langle u_i \rangle}{\partial t} + \frac{\partial \langle u_k \rangle \langle u_i \rangle}{\partial x_k} = -\frac{\partial \langle p \rangle}{\partial x_i} + \Gamma \frac{\partial^2 \langle u_i \rangle}{\partial x_k \partial x_k} - \frac{\partial \tau(u_k, u_i)}{\partial x_k} \tag{38b}$$

$$\frac{\partial \langle \phi_\alpha \rangle}{\partial t} + \frac{\partial \langle u_k \rangle \langle \phi_\alpha \rangle}{\partial x_k} = \Gamma \frac{\partial^2 \langle \phi_\alpha \rangle}{\partial x_k \partial x_k} - \frac{\partial \tau(u_k, \phi_\alpha)}{\partial x_k} \tag{38c}$$

$$\begin{aligned} \frac{\partial \tau(u_i, u_j)}{\partial t} &+ \frac{\partial \langle u_k \rangle \tau(u_i, u_j)}{\partial x_k} = \Gamma \frac{\partial^2 \tau(u_i, u_j)}{\partial x_k \partial x_k} - \tau(u_k, u_i) \frac{\partial \langle u_j \rangle}{\partial x_k} - \tau(u_k, u_j) \frac{\partial \langle u_i \rangle}{\partial x_k} + \\ &+ \left[G_{ik} \tau(u_k, u_j) + G_{jk} \tau(u_k, u_i) + C_0 \epsilon \delta_{ij} \right] - \frac{\partial \tau(u_k, u_i, u_j)}{\partial x_k} \end{aligned} \tag{39}$$

$$\begin{aligned} \frac{\partial \tau(\phi_\alpha, \phi_\beta)}{\partial t} &+ \frac{\partial \langle u_k \rangle \tau(\phi_\alpha, \phi_\beta)}{\partial x_k} = \Gamma \frac{\partial^2 \tau(\phi_\alpha, \phi_\beta)}{\partial x_k \partial x_k} - \tau(u_k, \phi_\alpha) \frac{\partial \langle \phi_\beta \rangle}{\partial x_k} - \tau(u_k, \phi_\beta) \frac{\partial \langle \phi_\alpha \rangle}{\partial x_k} + \\ &+ \left[2\Gamma \frac{\partial \langle \phi_\alpha \rangle}{\partial x_k} \frac{\partial \langle \phi_\beta \rangle}{\partial x_k} - (C_{\phi_\alpha} + C_{\phi_\beta}) \omega \tau(\phi_\alpha, \phi_\beta) \right] - \frac{\partial \tau(u_k, \phi_\alpha, \phi_\beta)}{\partial x_k} \end{aligned} \tag{40}$$

$$\frac{\partial \tau(u_i,\phi_\alpha)}{\partial t} + \frac{\partial \langle u_k\rangle \tau(u_i,\phi_\alpha)}{\partial x_k} = \Gamma \frac{\partial^2 \tau(u_i,\phi_\alpha)}{\partial x_k \partial x_k} - \tau(u_k,u_i)\frac{\partial \langle \phi_\alpha\rangle}{\partial x_k} - \tau(u_k,\phi_\alpha)\frac{\partial \langle u_i\rangle}{\partial x_k} + \\ + \left[G_{ik}\tau(u_k,\phi_\alpha) - C_{\phi_\alpha}\omega\tau(u_i,\phi_\alpha)\right] - \frac{\partial \tau(u_k,u_i,\phi_\alpha)}{\partial x_k} \tag{41}$$

Above set of equations will be solved using a finite difference scheme and the solution will be assessed for consistency with a solution from a Lagrangian Monte Carlo solver.

D Rotta's Closure and Model Constants

The GLM and LMSE have provided a stochastic closure for the LES system. However, we have not mentioned a proper form of G_{ij} tensor, nor the values of the closure coefficients. Pope[1,19] has derived an appropriate form of G_{ij} and suggested some guidelines for values of the closure coefficients.

$$G_{ij} = -\omega\left(\frac{1}{2} + \frac{3}{4}C_0\right)\delta_{ij} \tag{42}$$

where $\omega = \frac{\epsilon}{k}$, $\epsilon = C_\epsilon \frac{k^{3/2}}{\Delta_L}$, $k = \frac{1}{2}\tau\left(u_k,u_k\right)$, and Δ_L is the LES filter size.
The resulting closure for SGS velocity is equivalent to that of Rotta,[19]

$$-\left[\tau\left(u_i,\tfrac{\partial p}{\partial x_j}\right) + \tau\left(u_j,\tfrac{\partial p}{\partial x_i}\right) + 2\nu\tau\left(\tfrac{\partial u_i}{\partial x_k},\tfrac{\partial u_j}{\partial x_k}\right)\right] = \\ = \left[G_{ik}\tau(u_k,u_j) + G_{jk}\tau(u_k,u_i) + C_0\epsilon\delta_{ij}\right] = \\ = -\omega\left(1+\tfrac{3}{2}C_0\right)\left[\tau(u_i,u_j) - \tfrac{2}{3}k\delta_{ij}\right] - \tfrac{2}{3}\epsilon\delta_{ij} \tag{43}$$

for the SGS scalar we have,

$$-\left[2\Gamma^\alpha\tau\left(\tfrac{\partial \phi_\alpha}{\partial x_k},\tfrac{\partial \phi_\beta}{\partial x_k}\right)\right] = -\left[(C_{\phi_\alpha} + C_{\phi_\beta})\omega\tau(\phi_\alpha,\phi_\beta) - 2\Gamma\tfrac{\partial\langle\phi_\alpha\rangle}{\partial x_k}\tfrac{\partial\langle\phi_\beta\rangle}{\partial x_k}\right] \tag{44}$$

and for SGS velocity-scalar we have,

$$-\left[(\nu+\Gamma^\alpha)\tau\left(\tfrac{\partial u_i}{\partial x_k},\tfrac{\partial \phi_\alpha}{\partial x_k}\right) + \tau\left(\phi_\alpha,\tfrac{\partial p}{\partial x_i}\right) + \left(\tfrac{\nu-\Gamma^\alpha}{2}\right)\left(\tau\left(u_i,\tfrac{\partial^2\phi_\alpha}{\partial x_k\partial x_k}\right) - \tau\left(\phi_\alpha,\tfrac{\partial^2 u_i}{\partial x_k\partial x_k}\right)\right)\right] = \\ = \left[G_{ik}\tau(u_k,\phi_\alpha) - C_{\phi_\alpha}\omega\tau(u_i,\phi_\alpha)\right] = -\omega\left(\tfrac{1}{2} + \tfrac{3}{2}C_0 + C_\phi\right)\tau\left(u_i,\phi_\alpha\right) \tag{45}$$

The closure constants as proposed by Pope[19] are

$$C_0 = 2.1 \qquad C_\epsilon = 1.0 \qquad C_\phi = 1.0 \tag{46}$$

E Numerical Procedure

The solution of the VSFDF equation (Eqn. 18) provides all of the statistical information about velocity-scalar field. The most convenient way of solving this equation is by a Lagrangian Monte Carlo procedure. In the Lagrangian description, the FDF is represented by an ensemble of statistically identical Monte Carlo particles. These particles, in general, do not represent actual fluid particles, but rather serve as carriers of information about flow statistics. In a limited range of time scales, however, Monte Carlo particles do provide a direct model of fluid particle behavior.[1]

The information carried by the particles is updated through a temporal integration of the SDE's Eq.(36a-36c). The simplest way of performing this stochastic simulation is via the Euler approximation[10,21,22]

$$X_i^{n+1} = X_i^n + \left(D_i^X\right)^n \Delta t + \left(B^X\right)^n (\Delta t)^{1/2} \left(\zeta_i^X\right)^n \tag{47a}$$

$$U_i^{n+1} = U_i^n + \left(D_i^U\right)^n \Delta t + \left(B^U\right)^n (\Delta t)^{1/2} \left(\zeta_i^U\right)^n + \left(F_{ij}^{UX}\right)^n (\Delta t)^{1/2} \left(\zeta_j^X\right)^n \tag{47b}$$

$$\psi_\alpha^{n+1} = \psi_\alpha^n + \left(D_\alpha^\phi\right)^n \Delta t + \left(B^\phi\right)^n (\Delta t)^{1/2} \left(\zeta_\alpha^\phi\right)^n + \left(F_{\alpha j}^{\phi X}\right)^n (\Delta t)^{1/2} \left(\zeta_j^X\right)^n \tag{47c}$$

where D, B, and F are all functions of the state variables at a time step n, and ζ's are independent standardized Gaussian random variables. Higher order numerical schemes, such as Runge-Kutta, are also available for stochastic differential equations,[10,21,22] but caution is advised when selecting one for a Monte-Carlo simulation of LES. If the diffusion terms, B and F, strongly depend on the state variables, the numerical scheme may alter the solution in a way inconsistent with the true nature of undiscretized set of SDEs.[16] Numerical scheme must be consistent with Itô and Stratonovich calculus, and Euler approximation satisfies this condition.

The statistical information transported by Monte Carlo particles and evolving according to the SDE's is evaluated by considering a "finite area", for 2D, and "finite volume", for 3D, centered at a LES grid point. The area/volume is characterized by a length Δ_E. Statistics are computed based on an "ensemble" of approximately N_E particles residing inside it at a given time. This type of "ensemble" approach is necessary as the probability of finding a single, or multiple for that matter, Monte Carlo particle(s) at a given LES grid point is zero.[18] Fig.1 illustrates this concept. An alternative to the ensemble averaging is a method proposed by Pope.[1] This method uses least-squares continuous cubic splines with continuous first and second derivatives. It must be used when the number of Monte Carlo particles is too small to allow for smooth resolution of the first and second derivatives from the stochastic solver. Because the statistics are computed based on ensemble of Monte Carlo particles statistical errors are introduced into the simulation. Ideally, for reliable Eulerian statistics and minimum numerical dispersion, it is desired to minimize the size of ensemble domain while maximizing the number of Monte Carlo particles in it. Consequently the statistics would tend to their exact LES value.

$$\langle u_i \rangle_E \equiv \frac{1}{N_E} \sum_{n \in \Delta_E} U_i^{(n)} \xrightarrow[\substack{N_E \to \infty \\ \Delta_E \to 0}]{} \langle u_i \rangle \tag{48}$$

$$\tau\left(u_i, u_j\right)_E \equiv \frac{1}{N_E} \sum_{n \in \Delta_E} \left(U_i^{(n)} - \langle U_i \rangle_E\right)\left(U_i^{(n)} - \langle U_i \rangle_E\right) \xrightarrow[\substack{N_E \to \infty \\ \Delta_E \to 0}]{} \tau\left(u_i, u_j\right) \tag{49}$$

where subscript E indicates a statistical value obtained from the ensemble centered around the LES grid point. This procedure is termed "point estimator", because it ignores the ensemble average variations of the statistical value within the ensemble domain and uses the ensemble averaged value at the LES grid point only.

Solution of the Lagrangian stochastic system, as it is presented in Eq.(36a-36c), is not possible because SDE's contain filtered terms that can not be computed by the stochastic solver. To remedy this problem a finite difference LES code is developed and coupled with the stochastic solver. This combination yields a finite difference-stochastic hybrid LES solver.

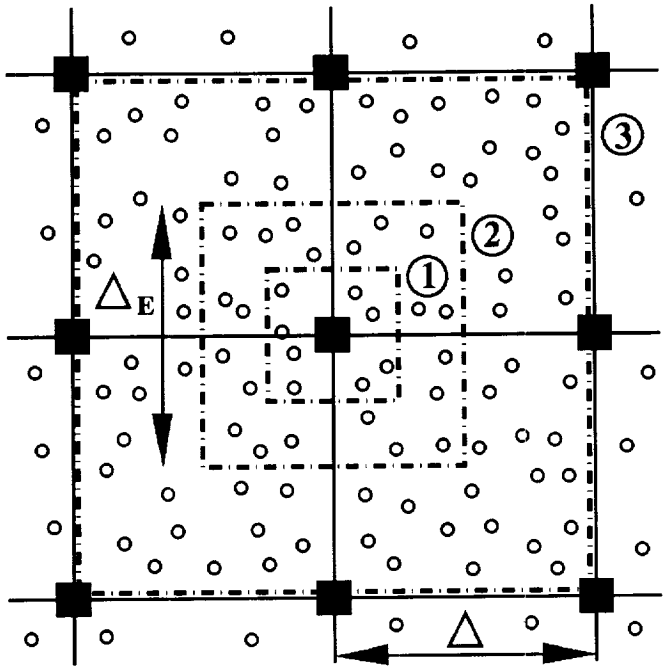

Figure 1: Concept of ensemble averaging. Shown are three different ensemble domains: $1(\Delta_E = 0.5\Delta, N_E \approx 10)$, $2(\Delta_E = \Delta, N_E \approx 40)$, $3(\Delta_E = 2.0\Delta, N_E \approx 160)$. Black squares indicate LES grid points, while small circles are Monte Carlo particles.

The filtered pressure field, velocity-scalar field and turbulent kinetic energy field appearing in Eqn. 36a-36c, are needed by the stochastic solver to advance the system in time. These quantities are computed via the finite-difference LES solver by a method based on the "compact parameter" finite difference scheme of Carpenter. This is a variant of the Mac Cormack scheme in which fourth-order compact differences are used to approximate the spatial derivatives, and second-order symmetric predictor-corrector sequence is employed for time discretization. All of the finite difference operations are conducted on a fixed and equally spaced grid points. The transfer of information from the LES grid points to the Lagrangian particles is accomplished via interpolation. A second-order interpolation scheme is used. The transfer of information from the Lagrangian particles to the finite difference solver is accomplished via ensemble averaging described earlier in this section. This procedure is shown schematically in Fig.2.

As can be seen in Table 2 a certain "redundancy" results from using a finite difference-stochastic hybrid LES solver. This is actually very useful as it allows for constant monitoring of the accuracy of the simulated results. This "redundancy" will also be used to show that the Lagrangian Monte Carlo solver is consistent with its finite difference counterpart.

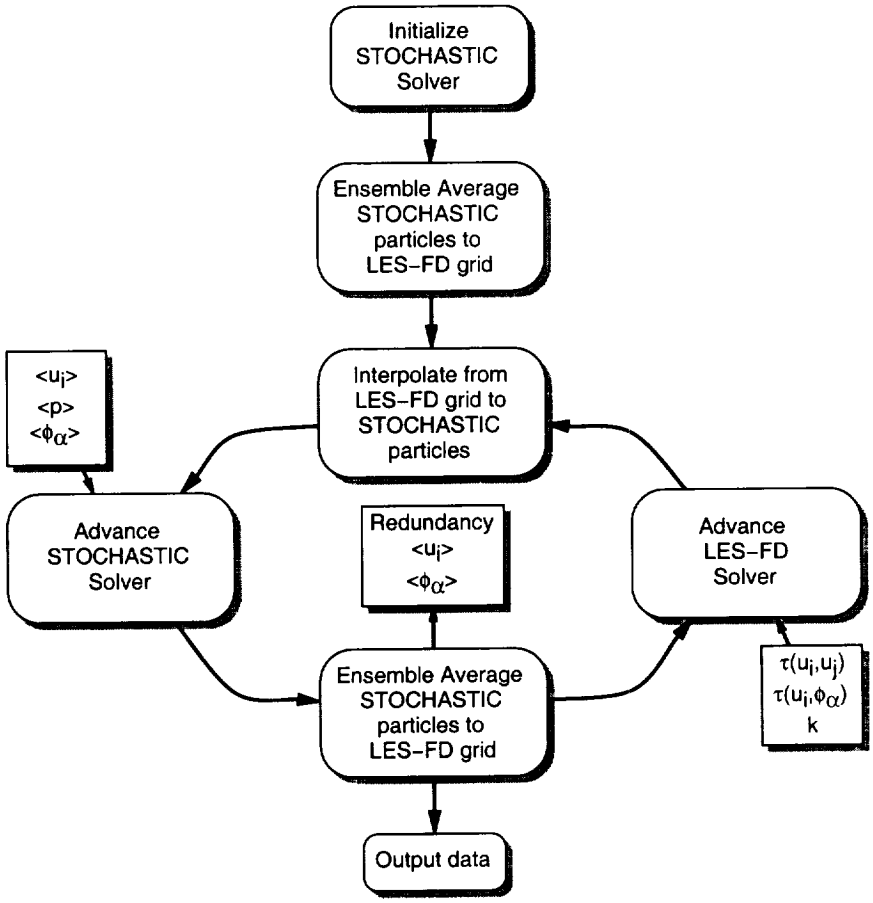

Figure 2: Numerical Procedure Flow Chart for VSFDF Hybrid Solver

	Finite Difference variables	Particle solver variables	Particle statistics used by the F.D solver	F.D. variables used by particle solver	Redundant quantities
VSFDF	$\langle p \rangle$, $\langle u_i \rangle$ $\langle \phi_\alpha \rangle$	X_i U_i ψ_α	$\tau(u_i, u_j)$ $\tau(u_i, \phi_\alpha)$	$\langle u_i \rangle$, $\frac{\partial \langle p \rangle}{\partial x_i}$ $\frac{\partial \langle u_i \rangle}{\partial x_k}$, $\frac{\partial^2 \langle u_i \rangle}{\partial x_k \partial x_k}$ $\langle \phi_\alpha \rangle$	$\langle u_i \rangle$ $\langle \phi_\alpha \rangle$
VSFDF Consistency	$\langle p \rangle$, $\langle u_i \rangle$ $\langle \phi_\alpha \rangle$ $\tau(u_i, u_j)$ $\tau(u_i, \phi_\alpha)$ $\tau(\phi_\alpha, \phi_\beta)$	X_i U_i ψ_α	$\tau(u_i, u_j), \tau(u_i, \phi_\alpha)$ $\tau(\phi_\alpha, \phi_\beta)$ $\tau(u_i, u_j, u_k)$ $\tau(u_i, u_j, \phi_\alpha)$ $\tau(u_i, \phi_\alpha, \phi_\beta)$	$\langle u_i \rangle$, $\frac{\partial \langle p \rangle}{\partial x_i}$ $\frac{\partial \langle u_i \rangle}{\partial x_k}$, $\frac{\partial^2 \langle u_i \rangle}{\partial x_k \partial x_k}$ $\langle \phi_\alpha \rangle$	$\langle u_i \rangle$,$\langle \phi_\alpha \rangle$ $\tau(u_i, u_j)$ $\tau(u_i, \phi_\alpha)$ $\tau(\phi_\alpha, \phi_\beta)$

Table 1: VSFDF Solution Procedure. VSFDF1 refers to actual production model, while VSFDF1 Consistency refers to the code used to demonstrate consistency with the finite difference LES solver.

3 Results

A Flow Simulated

Consistency simulations of the Lagrangian Monte Carlo solver were conducted for a 2D temporally developing mixing layer. A 2D simulation is sufficient to establish consistency and is chosen to preserve

computational resources.
The temporal mixing layer consists of two parallel streams traveling in opposite directions with the same speeds. Hyperbolic tangent functions are used to initialize both stream-wise velocity and scalar distributions profiles, while a form of exponential function is used to initialize the cross-stream velocity profile. The simulations are conducted for $0 \leq x \leq L$, and $-L/2 \leq y \leq L/2$, where x,y denote stream-wise and cross-stream directions, and the length L is specified such that $L = 2\pi N_r/\alpha_{us}$, where N_r is the number of successive vortex pairings and α_{us} is the wavelength of the most unstable linear mode corresponding to the mean stream-wise velocity profile at initial time.[4] The formation of large scale structures is facilitated by introducing small harmonic, phase-shifted, disturbances containing subharmonics of the most unstable mode into the stream-wise and cross-stream velocity profiles. This results in formation of two successive vortex pairings. For more detailed description of this "forcing" mechanism reader is referred to Ref. 4
The flow variables are normalized by the half initial vorticity thickness, $L_r = \frac{\delta_v|_0}{2}$, and half the velocity difference across the layer, $U_r = \frac{\Delta U}{2}$ ($\delta_v|_0 = \frac{\Delta U}{|\partial\langle u_1\rangle/\partial y|_{max}}$, and $\overline{\langle u_1\rangle}$ is the Reynolds averaged value of filtered stream-wise velocity)

B Numerical Specifications

All of the simulations are performed on the equally spaced finite difference grid, such that $\Delta x = \Delta y = \Delta$. The LES resolution used was 32x41 grid points. The choice for resolution was guided by the proper ratio of the resolved to total Reynolds stresses.[23] In general for LES, this ratio should be approximately 80%. The Reynolds number used for the simulations was, $Re = \frac{U_r L_r}{\nu} = 50$. A constant LES top-hat filter of size $\Delta_L = 2\Delta$ centered around a grid point is used such that,

$$G(x' - x) = \prod_{i=1}^{N_D} \tilde{G}(x_i' - x_i) \tag{50}$$

$$\tilde{G}(x_i' - x_i) = \begin{cases} \frac{1}{\Delta_L} & , |x_i' - x_i| \leq \frac{\Delta_L}{2} \\ 0 & , |x_i' - x_i| > \frac{\Delta_L}{2} \end{cases} \tag{51}$$

where N_D is the number of dimensions.

The Monte Carlo particles are initially distributed according to the uniform PDF scaled to fit the domain. All of these particles have equal "weight" in the solution. It is required that the particle distribution be approximately uniform to minimize the ensemble average bias and interpolating errors. The periodic boundary condition in stream-wise direction ensures that the particles leaving the domain are introduced at the opposite boundary with the same compositional values. The cross-stream direction has a free-slip boundary condition such that leaving particles are "mirror-reflected" back into the domain. The particle density is determined by counting the Monte Carlo particles residing inside the ensemble domain of size $\Delta_E \times \Delta_E (\times \Delta_E)$. The effects of average particle density (N_E) and ensemble domain size (Δ_E) on the LES solution will be assessed to ensure consistency and statistical accuracy of the VSFDF simulations.

The results will be analyzed both instantaneously, by visually comparing the finite difference and stochastic LES results at a specific time, and statistically, by Reynolds averaging the results at a specific time. In the case of a temporally developing shear layer the Reynolds average statistics are constructed by spatially averaging over the homogeneous direction and are denoted by an overbar.

C Consistency and Convergence Assessments

To show that the VSFDF formulation in consistent and that the Monte-Carlo simulation converges we will compare results obtained via VSFDF and LES-FD. This approach is valid because the accuracy and reliability of the finite-difference LES procedures is well established and consequently will provide a good means of assessing the quality of the Monte-Carlo simulation of the VSFDF. The comparison will consist of statistical and instantaneous values of all of the variables computed by the hybrid solver. No attempt is made to determine the appropriate values of the model coefficients, rather the values suggested in the literature are adopted (See section D).

Fig. 3 shows the distribution of the Monte-Carlo particles within the computational domain. Assuring that this distribution is uniform allows us to discount any differences between LES-FD and VSFDF as resulting form interpolation bias. The influence of the average particle density, N_E, on the first and second moments is shown in Figs. 4-12. It can be observed that N_E does not significantly influence the first nor the second moments. The differences displayed on these figures seem visually comparable to those due to changing random number generator seed. The later are shown explicitly for different values of Δ_E in Figs. 13-22. It is important to keep this influence in mind when dealing with Monte-Carlo type simulations as it is possible, but highly improbable, that two VSFDF simulations will yield identical results. Figs. 23-31 show the influence of the ensemble domain size (See Fig. 1) on the first and second moments. The first moments as obtained by VSFDF simulation agree very well with their LES-FD counterparts even for large values of Δ_E. The small differences in these moments can be contributed to the difference in the seed of the random number generator for different cases. However, the second moments exhibit significant differences. These differences exhibit a converging pattern of behavior as the ensemble domain is decreased. This was predicted and shown theoretically in Sec. E. As ensemble domain size decreases, the values of the SGS components predicted by the VSFDF simulation converge to their LES-FD values. Figs. 16-19, and 25-28 illustrate this behavior quite clearly. The scatter plots of first and second moments are presented in Figs. 32-34. The correlation and linear regression coefficients (denoted by ρ and r respectively on the figures) offer another set of indicators for consistency for VSFDF simulations. The ρ^2 indicates the percentage of variance of the VSFDF data accounted for by a linear fit. Figs. 35-44 provide a simple visual demonstration of the consistency of the VSFDF simulations and Figs. 45 and 46 show the consistency of the time evolution of the simulation.

4 Summary and Concluding Remarks

The Filtered Density Function (FDF) methodology has proven very effective in LES of turbulent reactive flows.[24,25,27,28,30] In all of the previous investigations, however, the FDF of either only the scalar[24](SFDF), or velocity[31](VFDF) were considered. The objective of present work is to develop and validate the FDF methodology for LES of the joint velocity-scalar field (VSFDF). For this purpose, a methodology for velocity FDF developed by Gicquel[31] is extended to include the scalar field resulting in a VSFDF method for LES. The exact transport equations governing the evolution of VSFDF are derived. It is shown that the effects of the SGS convection in these equations as well as the terms resulting from reaction source terms appear in the closed form. The remaining unclosed terms are modeled via VSFDF formulation with Generalized Langevin Model (GLM) for the Lagrangian velocity field evolution and Linear Mean Square Estimation (LMSE) Model for the Lagrangian scalar field evolution. The closure strategy is similar to that for PDF methods in Reynolds Averaged Navier-Stokes (RANS) simulations and consequently equivalent

to a second-order moment SGS closure.

The modeled VSFDF transport equations are solved numerically via a Lagrangian Monte Carlo scheme. The result of this simulation is then compared to a well established LES using a finite difference scheme (LES-FD). The consistency of the VSFDF method and the convergence of its Monte Carlo solutions are assessed. This assessment is done by comparing solutions of the first two filtered moments obtained via Monte Carlo procedure and LES-FD. The third order moment terms in the second filtered moment transport equations for LES-FD are closed by corresponding quantities obtained from VSFDF. The assessment itself contains the comparisons of Reynolds average quantities for varying ensemble domain size(Δ_E) and average particle density size(N_E). The theoretical predictions for these comparisons are validated. Additionally, instantaneous comparisons of data scatter, visual inspection of first and second moments, and time consistency of the simulations are examined. The consistency and convergence of the VSFDF simulation is demonstrated by good agreement of the first two moments as obtained with Monte Carlo simulations and LES-FD for all considered test cases.

Work is in progress on further evaluating the performance of VSFDF model by comparing the results obtained with a 3D homogeneous shear layer case with the DNS and experimental data. The effectiveness of the model as compared to some commonly used LES models such as Smagorinsky, or Dynamic Smagorinsky will also be evaluated as well its computational expense. Progress towards the development of VSFDF for LES of reaction flows will follow as the VSFDF's major advantages over its predecessors are the treatment of the convective transport and reactive terms in a closed form.

References

[1] Pope, S. B., "PDF methods for turbulent reactive flows," *Prog. Energy Combust. Sci.*, vol. 11, pp. 119–192, 1985.

[2] Haworth, D. C., Pope, S. B., "A Generalized Langevin Model for turbulent flows," *Phys. Fluids*, vol. 29, no. 2, pp. 387–405, 1986.

[3] Kosály, G., Givi, P., "Modeling of turbulent molecular mixing," *Combust. Flame*, vol. 70, pp. 101–118, 1987.

[4] Metcalfe, R. W., Orszag, S. A., Brachet, M. E., Menon, S., Riley, J. J., "Secondary instabilities of a temporally growing mixing layer," *J. Fluid Mech.*, vol. 184, pp. 207–243, 1987.

[5] Risken, H., *The Fokker-Planck Equation, Methods of Solution and Applications*, New York, NY: Springer-Verlag, 1989.

[6] Aldama, A. A., in Brebbia, C. A., Orszag, S. A., eds., "Filtering Techniques for Turbulent Flow Simulations," vol. 49 of *Lecture Notes in Engineering*, New York: Springer-Verlag, Inc., 1990.

[7] Pope, S. B., "Computations of turbulent combustion: Progress and challenges," in "Proceedings of 23rd Symp. (Int.) on Combustion," pp. 591–612, Pittsburgh, PA: The Combustion Institute, 1990.

[8] Valiño, L., Dopazo, C., "A binomial sampling model for scalar turbulent mixing," *Phys. Fluids*, vol. 2, no. 7, Jul. 1990.

[9] Papoulis, A., *Probability, Random Variables, and Stochastic Processes*, New York: McGraw-Hill, Inc., 3rd ed., 1991.

[10] Sobczyk, K., *Stochastic Differential Equations with Applications to Physics and Engineering*, vol. 40 of *Mathematics and its applications. East European Series*, Kluwer Academic Publishers, 1991.

[11] Germano, M., "Turbulence: The filtering approach," *J. Fluid Mech.*, vol. 238, pp. 325–336, 1992.

[12] Frankel, S. H., Adumitroaie, V., Madnia, C. K., Givi, P., "Large Eddy Simulations of turbulent reacting flows by assumed PDF methods," in Ragab, S. A., Piomelli, U., eds., "Engineering Applications of Large Eddy Simulations," pp. 81–101, New York, NY: ASME, FED-Vol. 162, 1993.

[13] Galperin, B., Orszag, S. A., eds., *Large Eddy Simulations of Complex Engineering and Geophysical Flows*, Cambridge, England: Cambridge University Press, 1993.

[14] Gao, F., O'Brien, E. E., "A large-eddy simulation scheme for turbulent reacting flows," *Phys. Fluids A*, vol. 5, no. 6, pp. 1282–1284, 1993.

[15] Madnia, C. K., Givi, P., "Direct numerical simulation and large eddy simulation of reacting homogeneous turbulence," in Galperin and Orszag,[13] chap. 15, pp. 315–346.

[16] Soong, T., Grigoriu, M., *Random Vibration of Mechanical and Structural Systems*, Prentice-Hall International, Inc., 1993.

[17] Cook, A. W., Riley, J. J., "A subgrid model for equilibrium chemistry in turbulent flows," *Phys. Fluids*, vol. 6, no. 8, pp. 2868–2870, 1994.

[18] Pope, S. B., "Lagrangian PDF methods for turbulent flows," *Ann. Rev. Fluid Mech.*, vol. 26, pp. 23–63, 1994.

[19] Pope, S. B., "On the relation between stochastic Lagrangian models of turbulence and second-moment closures," *Phys. Fluids*, vol. 6, no. 2, pp. 973–985, 1994.

[20] Vreman, B., Geurts, B., Kuerten, H., "Realizability conditions for the turbulent stress tensor in Large Eddy Simulation," *J. Fluid Mech.*, vol. 278, pp. 351–362, 1994.

[21] Kloeden, P. E., Platen, E., *Numerical Solution of Stochastic Differential Equations*, vol. 23 of *Applications of Mathematics, Stochastic Modeling and Applied Probability*, New York, NY: Springer-Verlag, 1995.

[22] Kloeden, P. E., Platen, E., Schurz, H., *Numerical Solution of Stochastic Differential Equations through Computer Experiments*, New York, NY: Springer-Verlag, corrected second printing ed., 1997.

[23] Vreman, B., Geurts, B., Kuerten, H., "Large Eddy Simulation of the turbulent mixing layer," *J. Fluid Mech.*, vol. 339, pp. 357–390, 1997.

[24] Colucci, P., Jaberi, F., Givi, P., Pope, S., "Filtered Density Function for Large Eddy Simulation of turbulent reacting flows," *Phys. Fluids*, vol. 20, no. 2, pp. 499–515, Feb. 1998.

[25] Colucci, P. J., *Large Eddy Simulation of Turbulent Reactive Flows: Stochastic Representation of the Subgrid Scale Scalar Fluctuations*, Ph.D. Dissertation, Dept. of Mechanical and Aerospace Engineering, State University of New York at Buffalo, Buffalo, NY, 1998, appendix C.

[26] Réveillon, J., Vervisch, L., "Subgrid-scale turbulent micromixing: Dynamic approach," *AIAA J.*, vol. 36, no. 3, pp. 336–341, 1998.

[27] Garrick, S. C., Jaberi, F. A., Givi, P., "Large Eddy Simulation of scalar transport in a turbulent jet flow," in Knight, D., Sakell, L., eds., "Recent Advances in DNS and LES," vol. 54 of *Fluid Mechanics and its Applications*, pp. 155–166, The Netherlands: Kluwer Academic Publishers, 1999.

[28] Jaberi, F. A., Colucci, P. J., James, S., Givi, P., Pope, S. B., "Filtered Mass Density Function for Large Eddy Simulation of turbulent reacting flows," *J. Fluid Mech.*, vol. 401, pp. 85–121, 1999.

[29] James, S., Jaberi, F. A., "Large scale simulations of two-dimensional nonpremixed methane jet flames," *Combust. Flame*, vol. 123, pp. 465–487, 2000.

[30] Pope, S. B., *Turbulent Flows*, Cambridge, UK: Cambridge University Press, 2000.

[31] Gicquel, L. Y., *Velocity Filtered Density Function for Large Eddy Simulation of Turbulent Flows. A stochastic methodology for the closure problem of LES*, Ph.D. Dissertation, Dept. of Mechanical and Aerospace Engineering, State University of New York at Buffalo, Buffalo, NY, 2001.

[32] Sagaut, P., *Large Eddy Simulation for Incompressible Flows: An Introduction*, New York: Springer-Verlag, Inc., Apr. 2001.

Figures

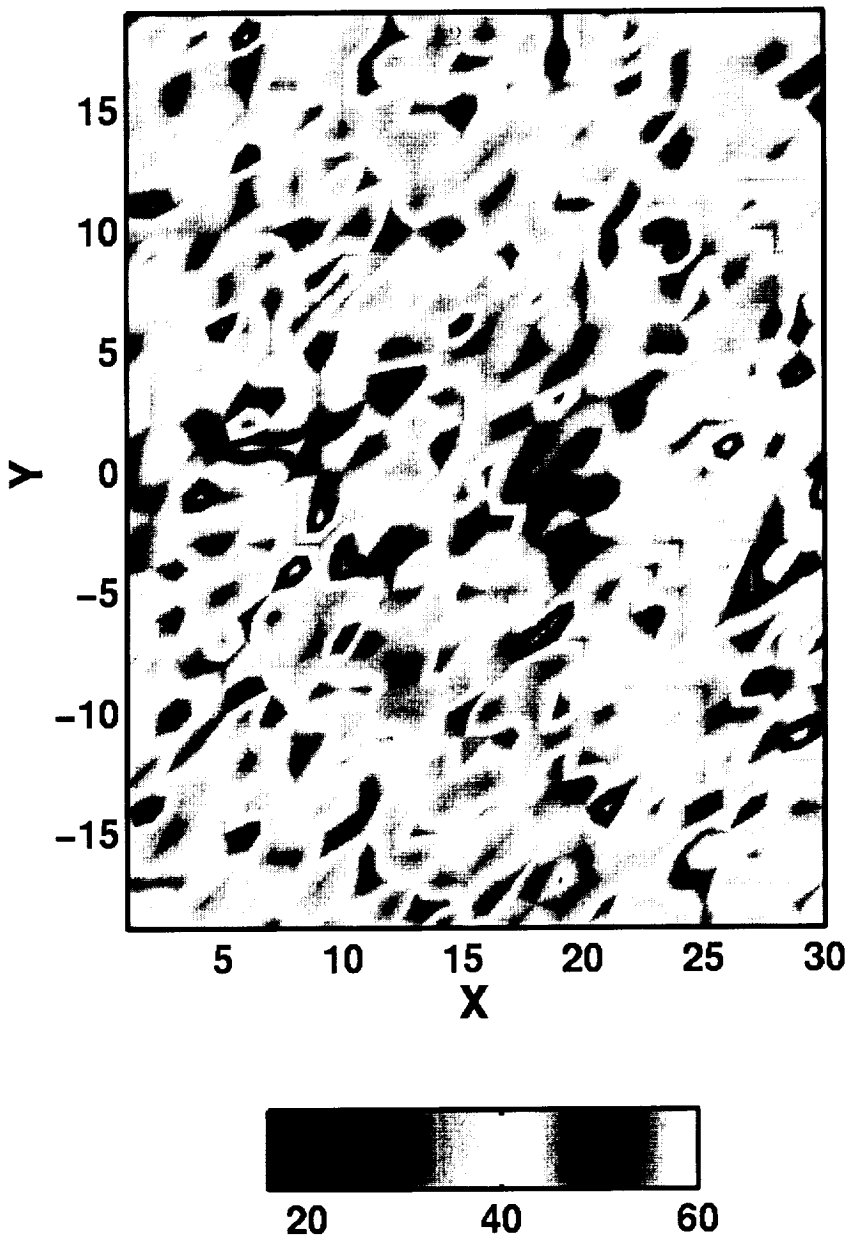

Figure 3: Particle density distribution per LES grid points for a typical VSFDF simulation for $\delta_E = 0.5\Delta$ and $N_E = 40$ at t=34.3

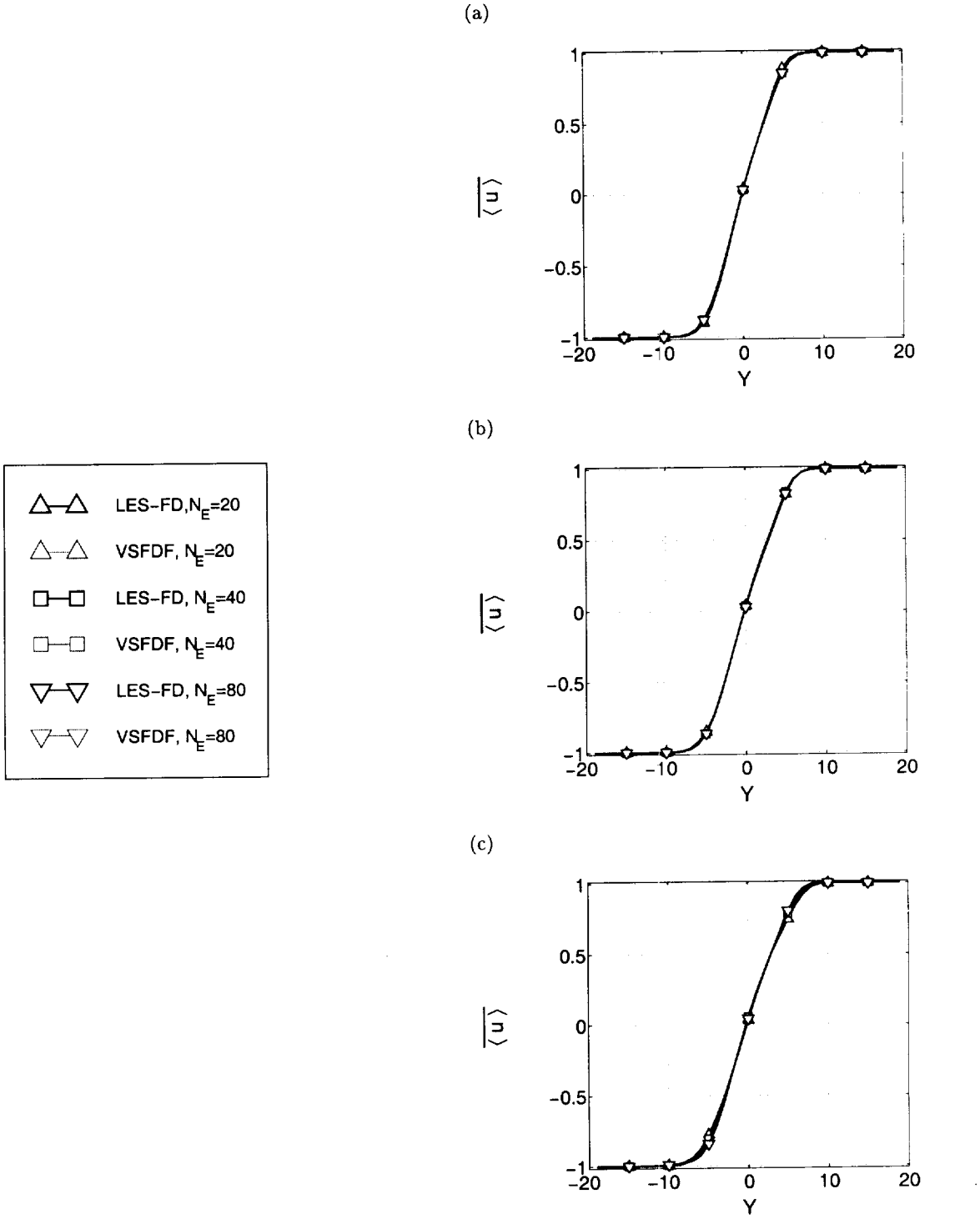

Figure 4: Cross-stream variation of the Reynolds averaged values of the $\langle u \rangle$ component of the velocity field: (a) $\Delta_E = 0.5\Delta$, (b) $\Delta_E = 1.0$, (c) $\Delta_E = 2.0$

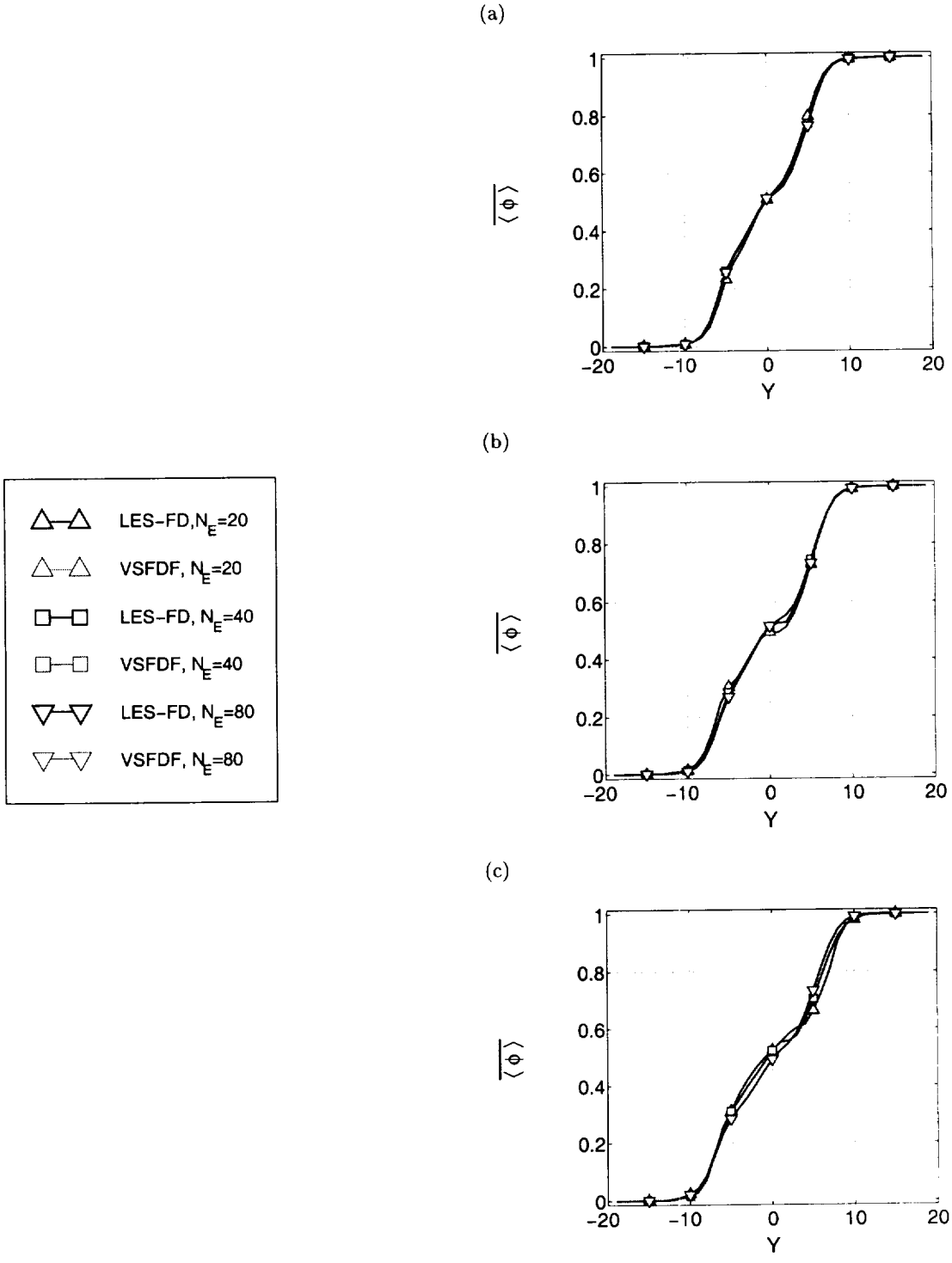

Figure 5: Cross-stream variation of the Reynolds averaged values of the $\langle\phi\rangle$, scalar field: (a) $\Delta_E = 0.5\Delta$, (b) $\Delta_E = 1.0$, (c) $\Delta_E = 2.0$

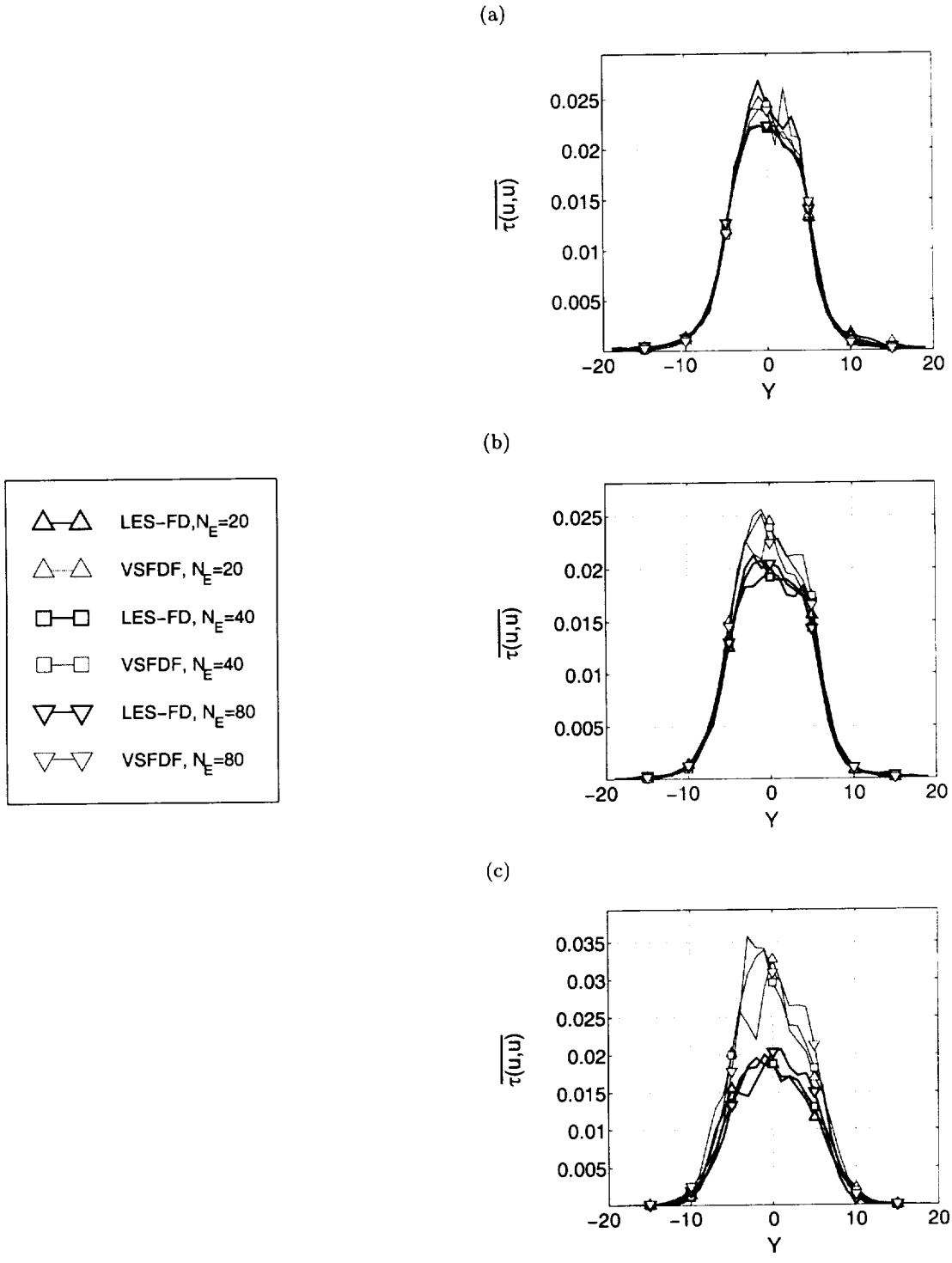

Figure 6: Cross-stream variation of the Reynolds averaged values of the $\tau(u,u)$ component of the SGS stress tensor: (a) $\Delta_E = 0.5\Delta$, (b) $\Delta_E = 1.0$, (c) $\Delta_E = 2.0$

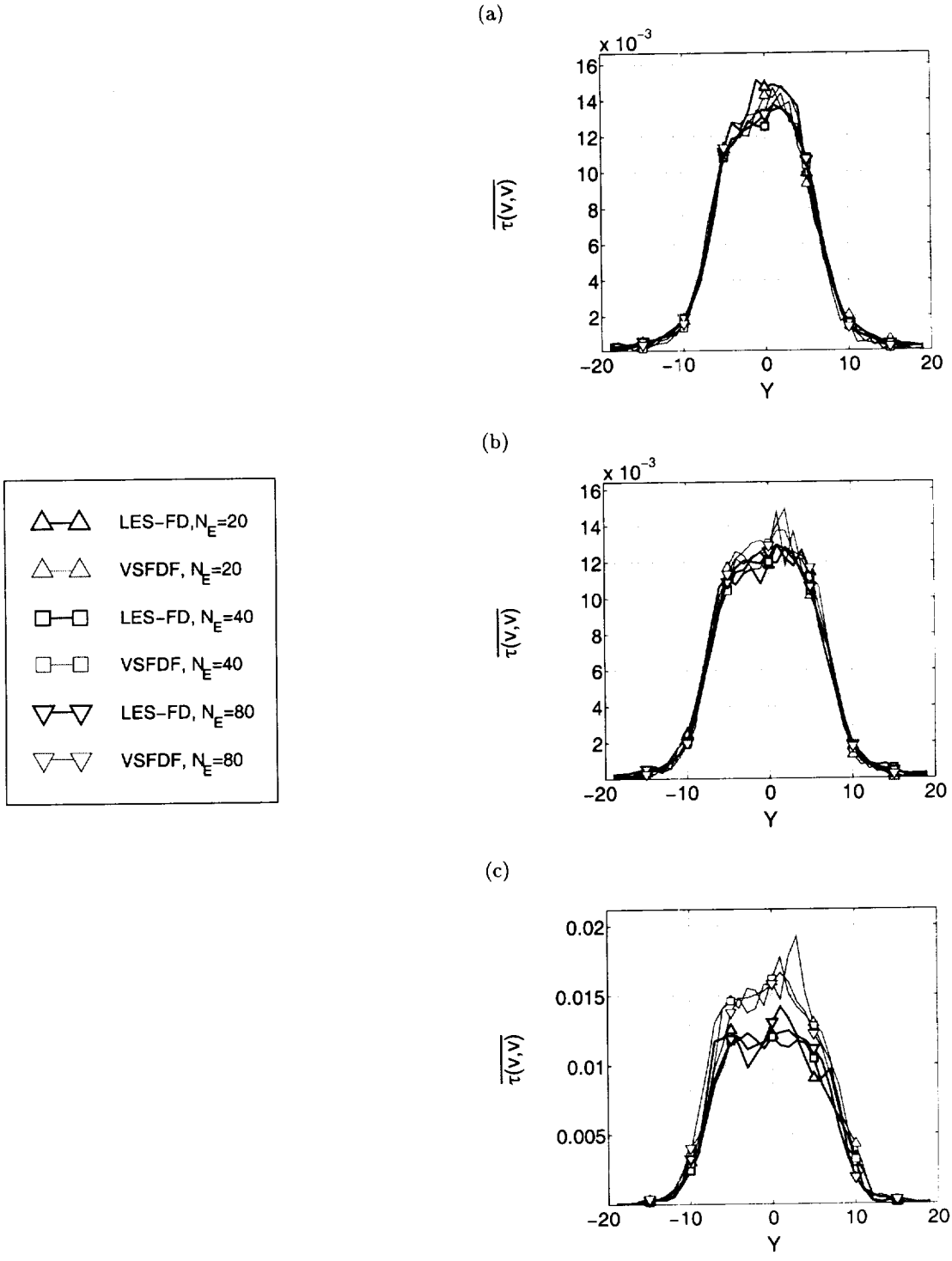

Figure 7: Cross-stream variation of the Reynolds averaged values of the $\tau(v,v)$ component of the SGS stress tensor: (a) $\Delta_E = 0.5\Delta$, (b) $\Delta_E = 1.0$, (c) $\Delta_E = 2.0$

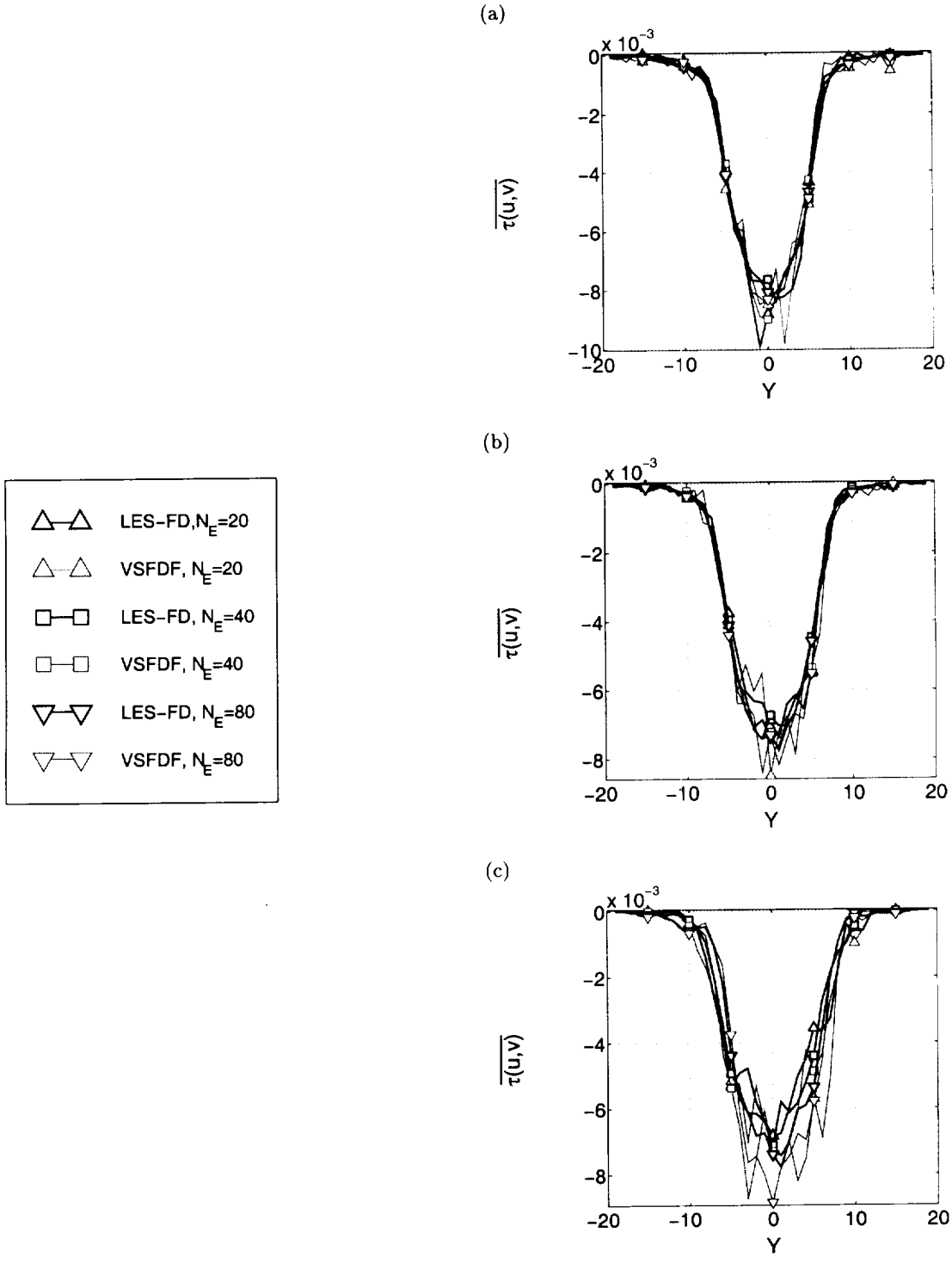

Figure 8: Cross-stream variation of the Reynolds averaged values of the $\tau(u,v)$, SGS stress tensor: (a) $\Delta_E = 0.5\Delta$, (b) $\Delta_E = 1.0$, (c) $\Delta_E = 2.0$

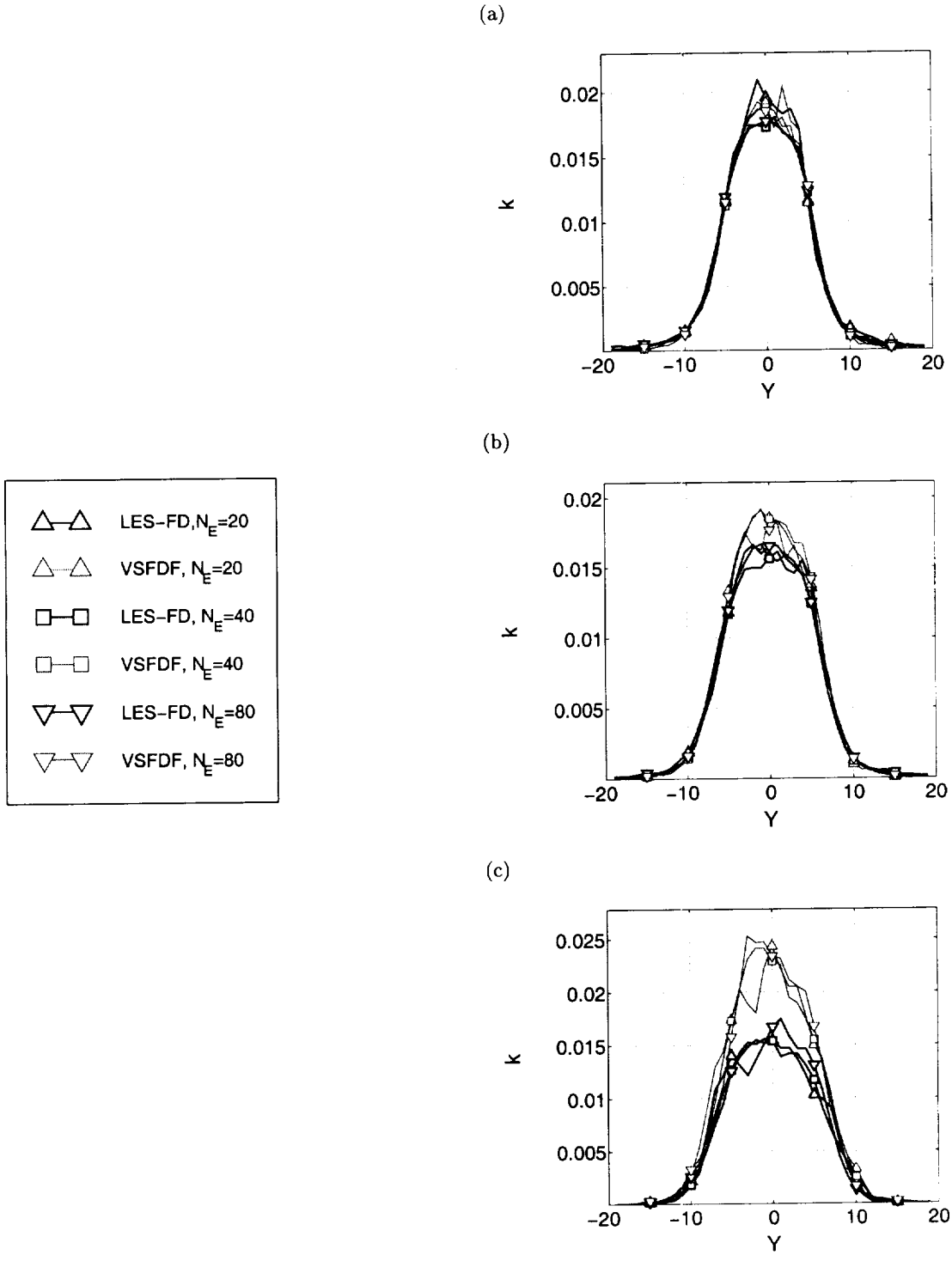

Figure 9: Cross-stream variation of the Reynolds averaged values of the turbulent kinetic energy, k: (a) $\Delta_E = 0.5\Delta$, (b) $\Delta_E = 1.0$, (c) $\Delta_E = 2.0$

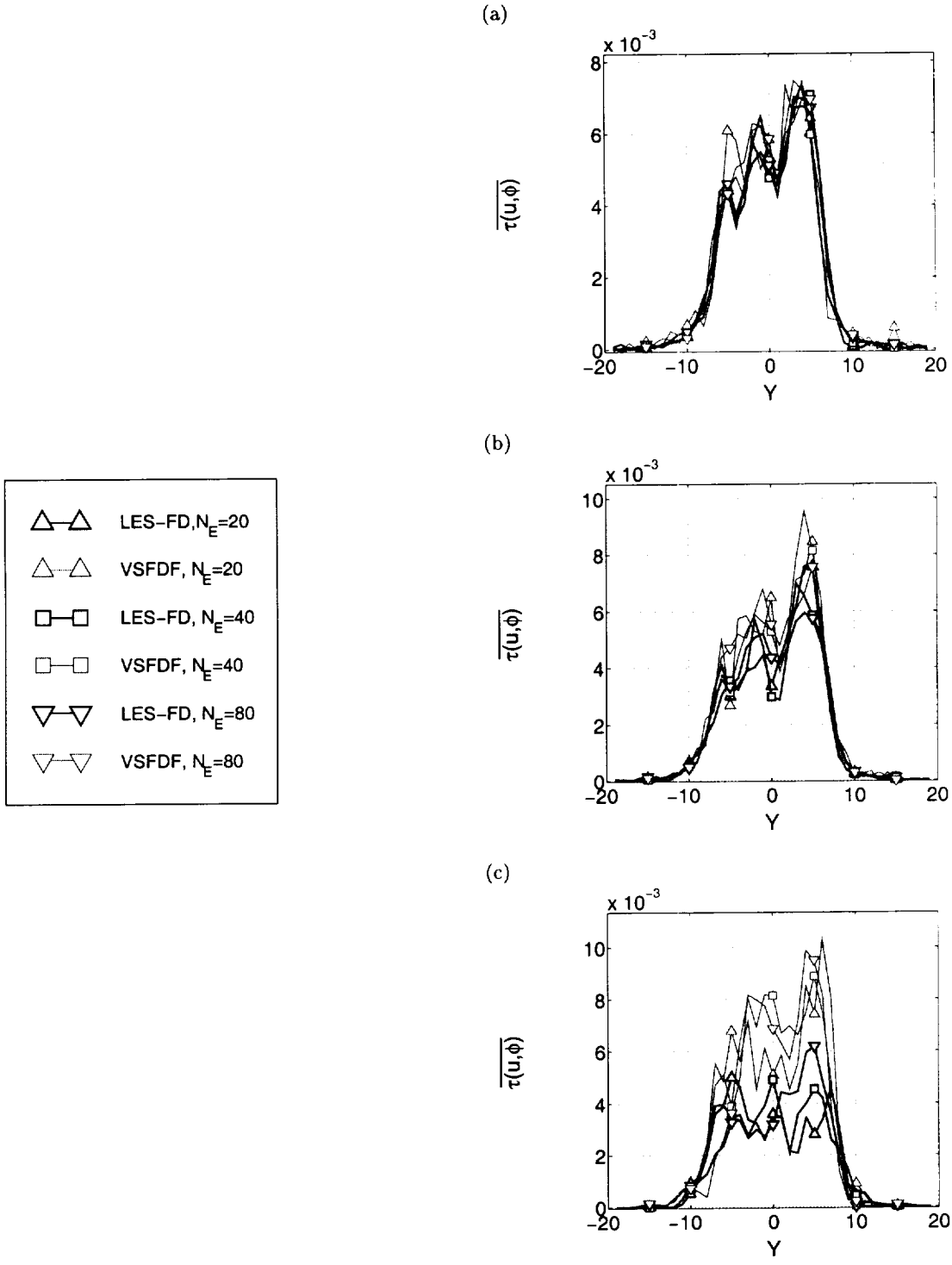

Figure 10: Cross-stream variation of the Reynolds averaged values of the $\tau(u,\phi)$, SGS tensor: (a) $\Delta_E = 0.5\Delta$, (b) $\Delta_E = 1.0$, (c) $\Delta_E = 2.0$

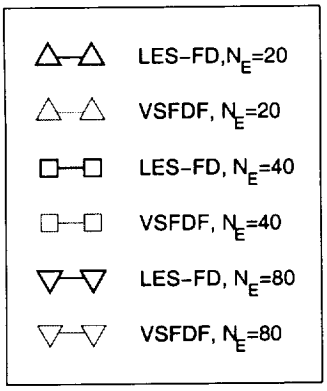

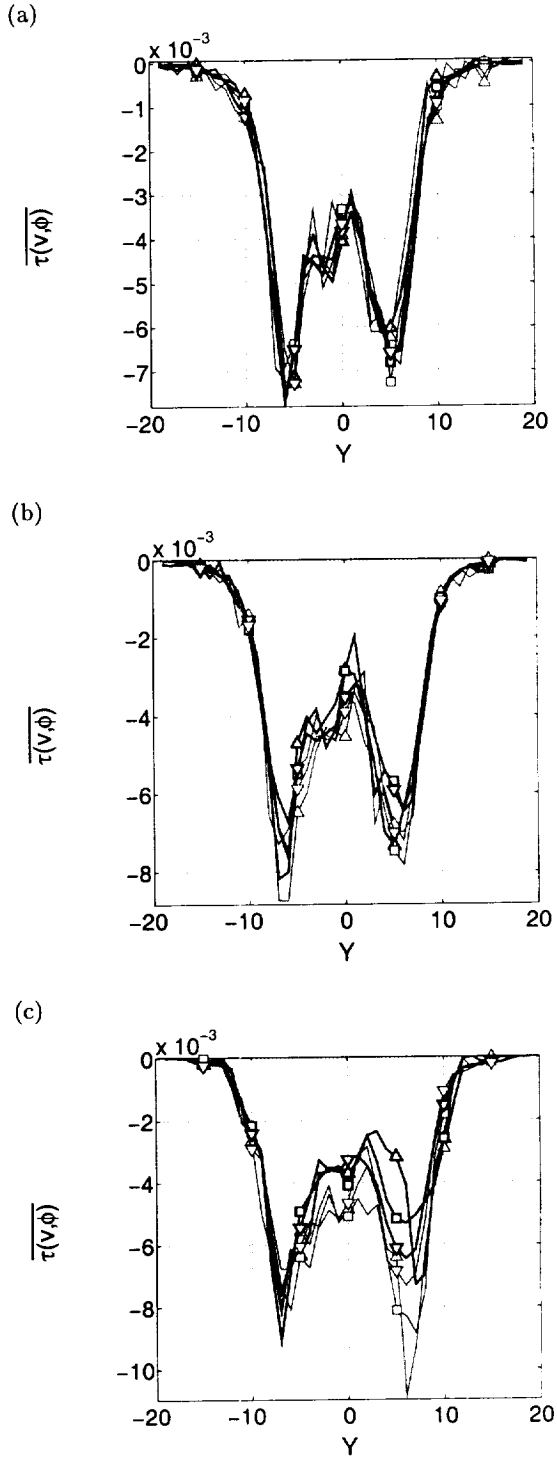

Figure 11: Cross-stream variation of the Reynolds averaged values of the $\tau(v,\phi)$, SGS tensor: (a) $\Delta_E = 0.5\Delta$, (b) $\Delta_E = 1.0$, (c) $\Delta_E = 2.0$

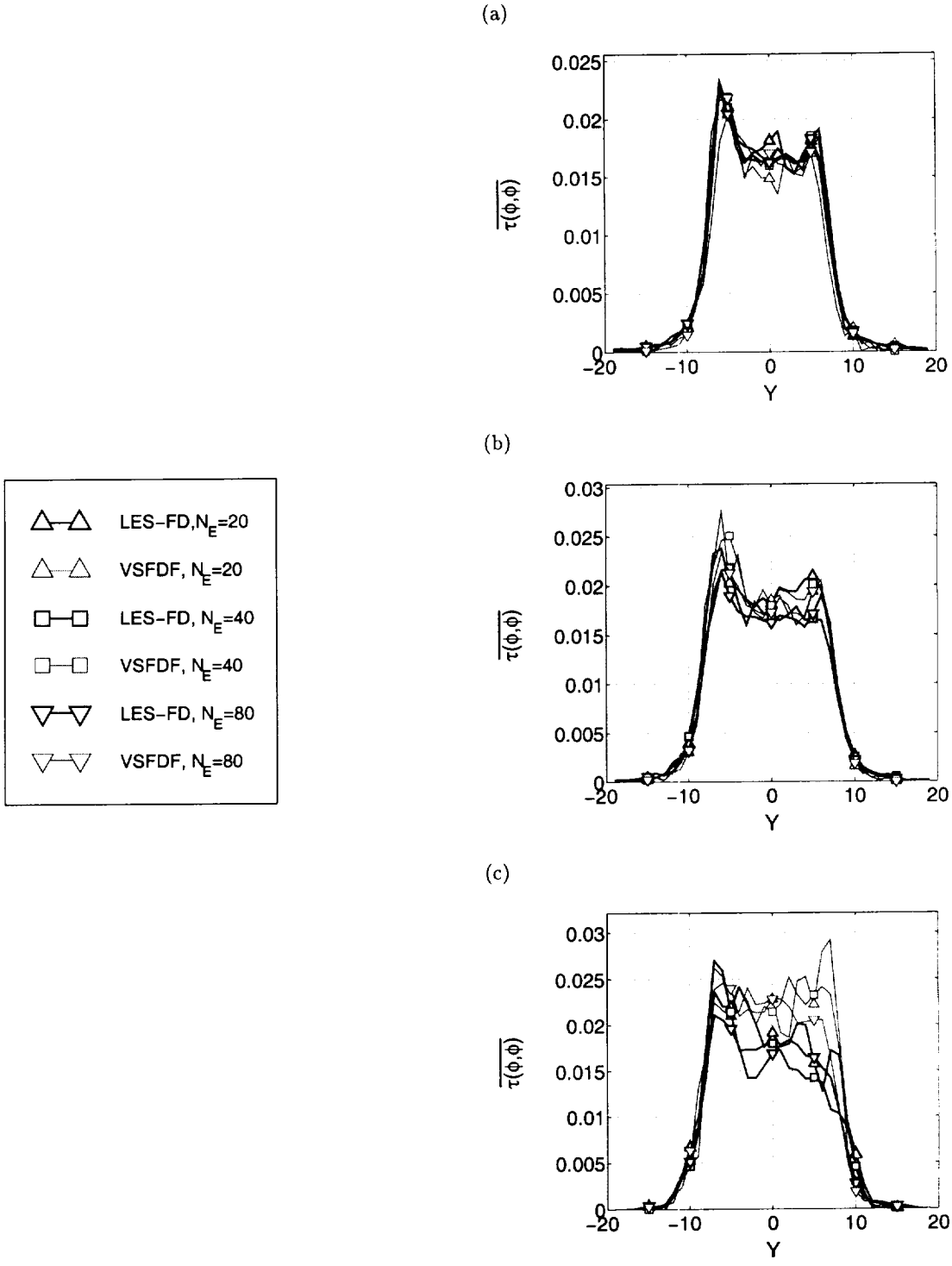

Figure 12: Cross-stream variation of the Reynolds averaged values of the $\tau(\phi, \phi)$, SGS tensor: (a) $\Delta_E = 0.5\Delta$, (b) $\Delta_E = 1.0$, (c) $\Delta_E = 2.0$

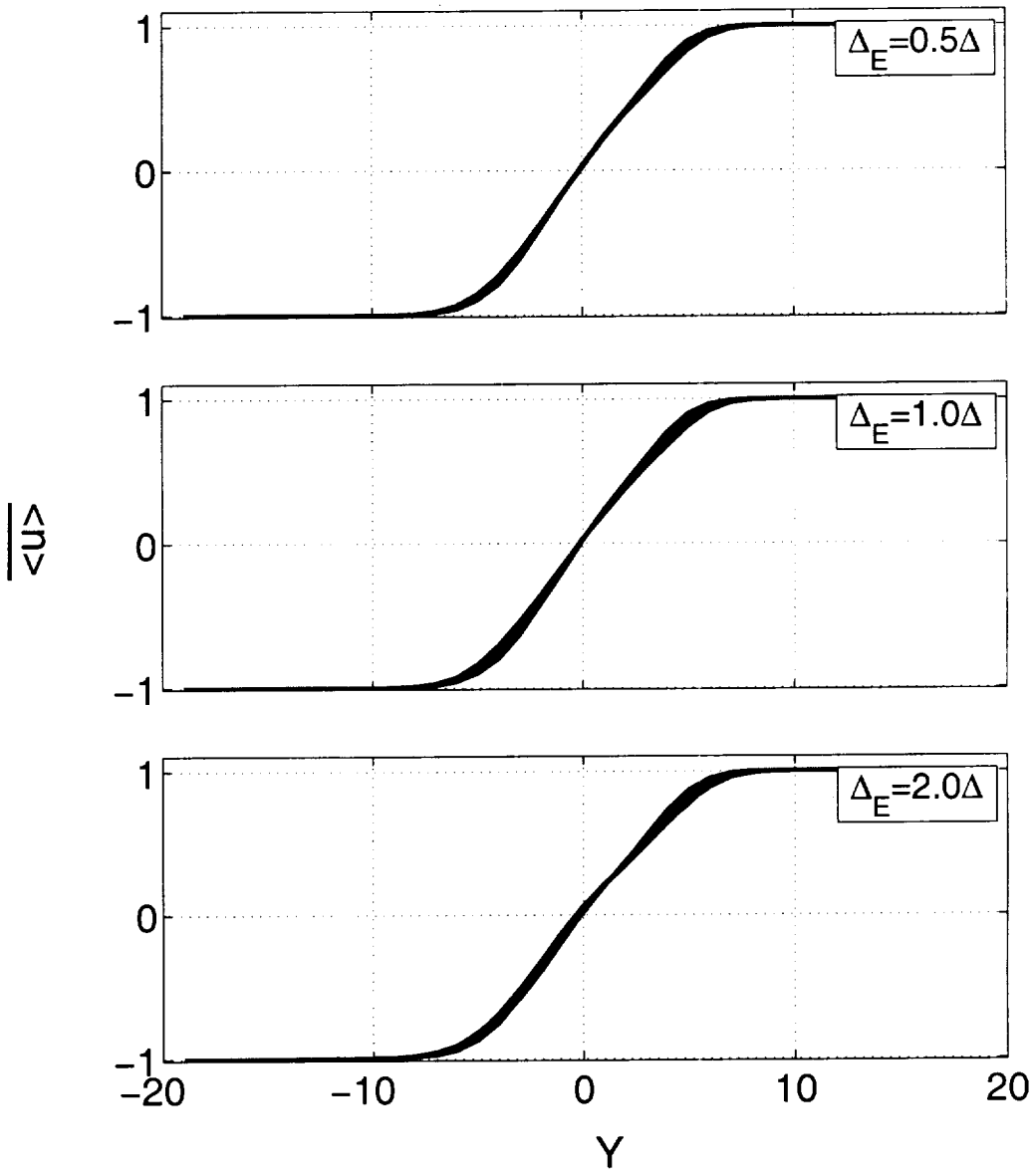

Figure 13: Effect of the random number sequence used in the Monte-Carlo solver with $N_E = 40$ on repeatability of the LES-FD and VSFDF simulations for Reynolds averaged values of $\langle u \rangle$ field. (– LES-FD, VSFDF)

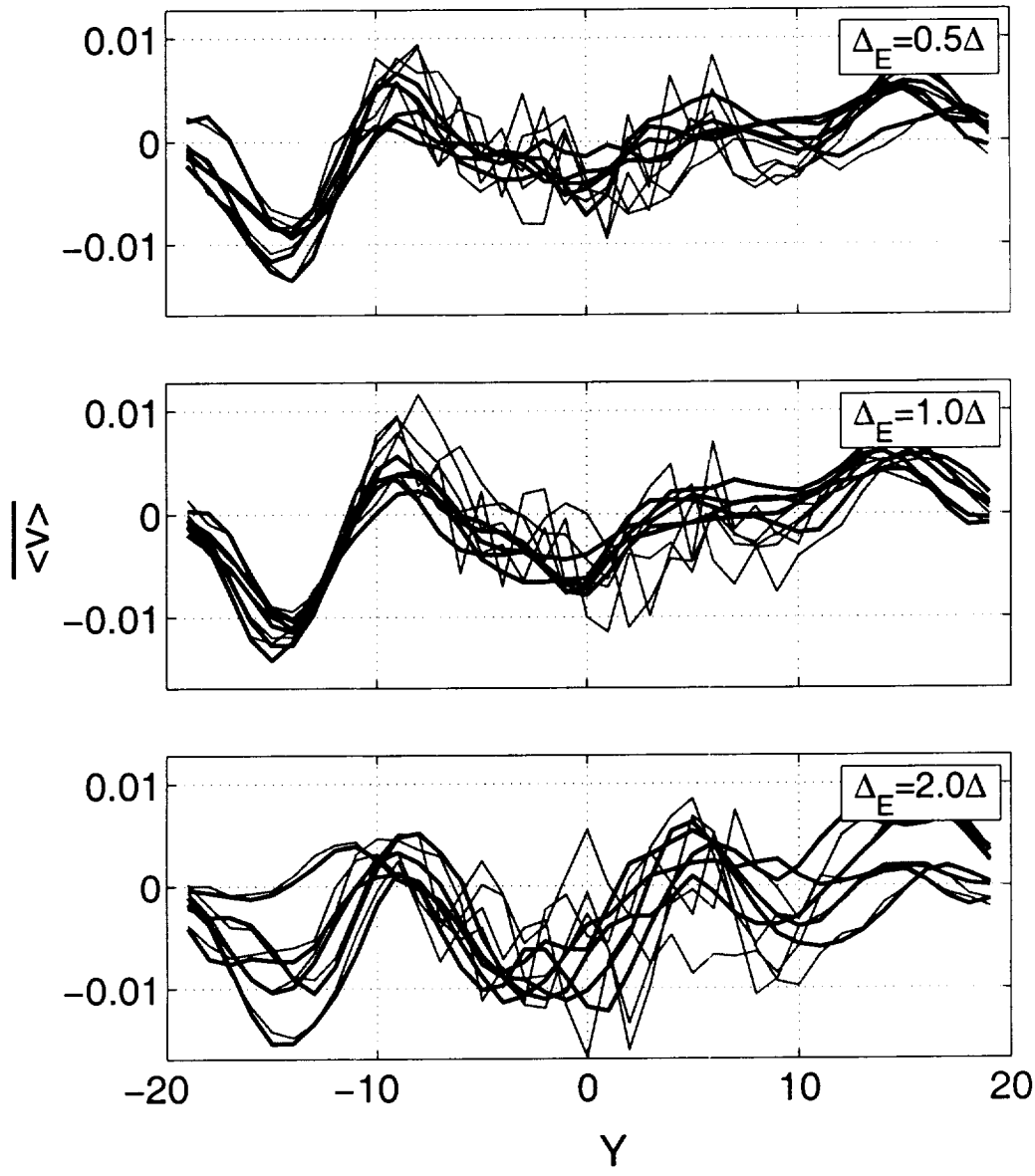

Figure 14: Effect of the random number sequence used in the Monte-Carlo solver with $N_E = 40$ on repeatability of the LES-FD and VSFDF simulations for Reynolds averaged values of $\langle v \rangle$ field. (– LES-FD, -- VSFDF)

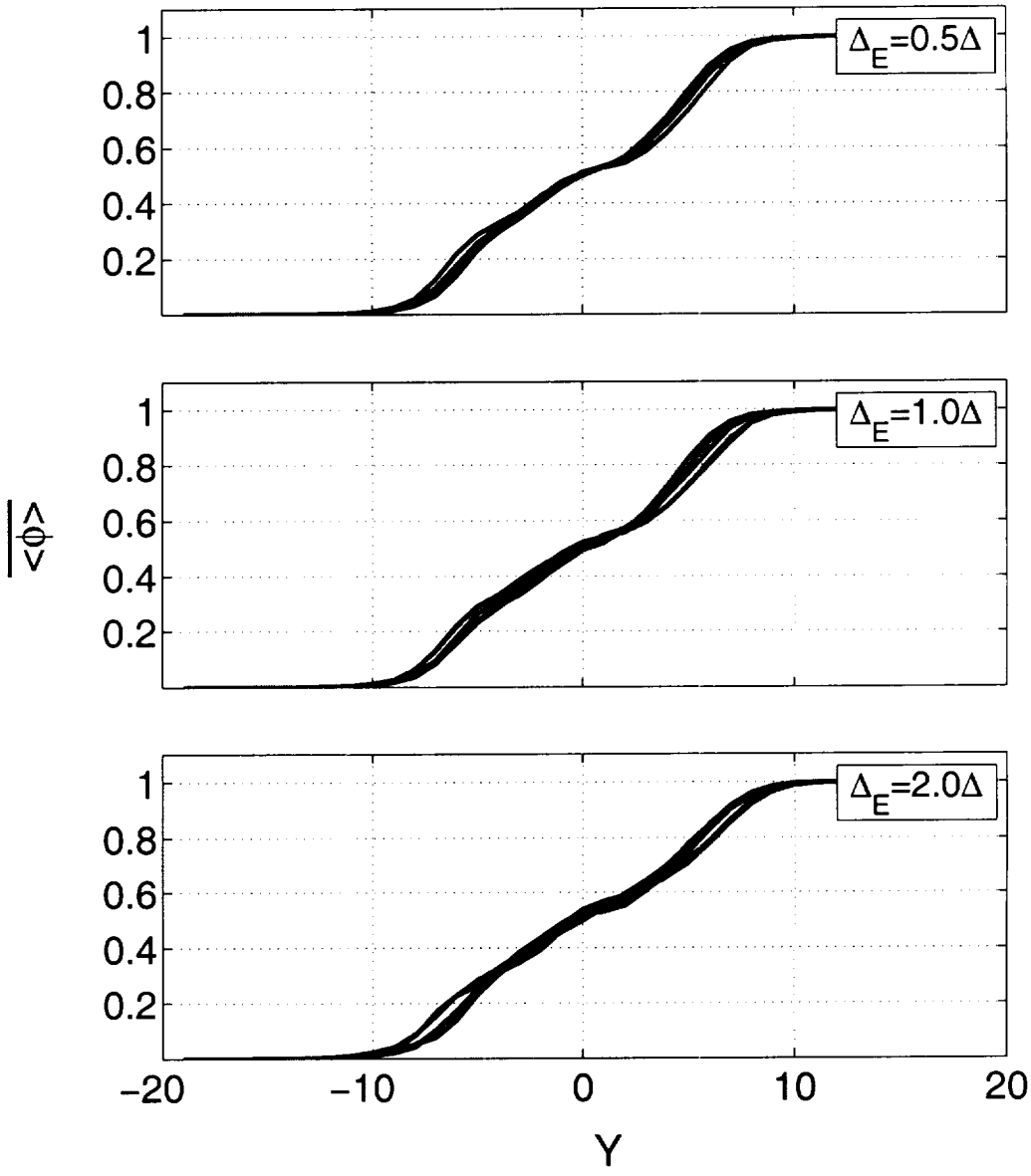

Figure 15: Effect of the random number sequence used in the Monte-Carlo solver with $N_E = 40$ on repeatability of the LES-FD and VSFDF simulations for Reynolds averaged values of $\langle\phi\rangle$ field. (– LES-FD, VSFDF)

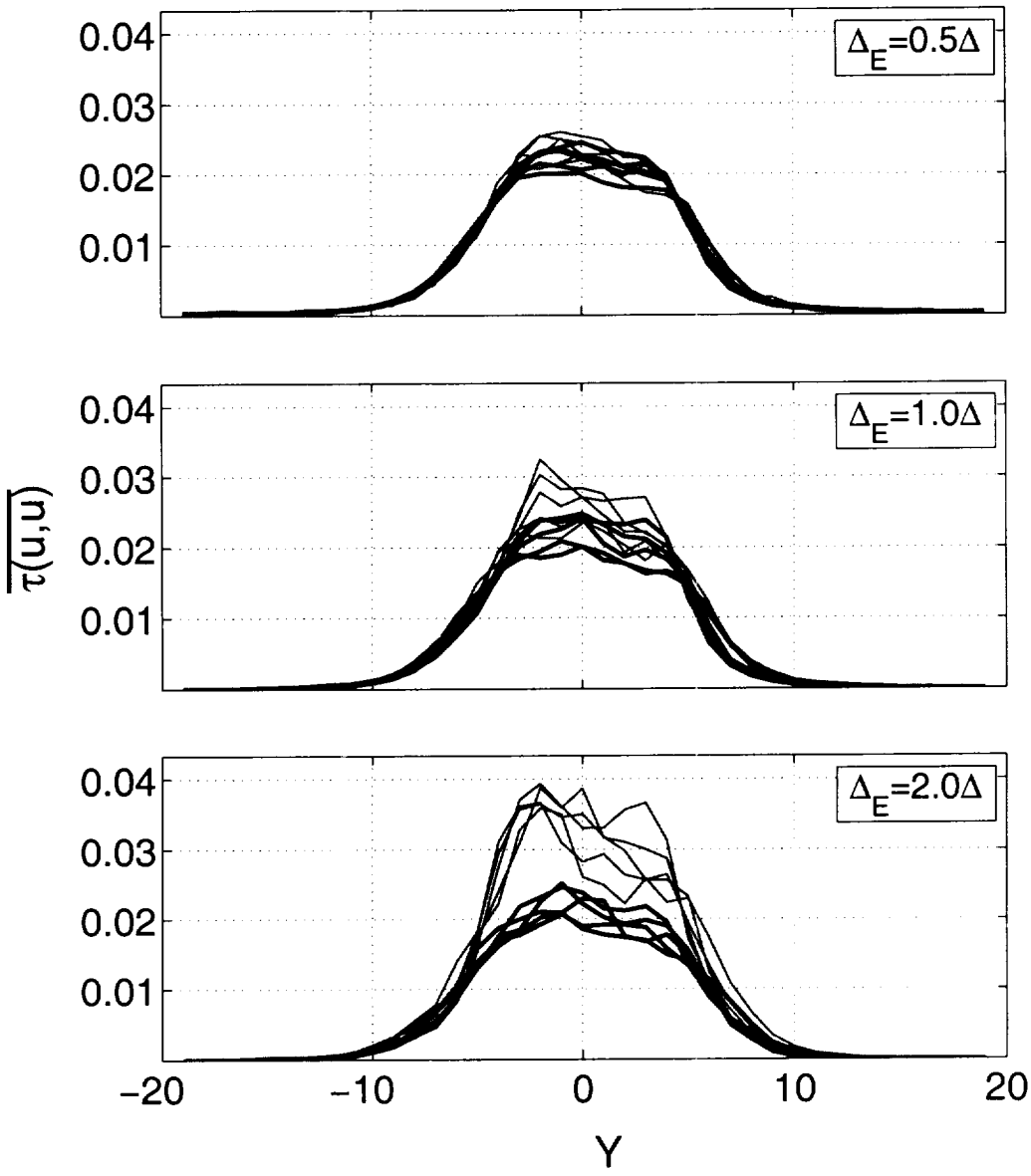

Figure 16: Effect of the random number sequence used in the Monte-Carlo solver with $N_E = 40$ on repeatability of the LES-FD and VSFDF simulations for Reynolds averaged values of $\tau(u,u)$ field. (– LES-FD, ··· VSFDF)

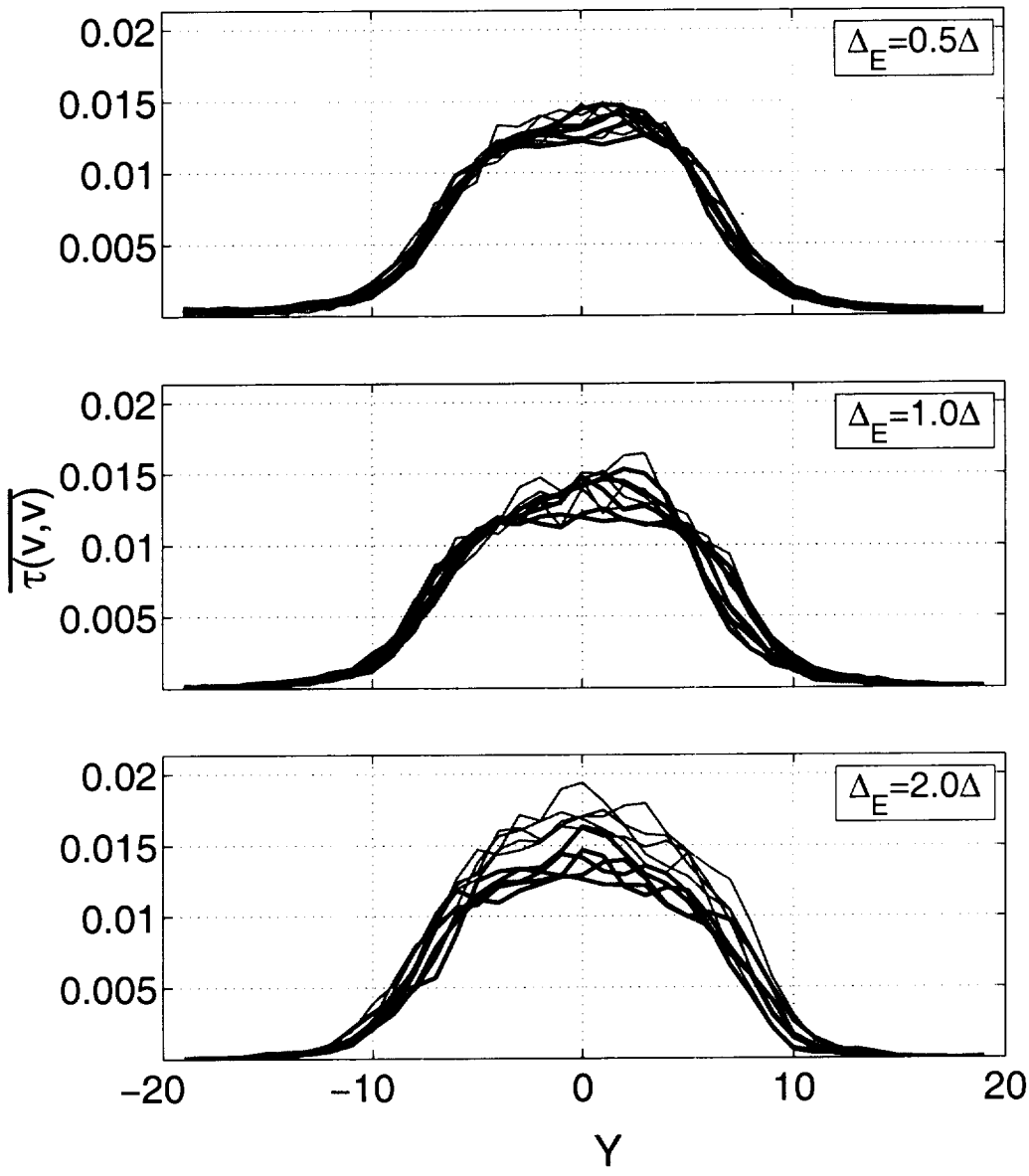

Figure 17: Effect of the random number sequence used in the Monte-Carlo solver with $N_E = 40$ on repeatability of the LES-FD and VSFDF simulations for Reynolds averaged values of $\tau(v, v)$ field. (– LES-FD, — VSFDF)

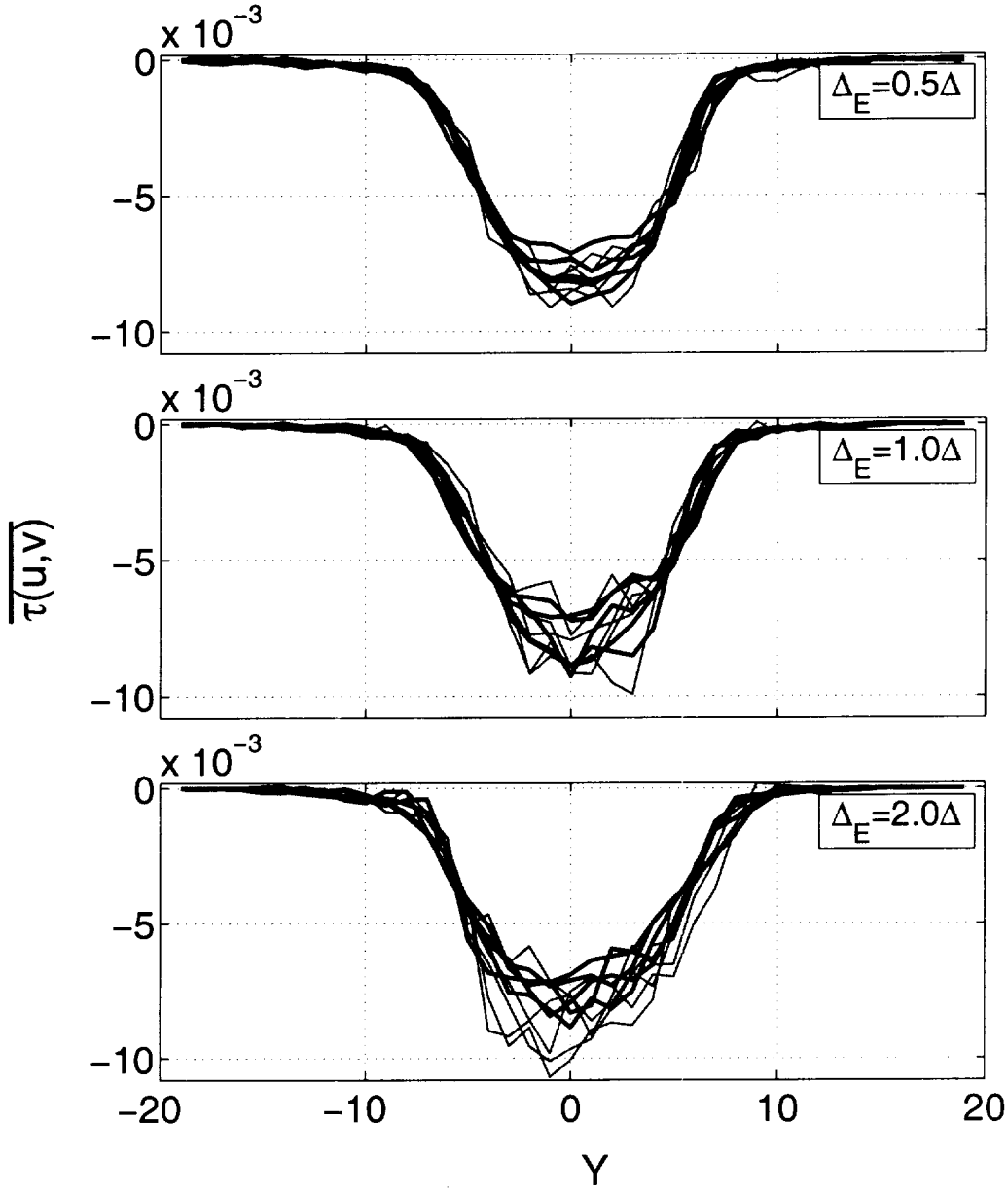

Figure 18: Effect of the random number sequence used in the Monte-Carlo solver with $N_E = 40$ on repeatability of the LES-FD and VSFDF simulations for Reynolds averaged values of $\tau(u, v)$ field. (– LES-FD, — VSFDF)

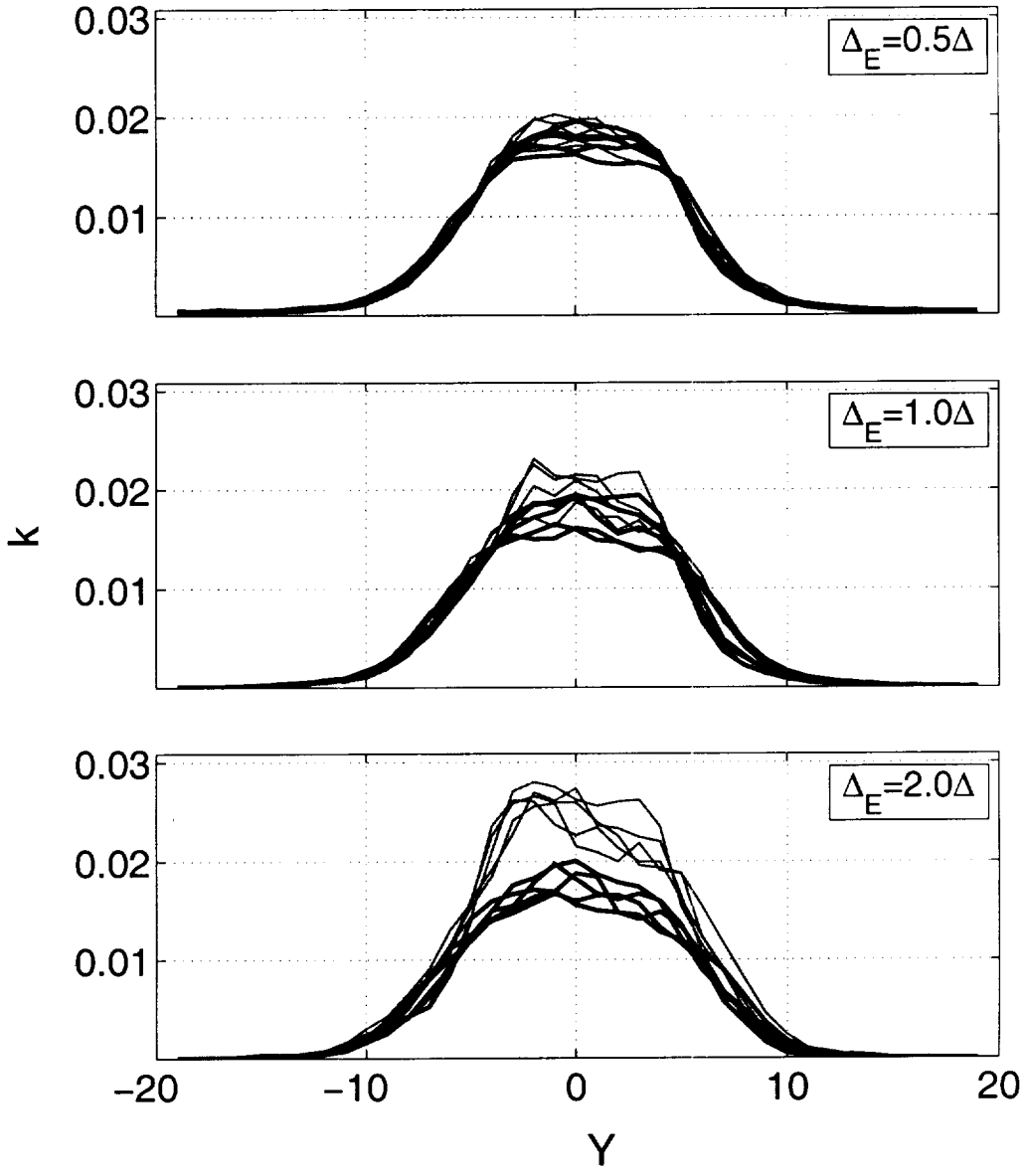

Figure 19: Effect of the random number sequence used in the Monte-Carlo solver with $N_E = 40$ on repeatability of the LES-FD and VSFDF simulations for Reynolds averaged values of turbulent kinetic energy, k, field. (– LES-FD, — VSFDF)

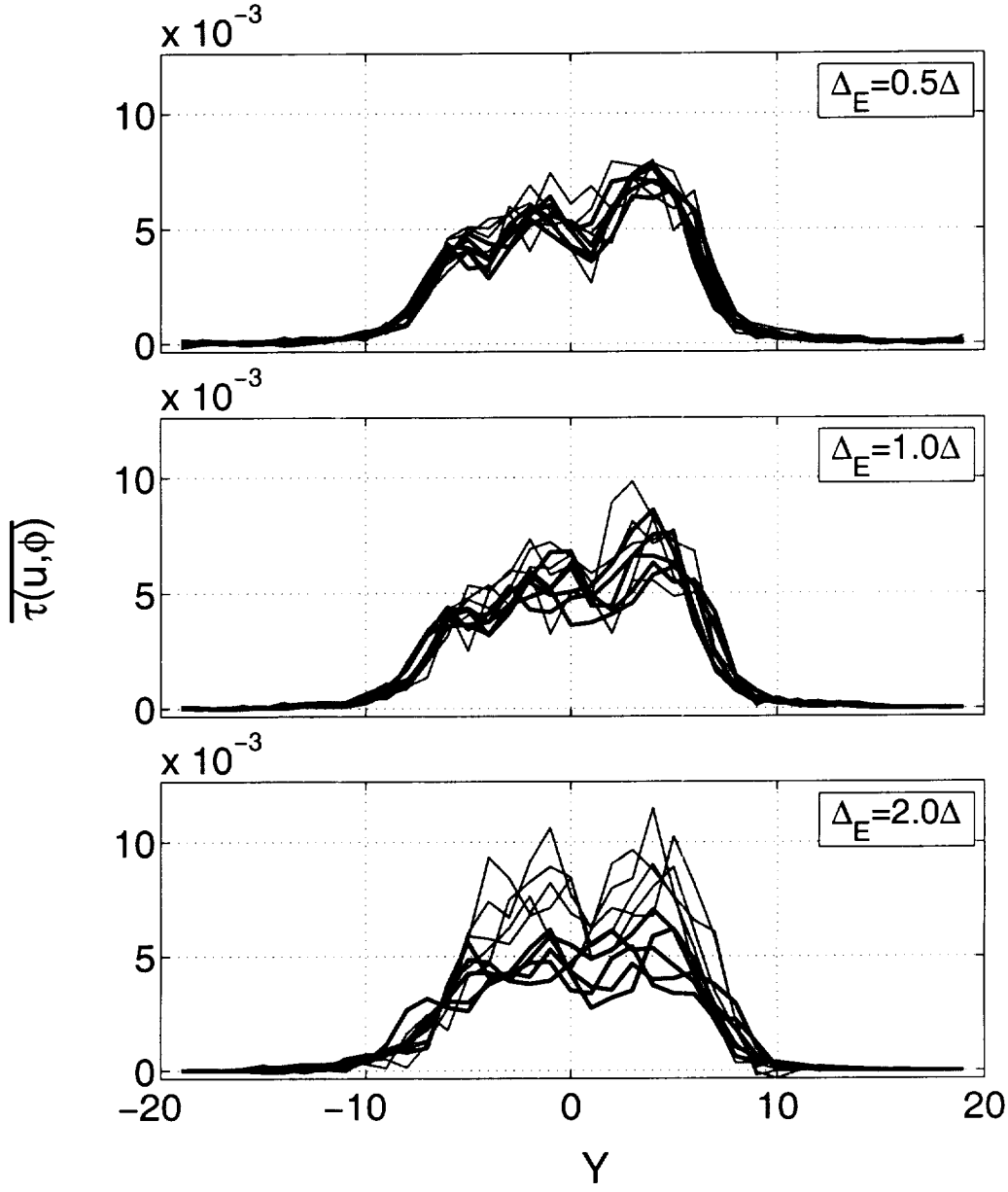

Figure 20: Effect of the random number sequence used in the Monte-Carlo solver with $N_E = 40$ on repeatability of the LES-FD and VSFDF simulations for Reynolds averaged values of $\tau(u, \phi)$ field. (– LES-FD, — VSFDF)

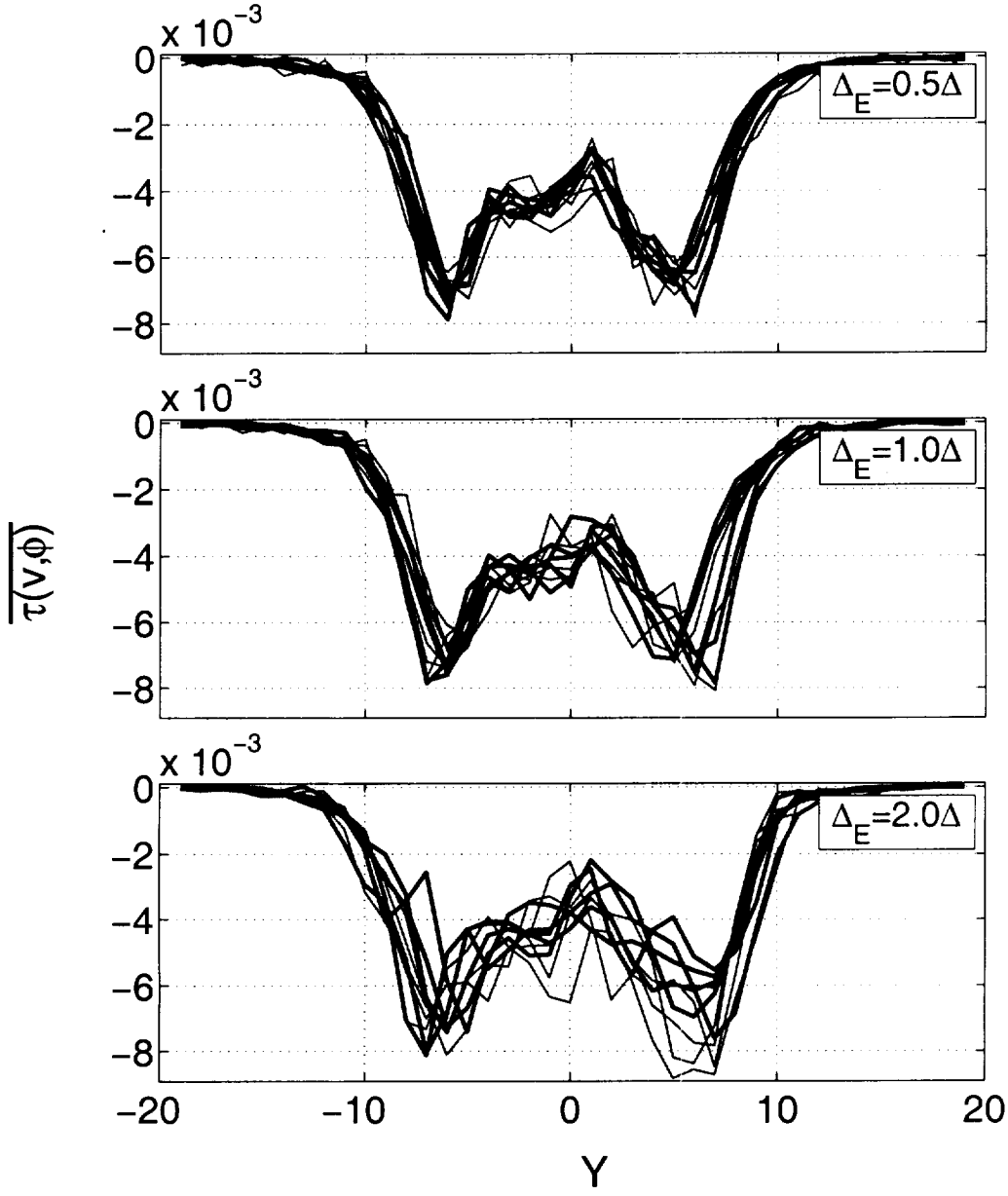

Figure 21: Effect of the random number sequence used in the Monte-Carlo solver with $N_E = 40$ on repeatability of the LES-FD and VSFDF simulations for Reynolds averaged values of $\tau(v, \phi)$ field. (– LES-FD, – VSFDF)

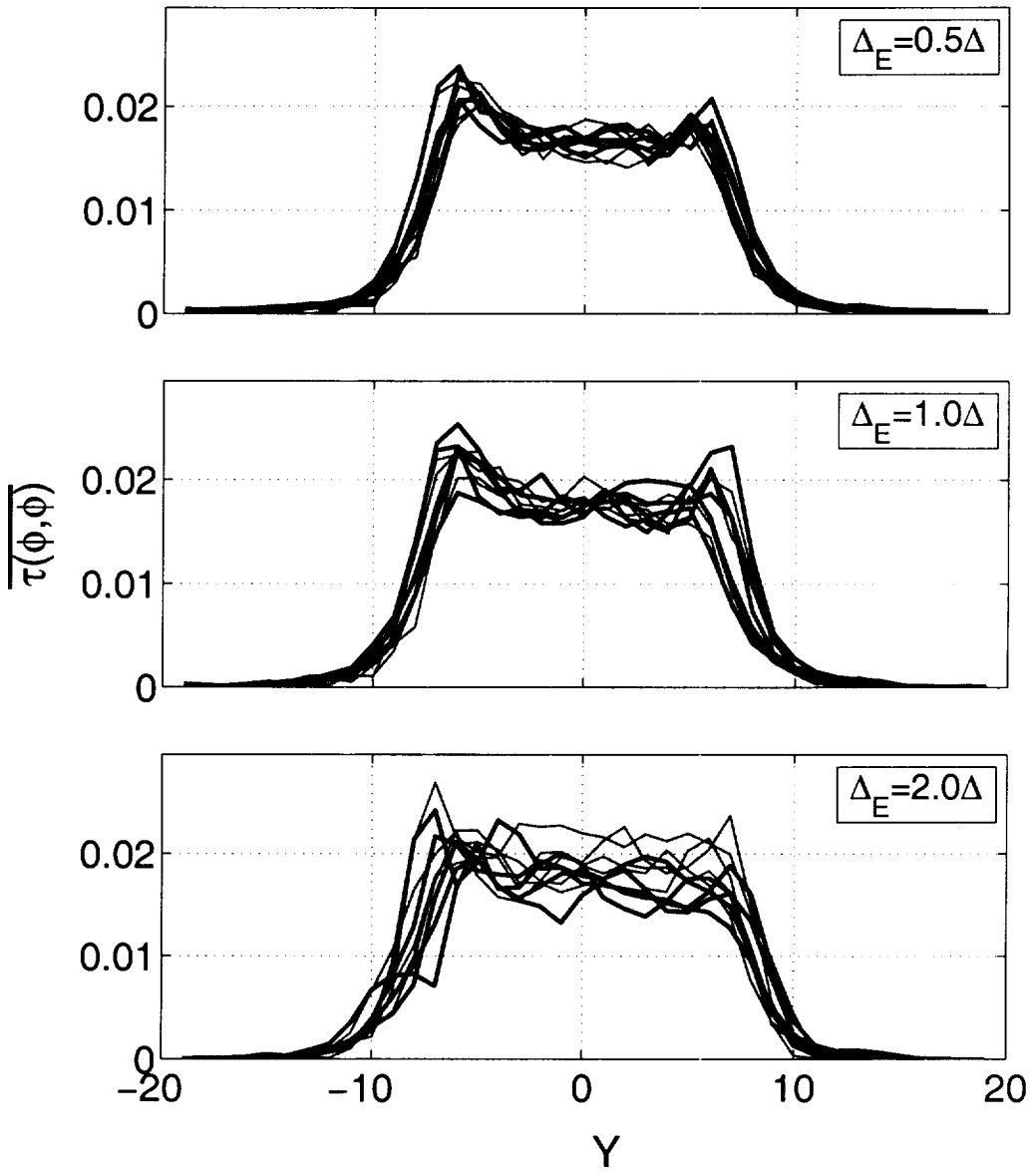

Figure 22: Effect of the random number sequence used in the Monte-Carlo solver with $N_E = 40$ on repeatability of the LES-FD and VSFDF simulations for Reynolds averaged values of $\tau(\phi, \phi)$ field. (– LES-FD, – VSFDF)

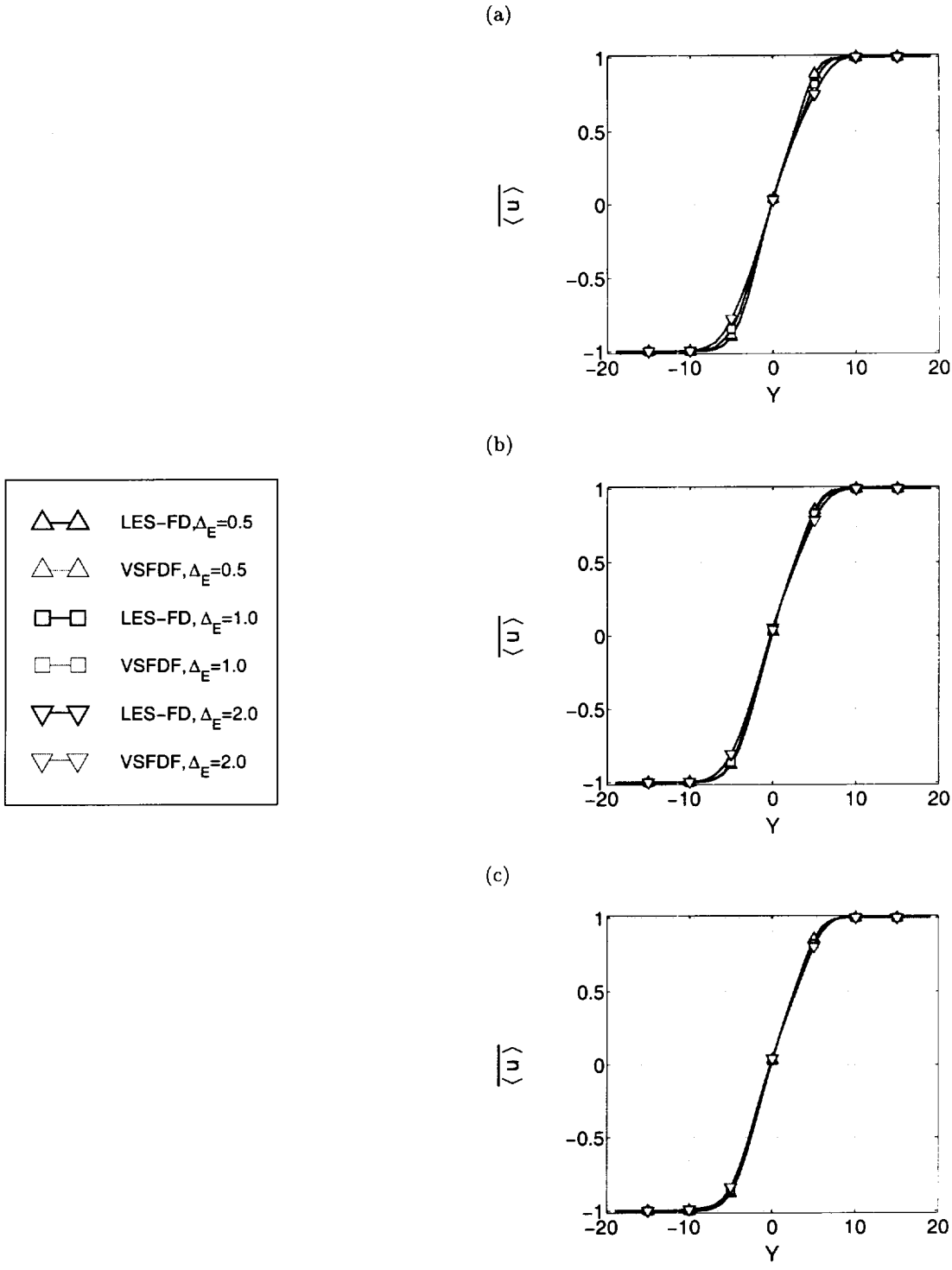

Figure 23: Cross-stream variation of the Reynolds averaged values of the $\langle u \rangle$ component of the velocity field: (a) $N_E = 20$, (b) $N_E = 40$, (c) $N_E = 80$

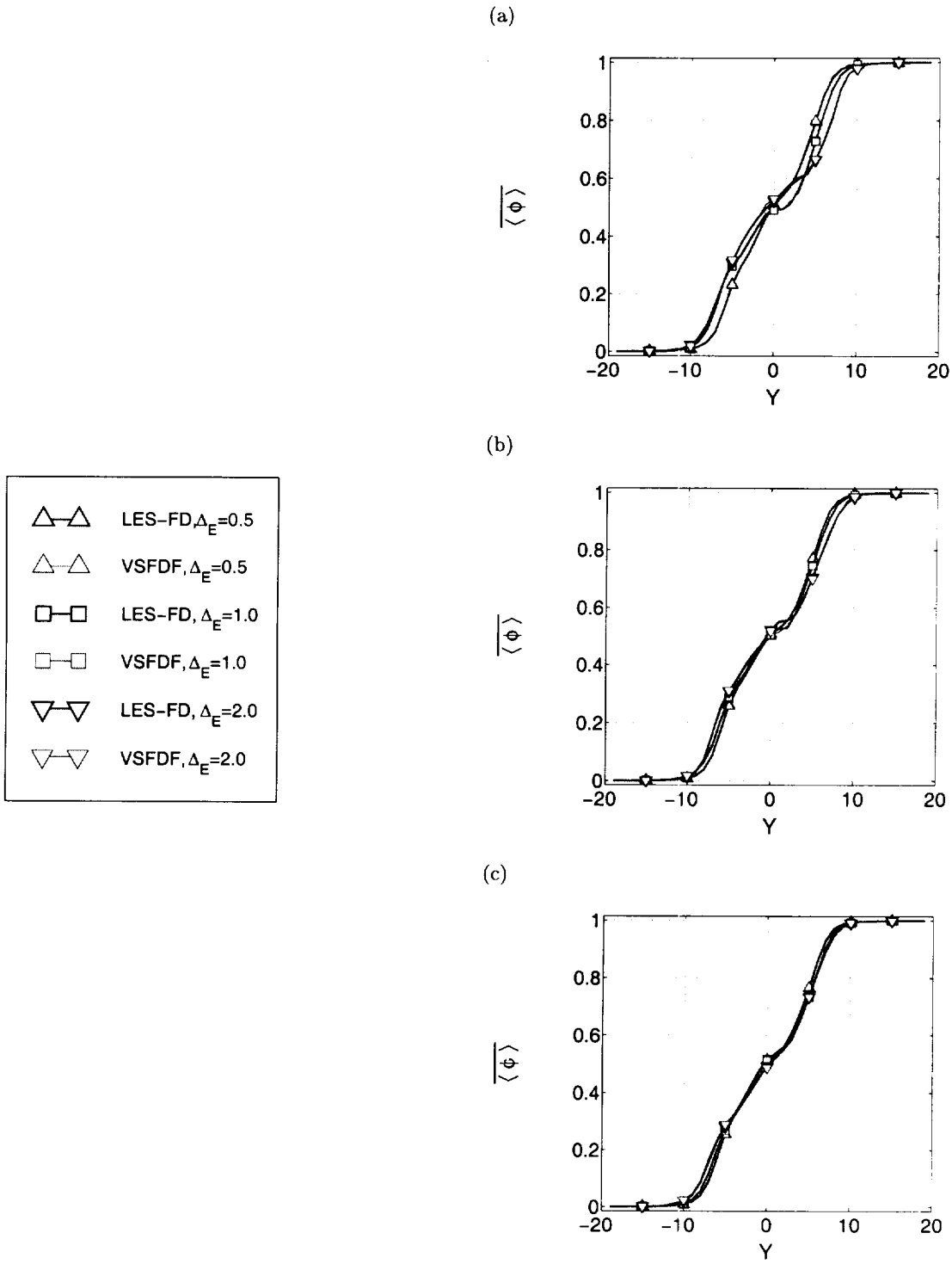

Figure 24: Cross-stream variation of the Reynolds averaged values of the $\langle\phi\rangle$, scalar field: (a) $N_E = 20$, (b) $N_E = 40$, (c) $N_E = 80$

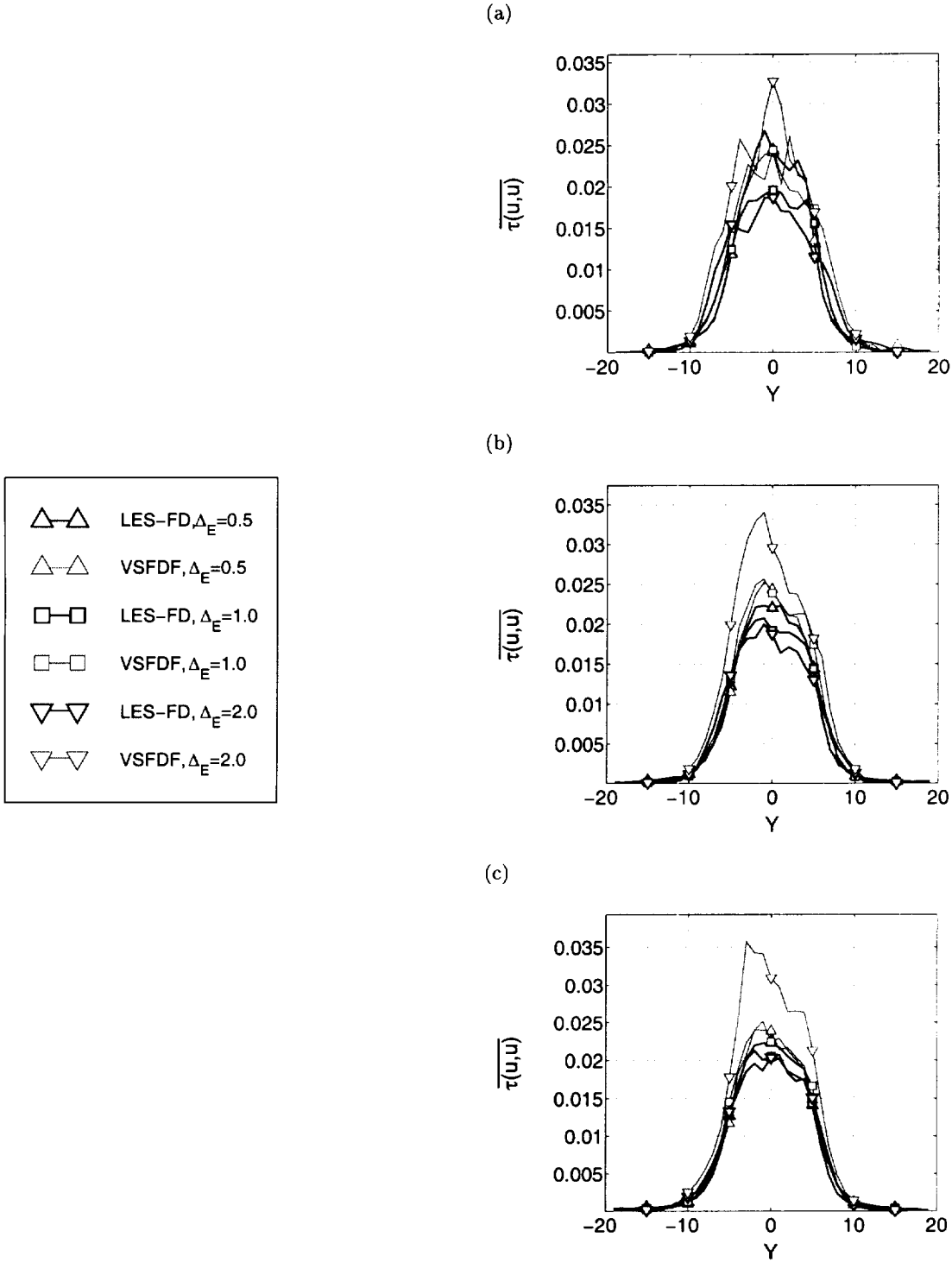

Figure 25: Cross-stream variation of the Reynolds averaged values of the $\tau(u,u)$ component of the SGS stress tensor: (a) $N_E = 20$, (b) $N_E = 40$, (c) $N_E = 80$

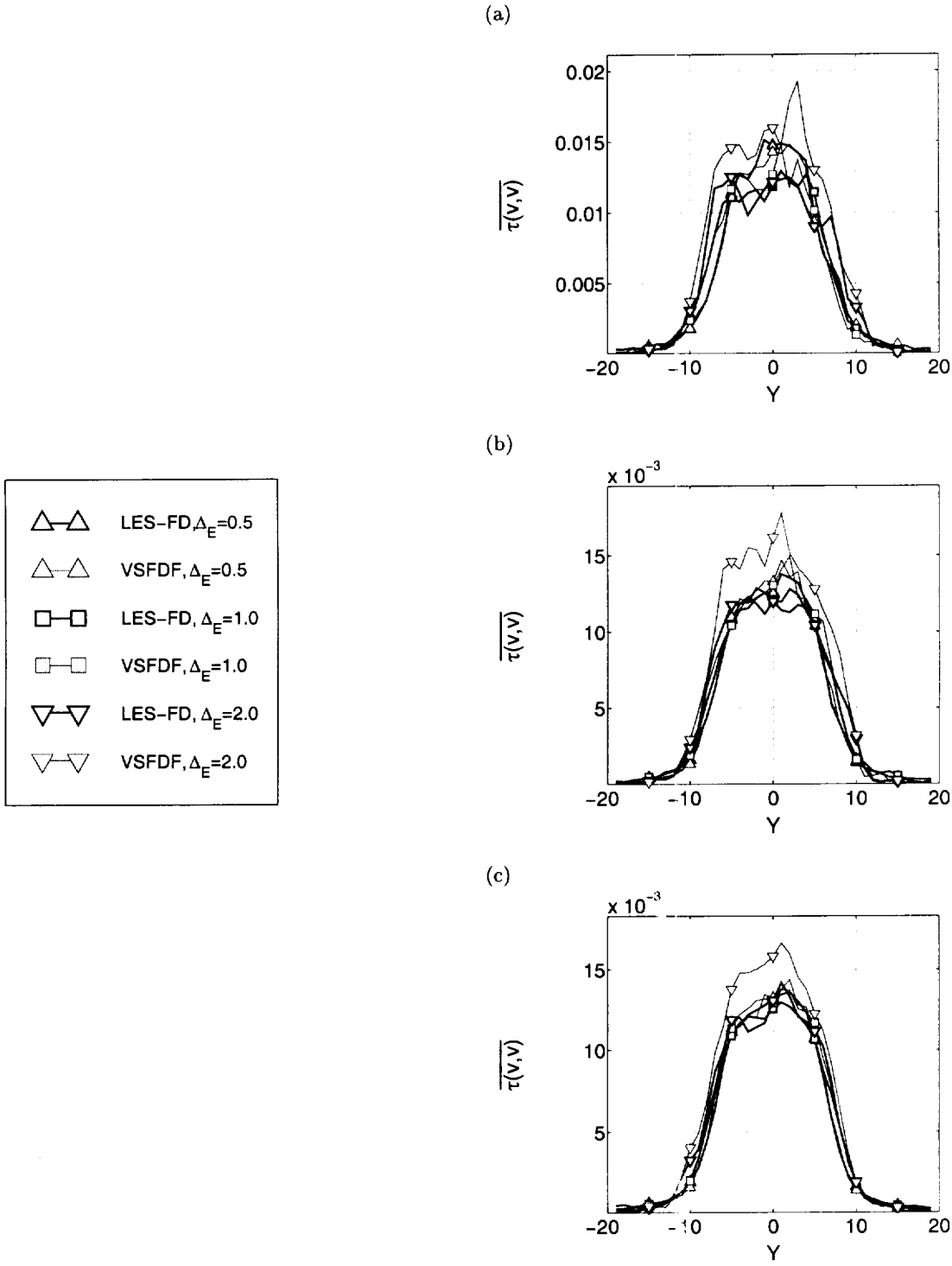

Figure 26: Cross-stream variation of the Reynolds averaged values of the $\tau(v,v)$ component of the SGS stress tensor: (a) $N_E = 20$, (b) $N_E = 40$, (c) $N_E = 80$

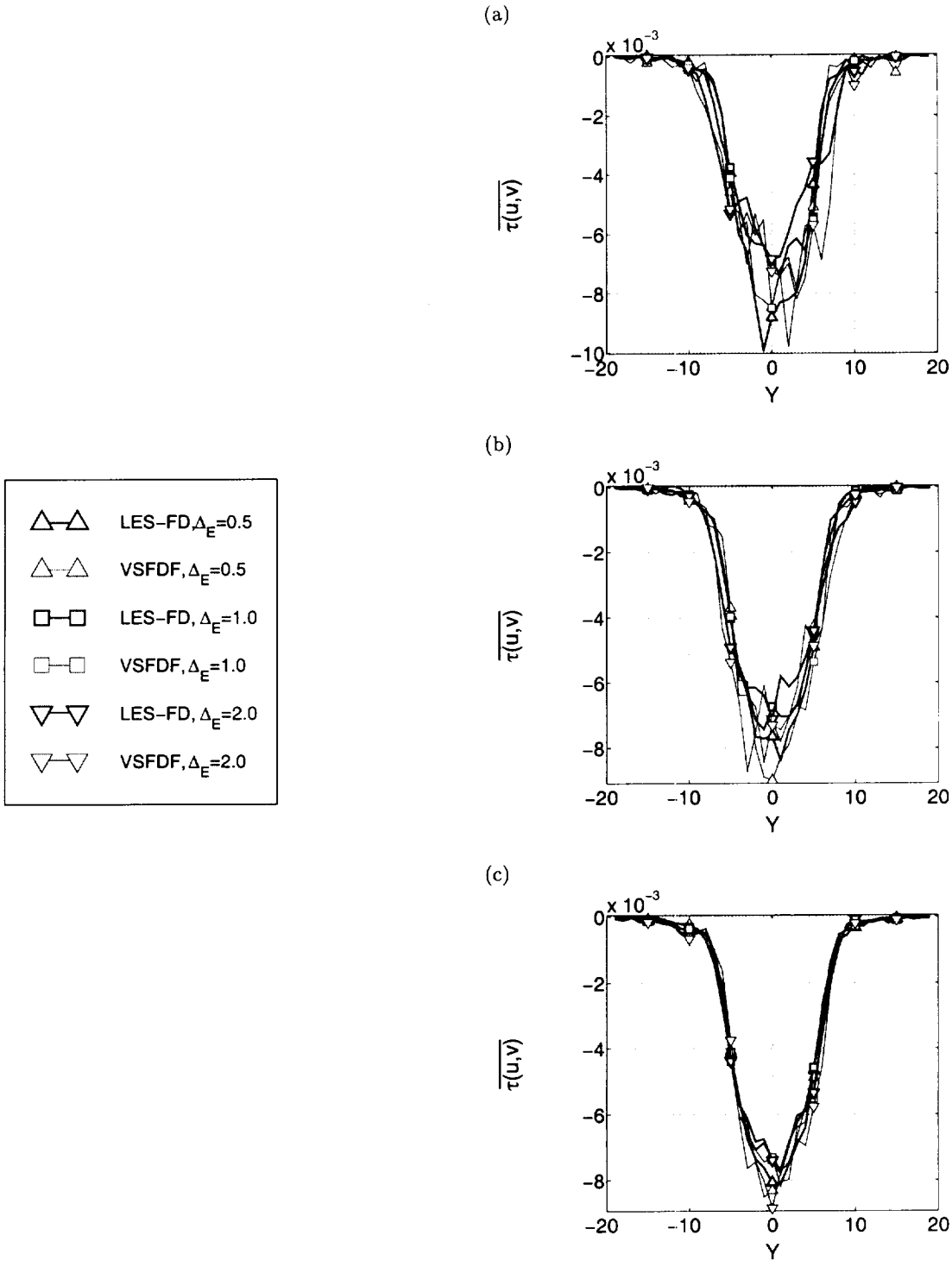

Figure 27: Cross-stream variation of the Reynolds averaged values of the $\tau(u,v)$, SGS stress tensor: (a) $N_E = 20$, (b) $N_E = 40$, (c) $N_E = 80$

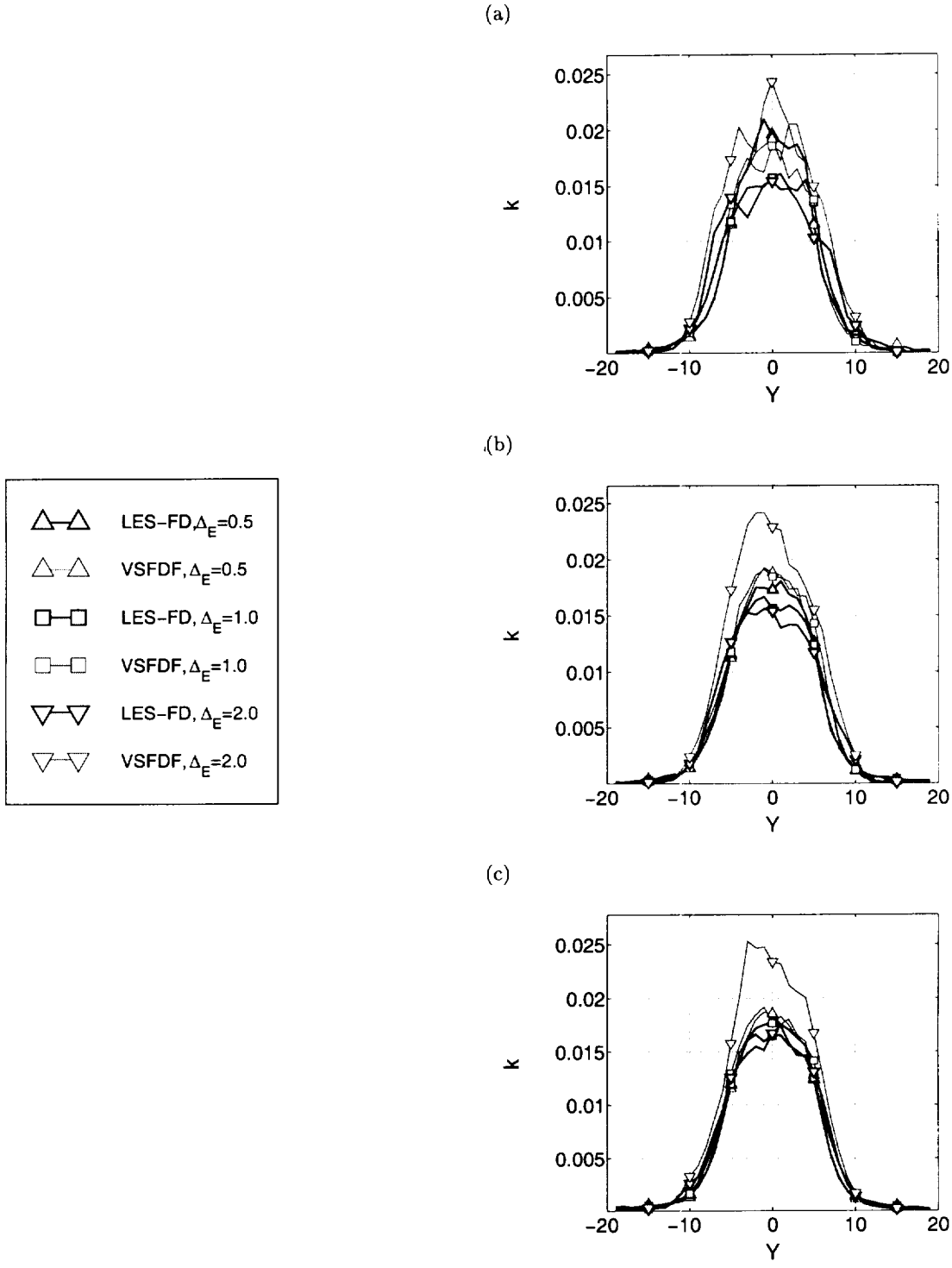

Figure 28: Cross-stream variation of the Reynolds averaged values of the turbulent kinetic energy, k: (a) $N_E = 20$, (b) $N_E = 40$, (c) $N_E = 80$

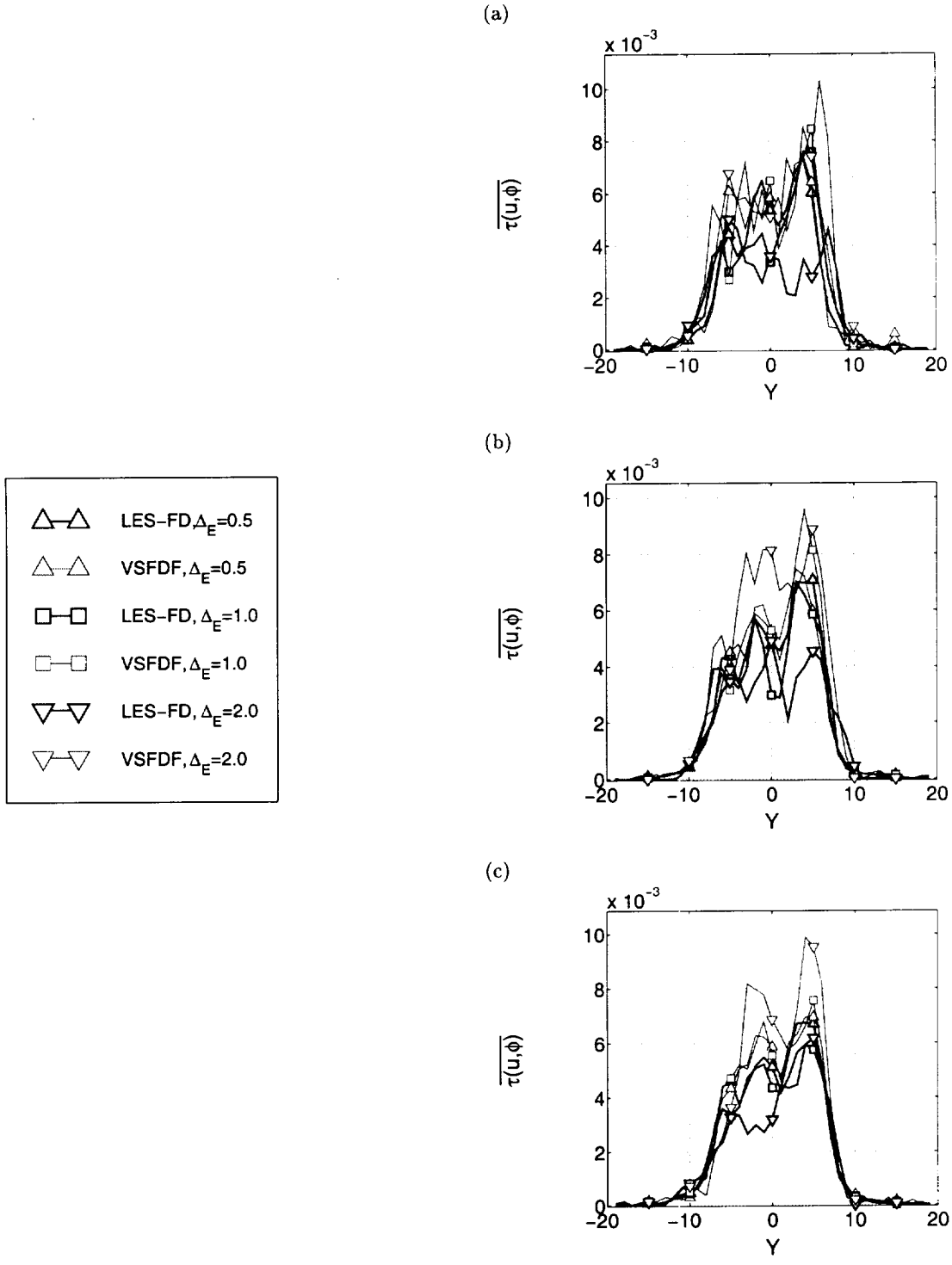

Figure 29: Cross-stream variation of the Reynolds averaged values of the $\tau(u, \phi)$, SGS tensor: (a) $N_E = 20$, (b) $N_E = 40$, (c) $N_E = 80$

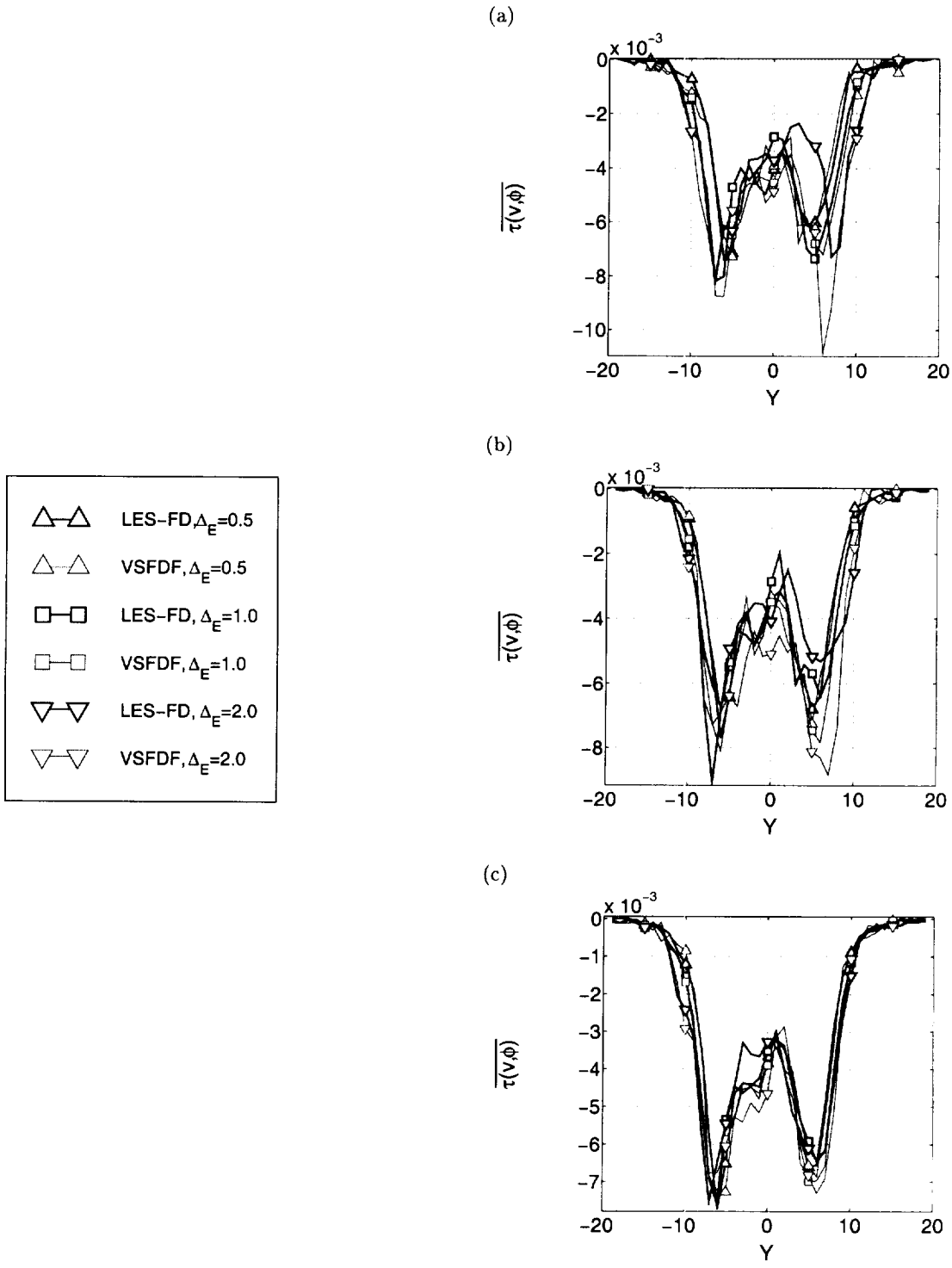

Figure 30: Cross-stream variation of the Reynolds averaged values of the $\tau(v, \phi)$, SGS tensor: (a) $N_E = 20$, (b) $N_E = 40$, (c) $N_E = 80$

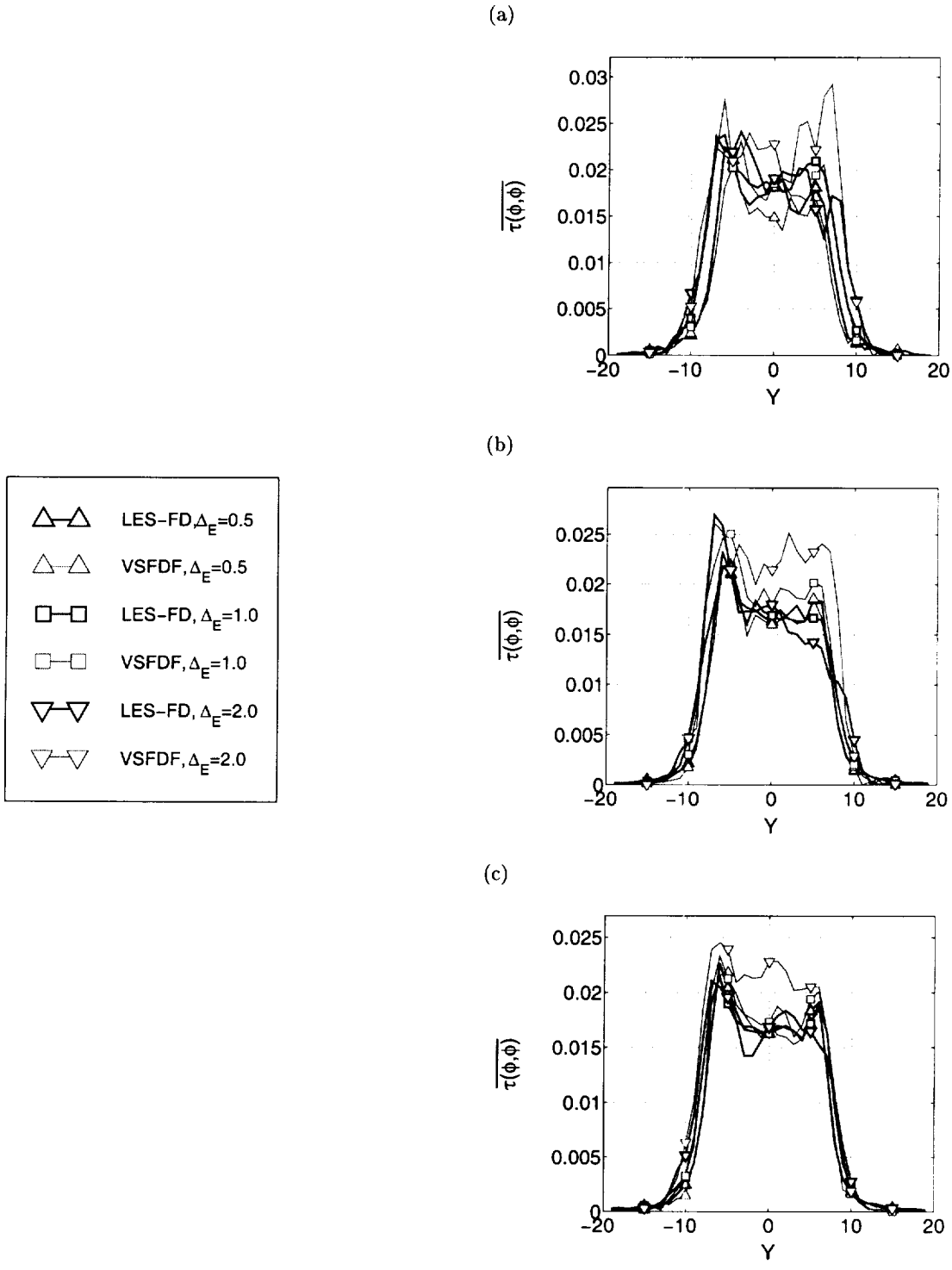

Figure 31: Cross-stream variation of the Reynolds averaged values of the $\tau(\phi, \phi)$, SGS tensor: (a) $N_E = 20$, (b) $N_E = 40$, (c) $N_E = 80$

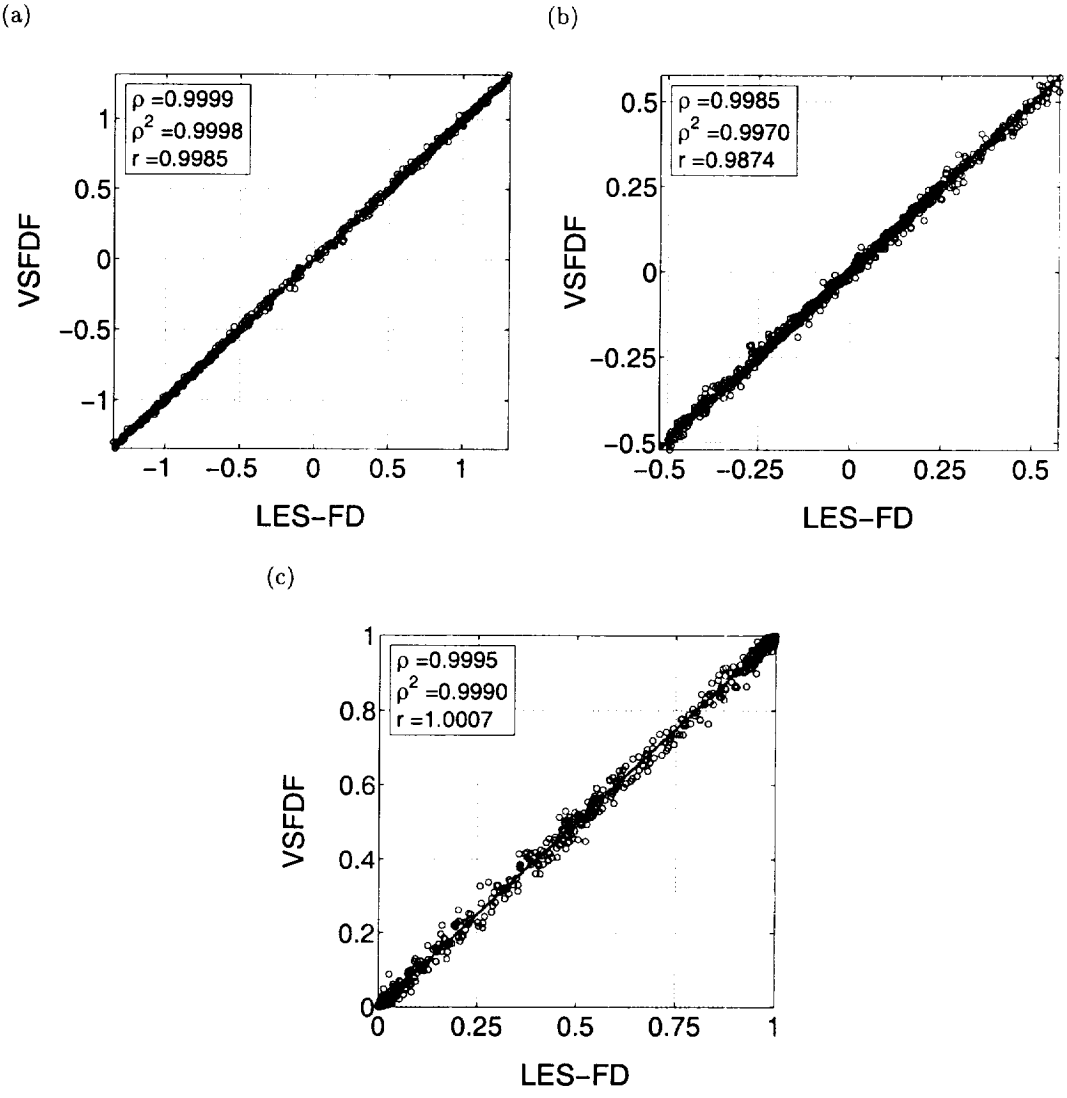

Figure 32: Scatter plot of the filtered velocity, $\langle u \rangle$ and $\langle v \rangle$, and scalar, $\langle \phi \rangle$ obtained via VSFDF and LES-FD for $\Delta_E = 0.5\Delta, N_E = 40$. (a) $\langle u \rangle$, (b) $\langle v \rangle$, (c) $\langle \phi \rangle$. - - least-squares-fit line, - 1:1 fit line. ρ is the correlation coefficient, r is the linear regression coefficient

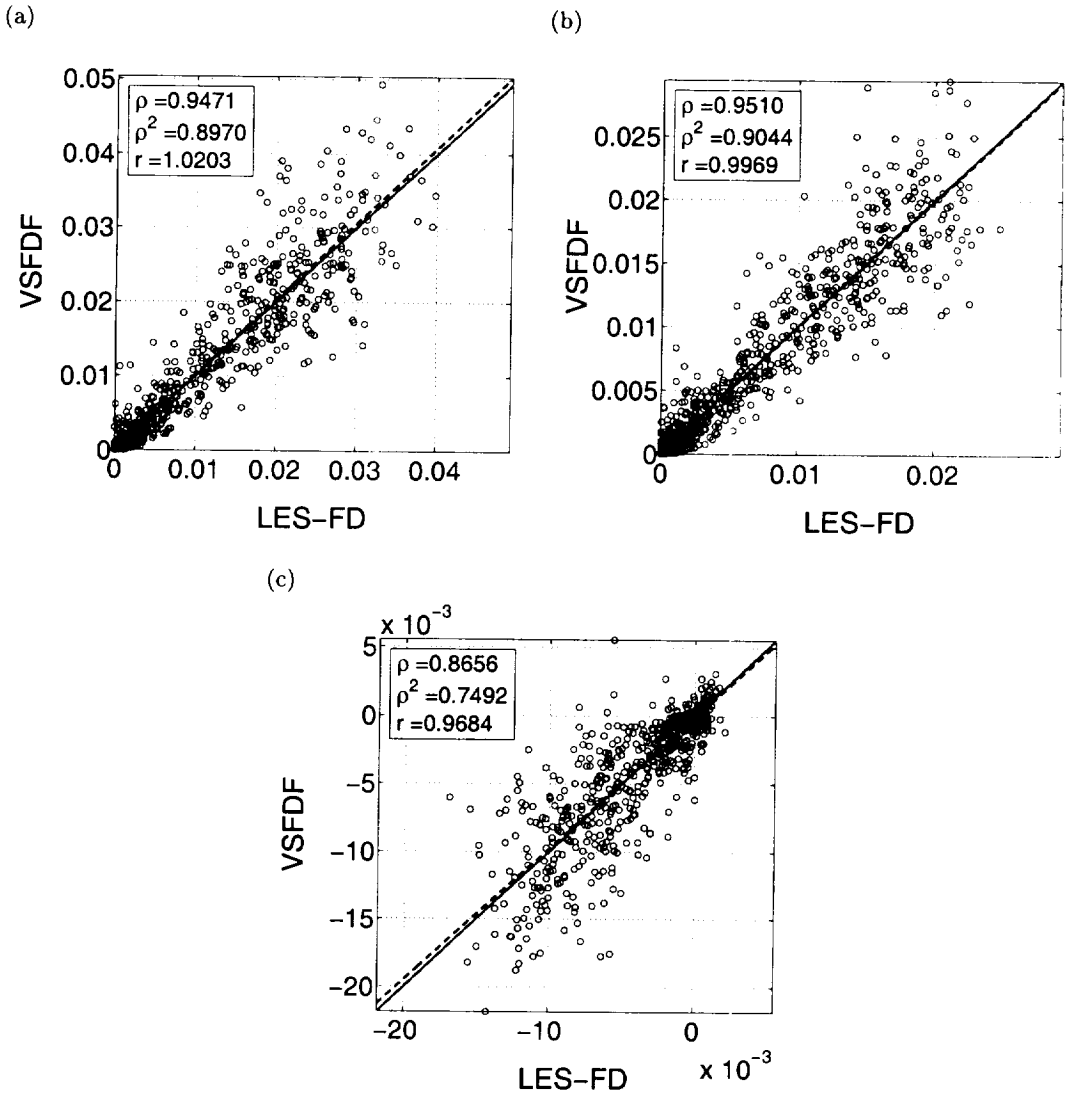

Figure 33: Scatter plot of the components of the SGS stress tensor, $\tau(u,u)$, $\tau(v,v)$, and $\tau(u,v)$ obtained via VSFDF and LES-FD for $\Delta_E = 0.5\Delta$,$N_E = 40$. (a) $\tau(u,u)$, (b) $\tau(v,v)$, (c) $\tau(u,v)$. - - least-squares-fit line, - 1:1 fit line. ρ is the correlation coefficient, r is the linear regression coefficient

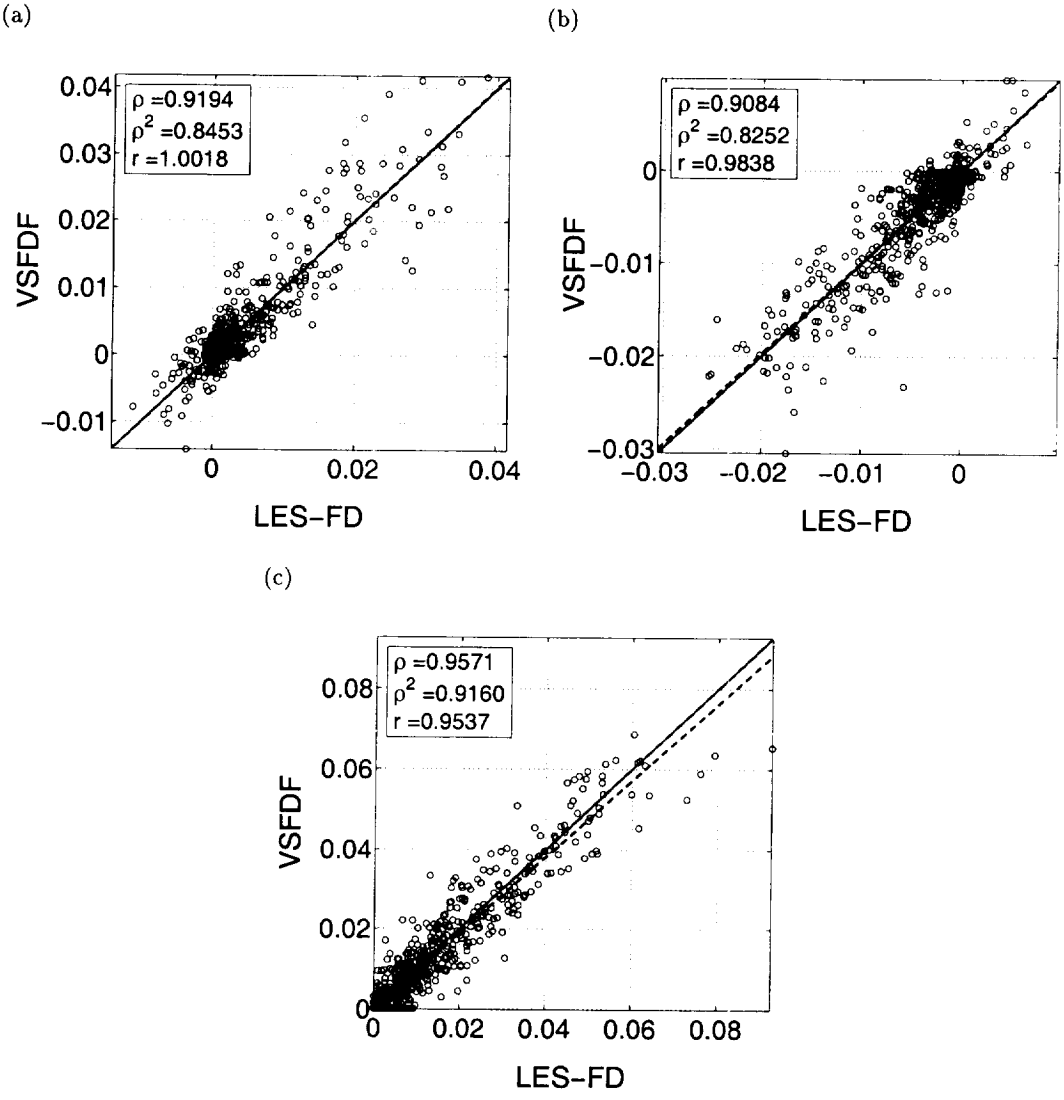

Figure 34: Scatter plot of the components of the SGS tensor, $\tau(u,\phi)$, $\tau(v,\phi)$, and $\tau(\phi,\phi)$ obtained via VSFDF and LES-FD for $\Delta_E = 0.5\Delta$,$N_E = 40$. (a) $\tau(u,\phi)$, (b) $\tau(v,\phi)$, (c) $\tau(\phi,\phi)$. - - least-squares-fit line, - 1:1 fit line. ρ is the correlation coefficient, r is the linear regression coefficient

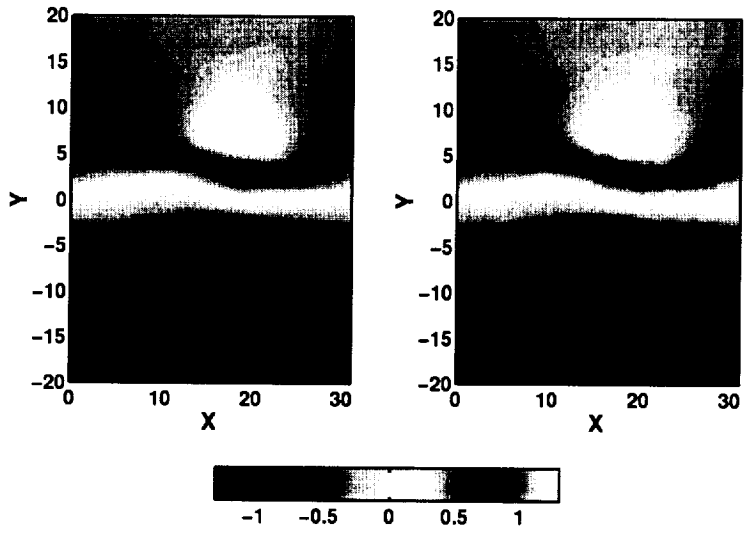

Figure 35: Visual consistency for stream-wise velocity field, $\langle u \rangle$. The LES-FD results are obtained for $\Delta_E = 0.5\Delta$, $N_E = 40$ at t=34.3. (Captions: Left - LES-FD, Right - VSFDF)

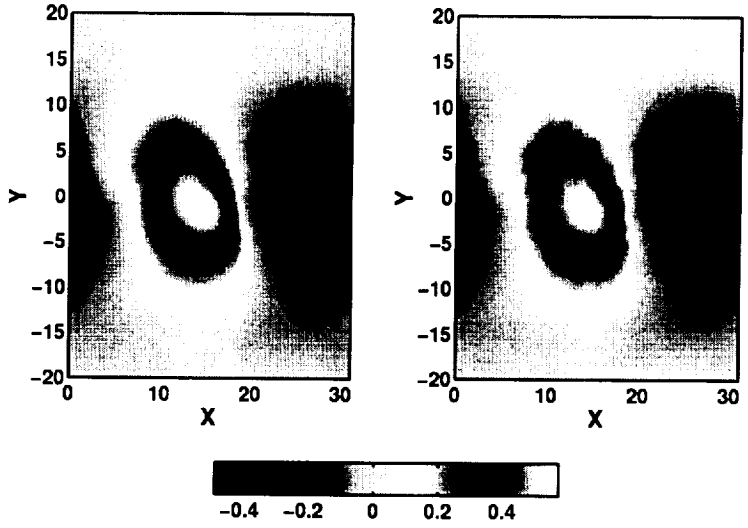

Figure 36: Visual consistency for span-wise velocity field, $\langle v \rangle$. The LES-FD results are obtained for $\Delta_E = 0.5\Delta$, $N_E = 40$ at t=34.3. (Captions: Left - LES-FD, Right - VSFDF)

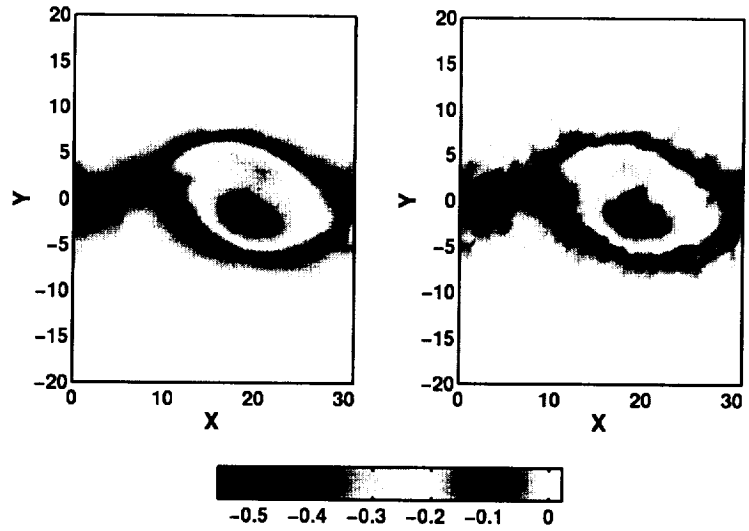

Figure 37: Visual consistency for the vorticity field. The LES-FD results are obtained for $\Delta_E = 0.5\Delta$, $N_E = 40$ at t=34.3. (Captions: Left - LES-FD, Right - VSFDF)

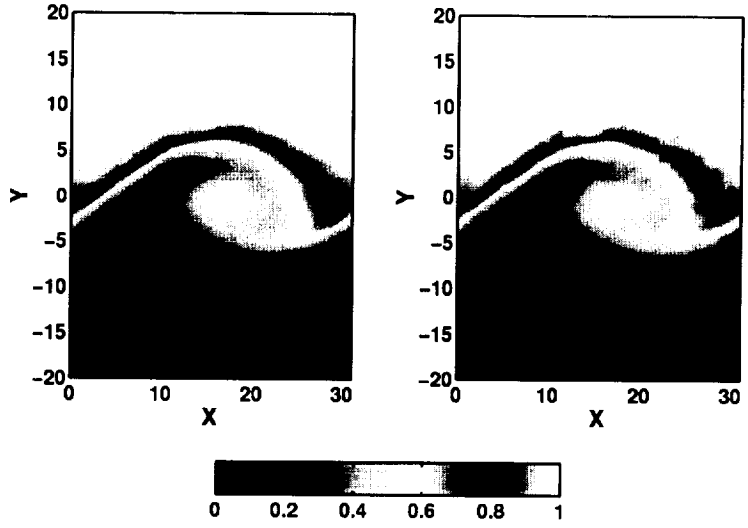

Figure 38: Visual consistency for the scalar field. The LES-FD results are obtained for $\Delta_E = 0.5\Delta$, $N_E = 40$ at t=34.3. (Captions: Left - LES-FD, Right - VSFDF)

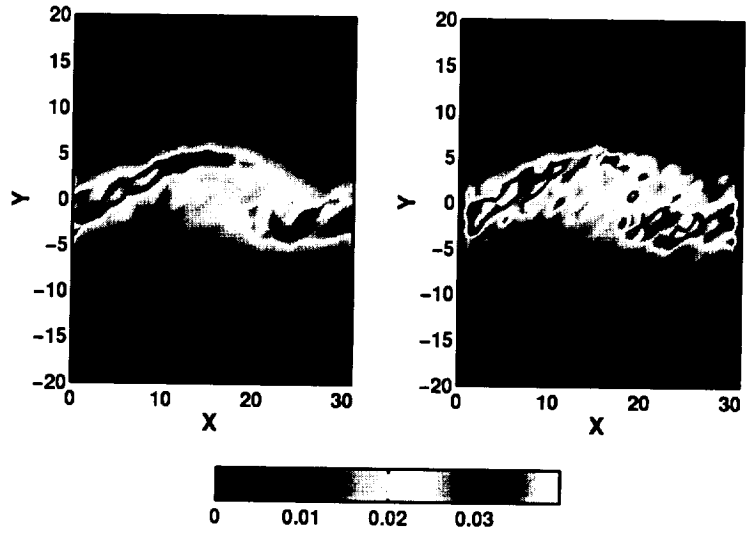

Figure 39: Visual consistency for the $\tau(u,u)$ component of the SGS stress tensor. The LES-FD results are obtained for $\Delta_E = 0.5\Delta$, $N_E = 40$ at t=34.3. (Captions: Left - LES-FD, Right - VSFDF)

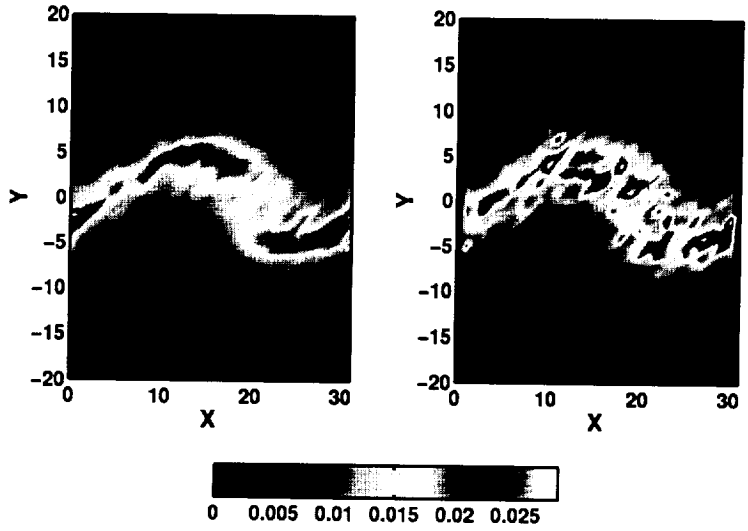

Figure 40: Visual consistency for the $\tau(v,v)$ component of the SGS stress tensor. The LES-FD results are obtained for $\Delta_E = 0.5\Delta$, $N_E = 40$ at t=34.3. (Captions: Left - LES-FD, Right - VSFDF)

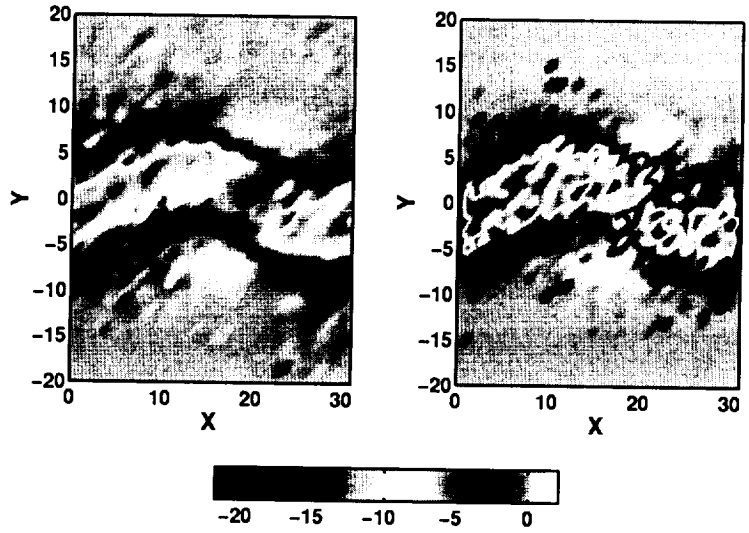

Figure 41: Visual consistency for the $\tau(u, v)$ component of the SGS stress tensor. The LES-FD results are obtained for $\Delta_E = 0.5\Delta$, $N_E = 40$ at t=34.3. (Captions: Left - LES-FD, Right - VSFDF)

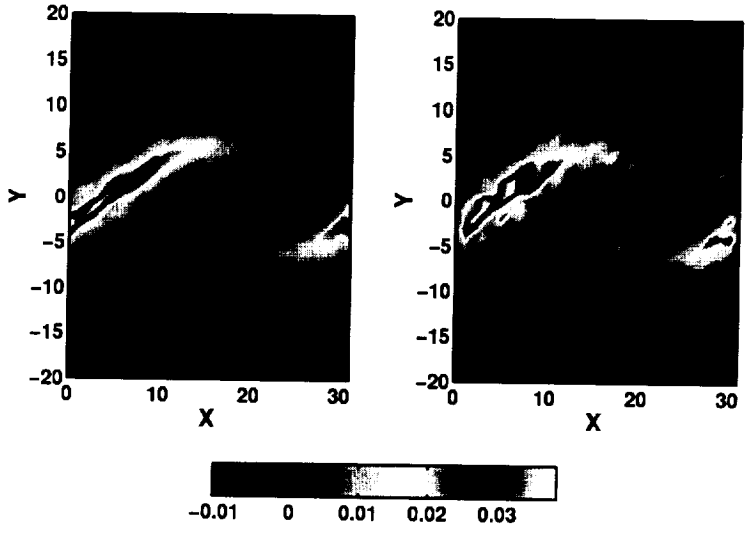

Figure 42: Visual consistency for the $\tau(u, \phi)$ component of the SGS stress tensor. The LES-FD results are obtained for $\Delta_E = 0.5\Delta$, $N_E = 40$ at t=34.3. (Captions: Left - LES-FD, Right - VSFDF)

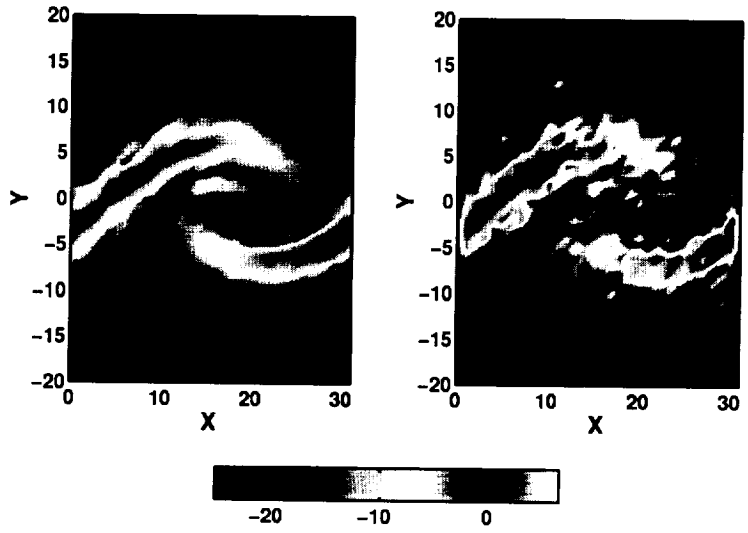

Figure 43: Visual consistency for the $\tau(v, \phi)$ component of the SGS stress tensor. The LES-FD results are obtained for $\Delta_E = 0.5\Delta$, $N_E = 40$ at t=34.3. (Captions: Left - LES-FD, Right - VSFDF)

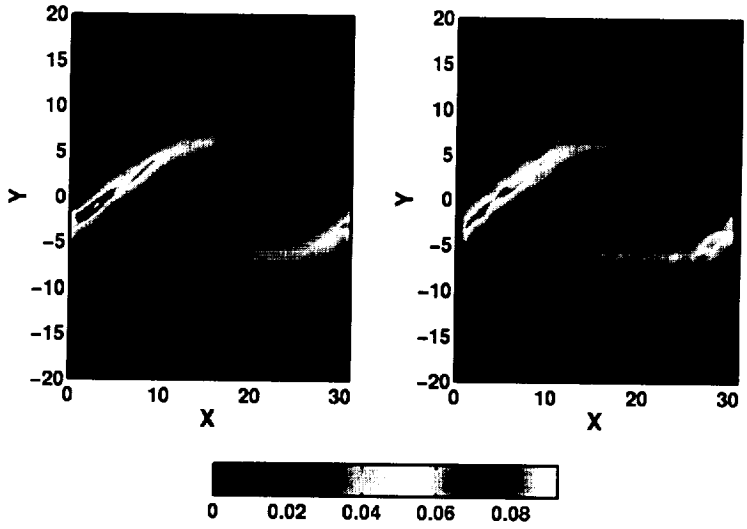

Figure 44: Visual consistency for the $\tau(\phi, \phi)$ component of the SGS stress tensor. The LES-FD results are obtained for $\Delta_E = 0.5\Delta$, $N_E = 40$ at t=34.3. (Captions: Left - LES-FD, Right - VSFDF)

(a) t=9.00

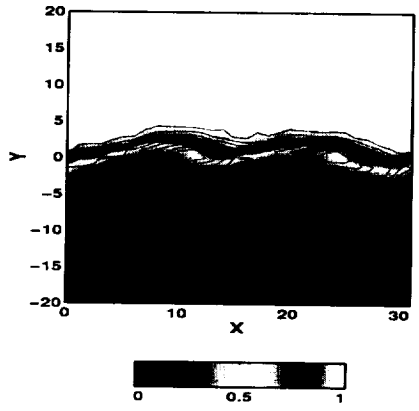

(b) t=9.00

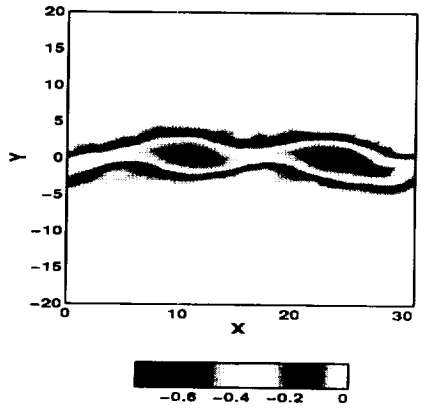

(c) t=13.98

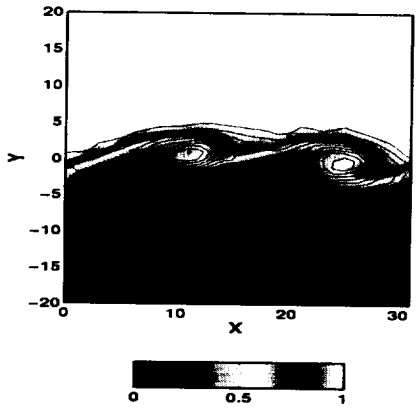

(d) t=13.98

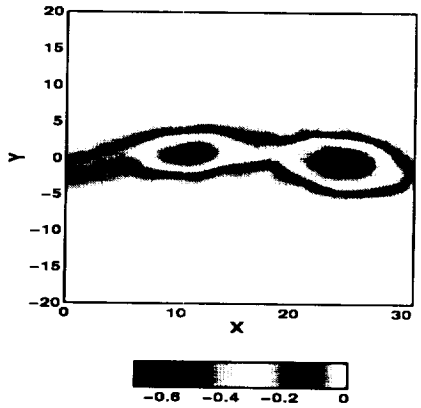

(e) t=18.96

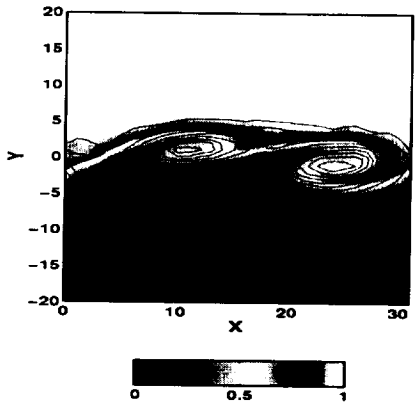

(f) t=18.96

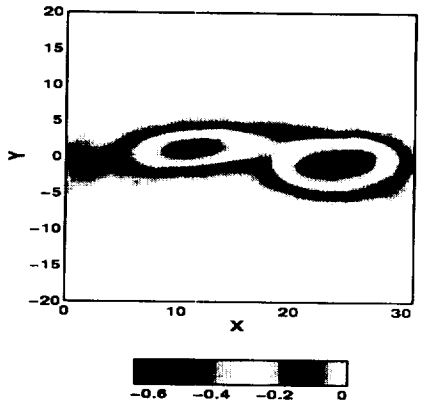

(g) t=23.94

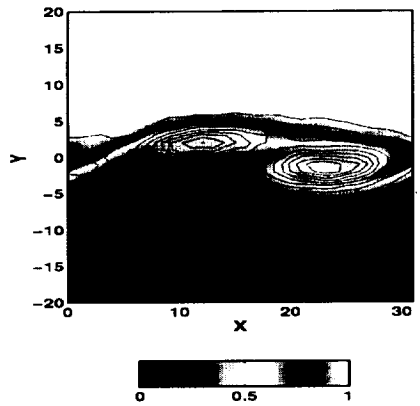

(h) t=23.94

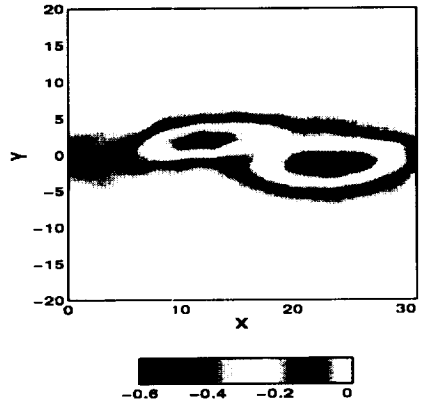

(i) t=28.92

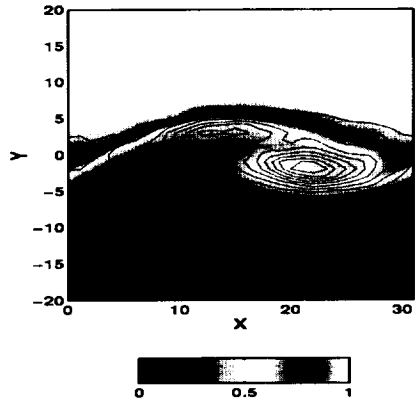

(j) t=28.92

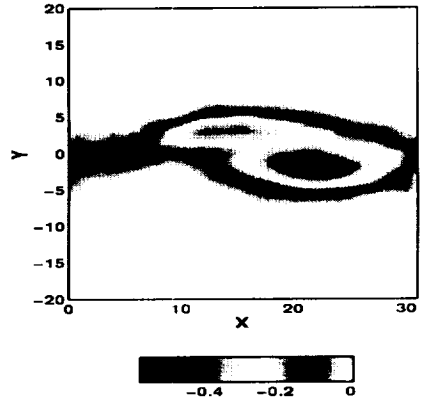

(k) t=33.90

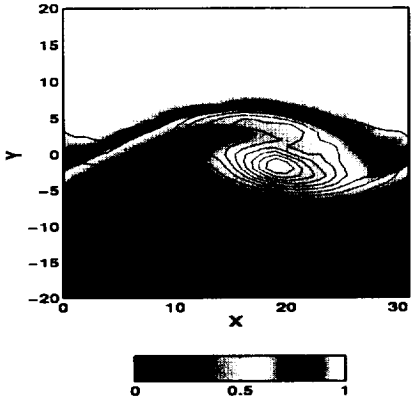

(l) t=33.90

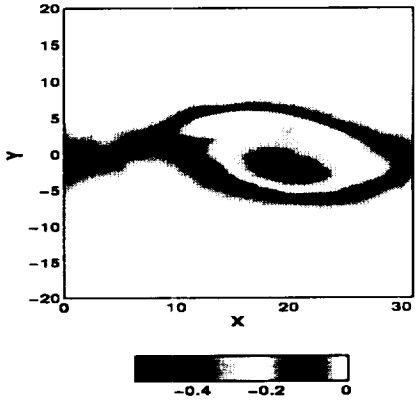

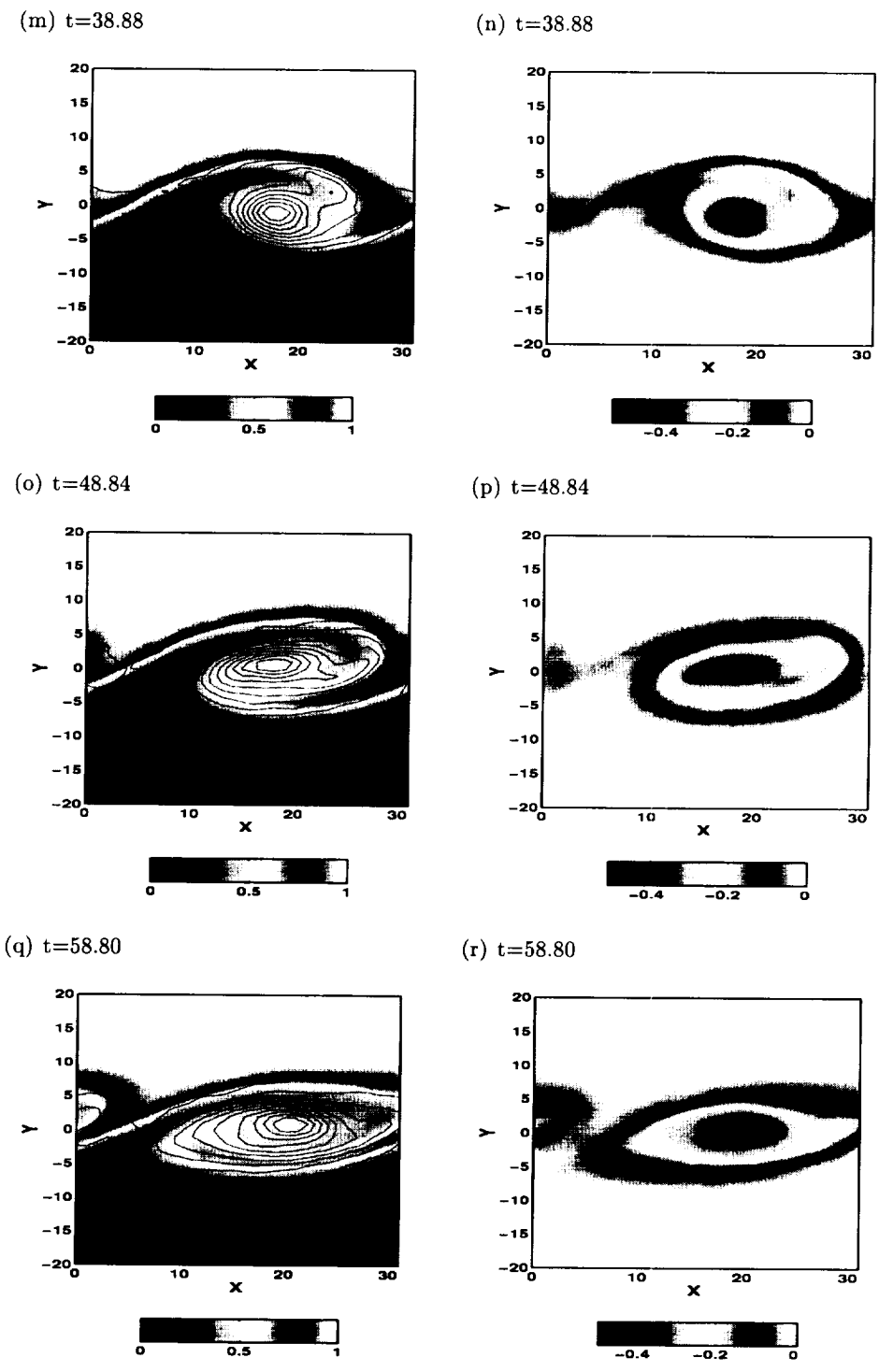

Figure 45: Time evolution of the scalar(with superimposed vorticity isolines) and vorticity fields for LES-FD obtained with $\Delta_E = 0.5\Delta$ and $N_E = 40$

(a) t=9.00

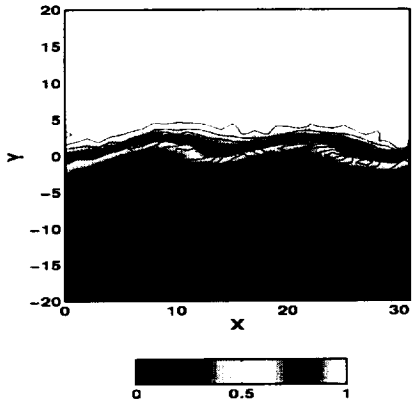

(b) t=9.00

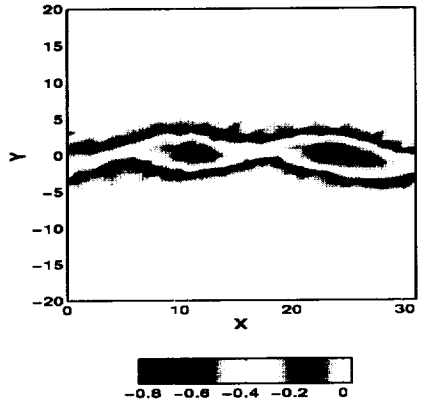

(c) t=13.98

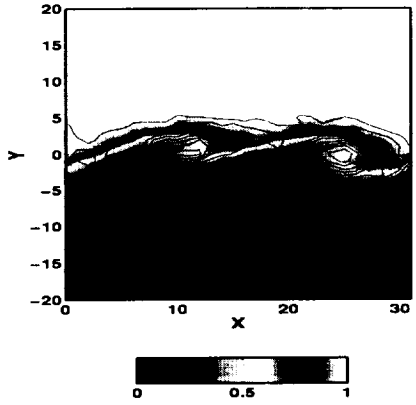

(d) t=13.98

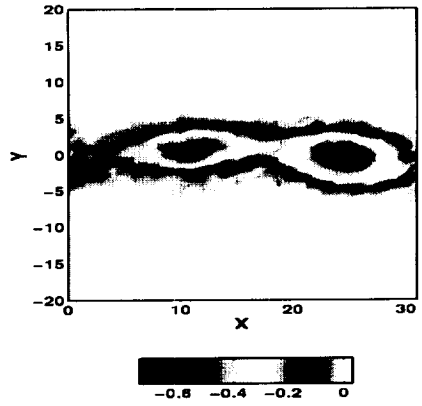

(e) t=18.96

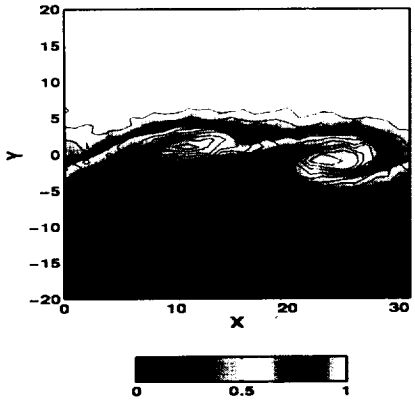

(f) t=18.96

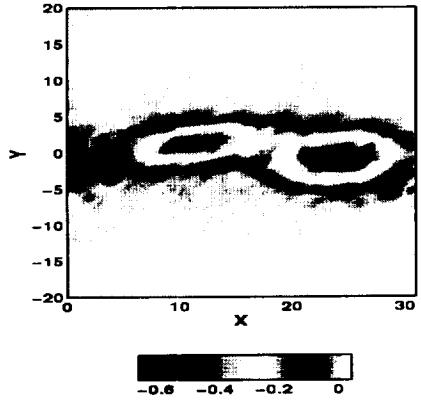

(g) t=23.94

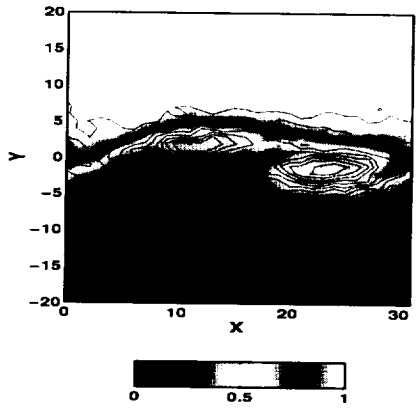

(h) t=23.94

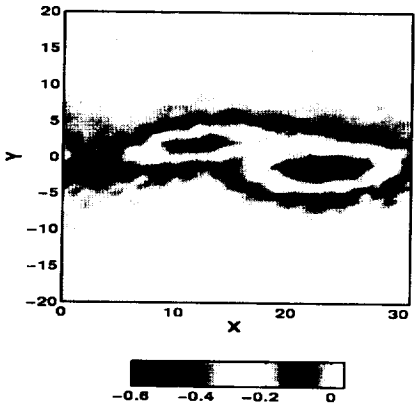

(i) t=28.92

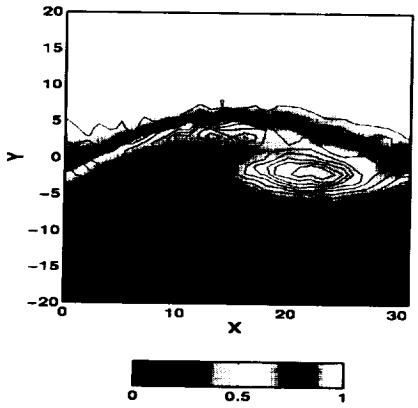

(j) t=28.92

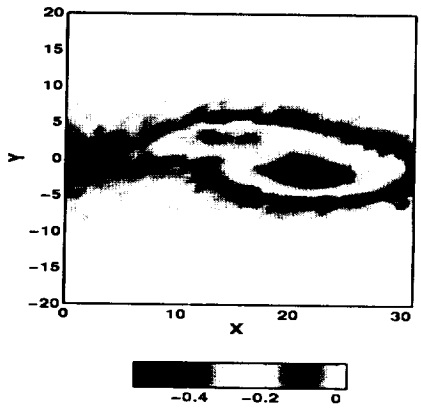

(k) t=33.90

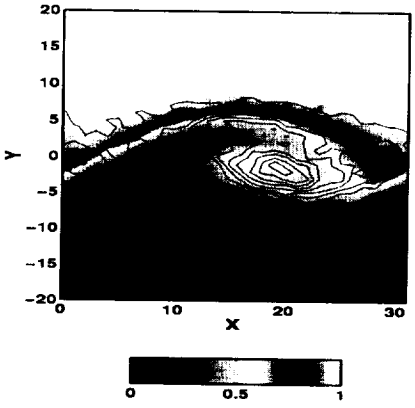

(l) t=33.90

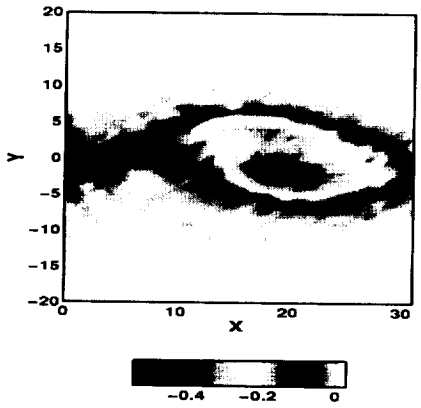

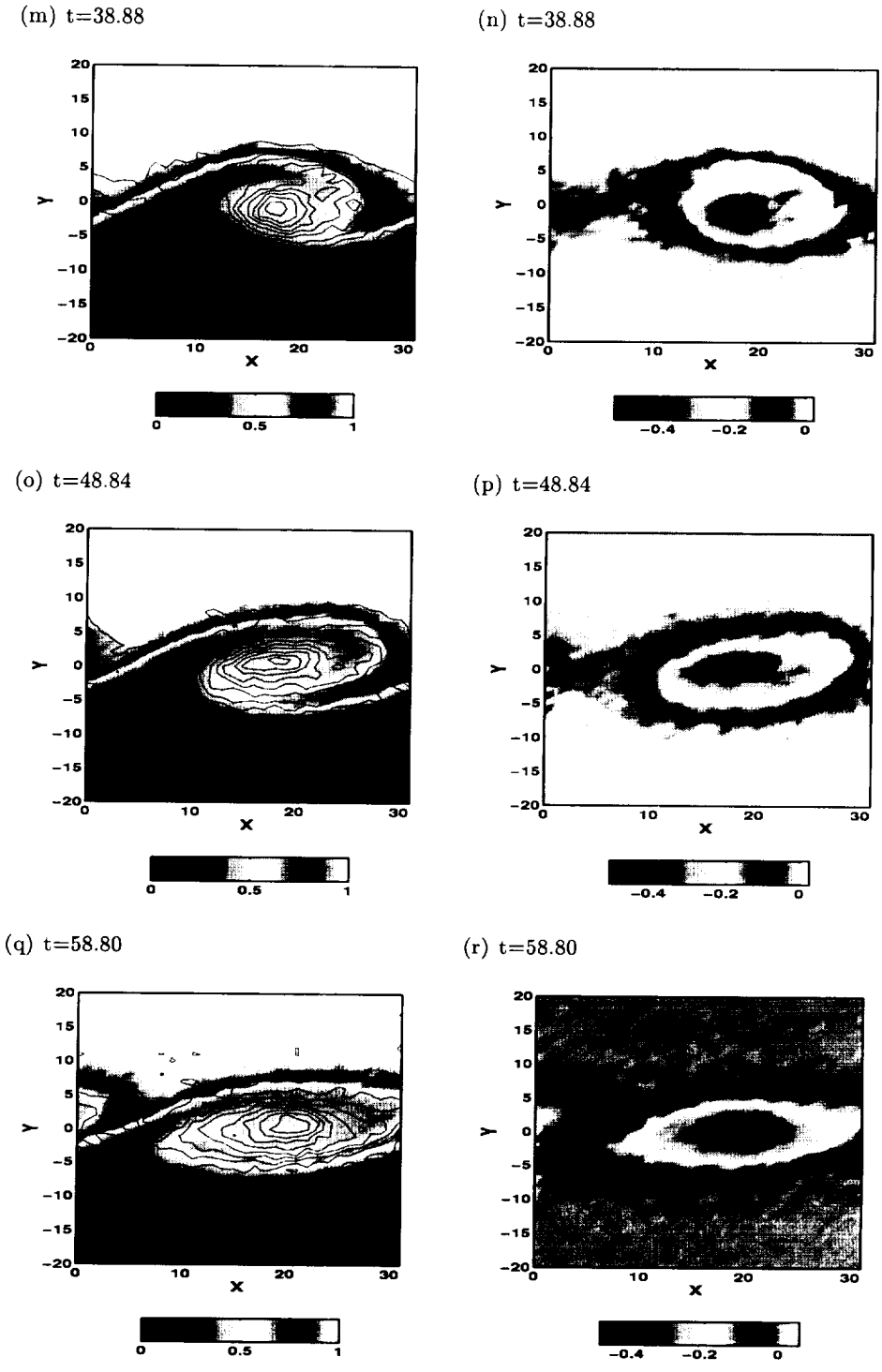

Figure 46: Time evolution of the scalar(with superimposed vorticity isolines) and vorticity fields for VSFDF